The Synthesis and Single-Molecule Conductance of Conjugated Molecular Wires

ZHAO, XIAOTAO

The Synthesis and Single-Molecule Conductance of Conjugated Molecular Wires

Xiaotao Zhao

Josephine Butler College

Department of Chemistry

Durham University

A thesis submitted for the degree of Doctor of Philosophy at Durham University

March 2014

Declaration

The work described in this thesis was carried out in the Department of Chemistry at Durham University between October 2010 and March 2014. All the work was carried out by the author unless otherwise stated and has not been previously submitted for a degree at this or any other university.

Table of Contents

Abstract

The Synthesis and Single-Molecule Conductance of Conjugated Molecular Wires

Xiaotao Zhao, Durham University, 2014

The past decades have seen the fast development of electronic devices in the industrial sector. There is increasingly rapid growth in the demand for alternative electronic building blocks to compliment, and possibly replace, the conventional silicon-based products. Electronic devices based on organic molecules, especially those based on single molecules, receive intense studies both theoretically and experimentally.

In this presented work, a new family of oligo(aryleneethenylene)s (OAE)s with molecular lengths (N…N distance) of ca. 2-6 nm were designed to investigate the length dependence of conductance at the single molecule level. X-ray molecular structures of OAEs with a molecular length up to 5.3 nm were successfully analysed and presented.

Secondly, four groups of pyridyl terminated oligo(phenyleneethylene) (OPE) derivatives were studied for the quantum interference effects. A dramatic destructive quantum interference effect was observed which decreased the single molecule conductance by several orders of magnitude. Unsymmetrical molecules with only one anchor group were noticed to form π-π stacking between two molecules.

Thirdly, amino terminated OPEs bearing various substituents on the central phenyl rings were explored to present the robustness of the central OPE backbone towards various functionalising substituents.

Fourthly, diaryloligoynes with different anchor groups were synthesised and the single-molecule conductances were studied. The stability of the tetrayne compounds is discussed and X-ray crystal structures of the stable tetraynes are presented.

Finally, pyridyl terminated OAE derivatives bearing an anthraquinone core were synthesised to investigate the charge transport through the central anthraquinone core, with special purpose of investigating quantum interference effects and the switching process of the central anthraquinone core.

Acknowledgement

Firstly, I would like to thank my supervisor Prof. Martin R. Bryce for accepting me in his lovely research group. I had a really good time in Durham for the last few years and it was a great experience for me to work with both past and present members of the group. I would like to thank Dr. Murat Gulcur for sharing his knowledge and experiences with me, and proof reading this thesis as well. I would also like to thank Dr. Daniel Welsh for his dedication in proof reading this thesis. I would like to thank Dr. Steven Zheng and Dr. Jose Santos for their help. And many thanks to all the other group members who have left wonderful memories.

Secondly, I would like to thank Prof. Thomas Wandlowski and his research group members at the University of Bern. I wish that Prof. Wandlowski will get well soon after a brain haemorrhage. Many thanks to Cancan Huang, Masoud Baghernejad, Dr. Wenjing Hong and Dr. Pavel Moreno-García for their efforts in single-molecule conductance measurements.

I would like to thank Prof. Nicolás Agraït and his research group at IMDEA-Nanociencia, Madrid, especially Dr. Maria Teresa González for the efforts they made in single-molecule conductance measurements.

I would like to thank Prof. Colin Lambert and his research group at the Lancaster University, especially Dr. David Manrique for theoretical calculations.

I would also like to thank Dr. Andrei S. Batsanov for the amazing job he has done in X-ray crystal structure elucidation.

Finally, I would like to thank my parents for supporting me throughout my study in Durham. I would like to give my special gratefulness to my lovely wife Lu Liu for her continuous support and motivating me to keep looking forward.

Publications and Presentations

The following papers are based on work described in this thesis:

- C. Huang, M. Baghernejad, X. Zhao, D. Z. Manrique, V. Kaliginedi, M. Gulcur, W. Hong, T. Wandlowski, C. J. Lambert, M. R. Bryce. **Tandem Controlling of Single-Molecule Conductance in Pyridyl Terminal Oligo(phenyleneethynylene)s.** Manuscript in preparation.
- M. González, X. Zhao, D. Manrique, D. Miguel, E. Leary, M. Gulcur, A. S. Batsanov, G. Bollinger, C. Lambert, M. R. Bryce, and N. Agraït. **Conductance Invariance towards Functionalisation in Oligo(phenylenethynylene) Molecular Junctions.** Manuscript for submission in April 2014.
- M. Gulcur, P. Moreno-García, X. Zhao, M. Baghernejad, A. S. Batsanov, W. Hong, M. R. Bryce and T. Wandlowski. **The Synthesis of Functionalised Diaryltetraynes and their Transport Properties in Single-Molecule Junctions.** *Chem. Eur. J.* Accepted.
- X. Zhao, C. Huang, M. Gulcur, A. S. Batsanov, M. Baghernejad, W. Hong, M. R. Bryce, and T. Wandlowski. **Oligo(aryleneethynylene)s with Terminal Pyridyl Groups: Synthesis and Length Dependence of the Tunneling to Hopping Transition of Single-Molecule Conductances.** *Chem. Mater.*, 2013, 25 (21), 4340–4347.
- I. Kaur, X. Zhao, M. R. Bryce, P. Schauer, P. J. Low and R. Kataky. **Modification of Electrode Surfaces by Self-Assembled Monolayers of Thiol-Terminated Oligo(Phenyleneethynylene)s.** *ChemPhysChem,* 2013, 14, 431-440.

The following presentations were based on work described in this thesis:

- The 11th International Symposium on Functional π-electron systems (Fπ-11) , June, 2013, Arcachon, France; poster presentation
- Durham University Postgraduate Gala Symposium, Durham, UK; oral presentation (best talk)
- FUNMOLS Workshop, February 2013, Madrid, Spain; oral presentation
- FUNMOLS Workshop, September 2012, Newcastle, UK; poster presentation
- FUNMOLS Workshop, May, 2012, Erlangen, Germany; poster presentation
- FUNMOLS Workshop, January 2012, Zurich, Switzerland; poster presentation
- FUNMOLS Workshop, September 2011, Barcelona, Spain; poster presentation
- European Conference on Molecular Electronics (ECME), September 2011, Barcelona, Spain; poster presentation

List of Abbreviations

A	Acceptor
ASAP	Atmospheric solids analysis probe
abs	Absorbance
Ac	Acetyl
AFM	Atomic force microscope
β	Attenuation factor
BDTMS	1,4-Bis(trimethylsilyl)buta-1,3-diyne
BJ	Break junction
bp	Boiling point
BPDN-DT	Bipyridyl-dinitro oligo(phenyleneethynylene) dithiol
CV	Cyclic voltammetry
D	Donor
D-A	Donor-acceptor
DCM	Dichloromethane
DMF	*N*,*N*-Dimethylformamide
DMSO	Dimethyl sulfoxide
EtOAc	Ethyl acetate
EtOH	Ethanol
Et_2O	Diethyl ether
eV	Electron volts
HOMO	Highest occupied molecular orbital
I	Current
IET	Intramolecular electron-transfer
IP	Ionization potential
I-V	Current-voltage
JFP	Junction formation probability
LUMO	Lowest occupied molecular orbital
M	Molar/Molecular Junctions
Me	Methyl
MeOH	Methanol
MCBJ	Mechanically controllable break junction

mp	Melting point
MS	Mass spectroscopy
NMR	Nuclear magnetic resonance
OAE	Oligo(aryleneethynylene))
OP	Oligophenylene
OPE	Oligo(phenyleneethynylene)
OPV	Oligo(phenylenevinylene)
PE	Petroleum ether (b.p. 40° - 60°C)
Rt	room temperature
QI	Quantum interference
SAM	Self-assembled monolayer
SPM	Scanning probe microscopy
STM	Scanning tunneling microscopy
STS	Scanning tunneling spectroscopy
T	Tunneling
TBAF	Tetrabutylammonium fluoride
TCB	1,2,4-Trichlorobenzene
TCNQ	Tetracyanoquinodimethane
THF	Tetrahydrofuran
TMB	1,3,5-Trimethylbenzene
TMS	Trimethylsilyl
TMSA	Trimethylsilylacetylene
TTF	Tetrathiafulvalene
UV-Vis	Ultraviolet- visible

Chapter 1. Introduction to Molecular Electronics

1.1 An overview

Three key components which have dominated the development of electronics spanning two centuries are the vacuum tube, the transistor and the integrated circuit. In 1883, the discovery of electrons flowing from one metal conductor to another through a vacuum was made by Thomas Alva Edison, and is known as the Edison effect. John Fleming applied this effect in inventing the diode in 1904 and Lee De Forest followed with the triode in 1906. These inventions made it possible to amplify and transmit electrical energy.

After World War II, researchers tried to use electron tubes to develop early stage computers. However, it was impractical due to the sizes of the electronic components at that time. The transistors were invented by John Bardeen, Walter Brattain and William Shockley in 1947, who were awarded the Nobel Prize in Physics (1956) for their work. In 1952, Geoffrey Dummer proposed the concept of the integrated circuit which led to the booming of the silicon integrated circuits industry for the following decades.

In 1965, Intel co-founder Gordon Moore wrote one of the first reviews of the progress in the semiconductor industry.[2] Six years after the first commercial planar transistor was introduced in 1959, Moore noted that the number of the components on a single chip was approximately doubling every year. There were 64 components on a single chip in 1965. According to this trend, Moore predicted that in ten years' time, chips with 65000 components would be available (Fig. 1.1). Moore's law of exponential growth in circuit density has become known as one of the best predictions in modern science.

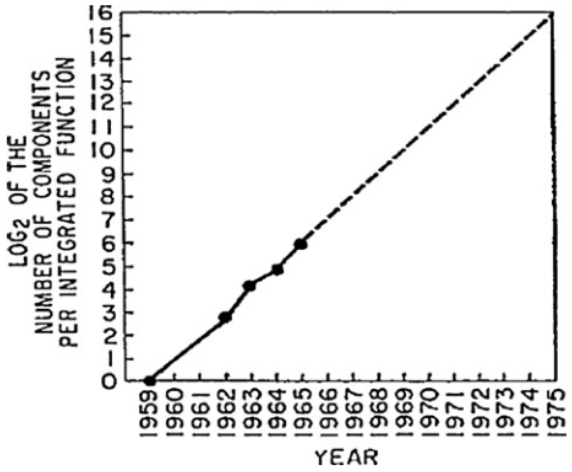

Fig. 1.1 Based on the historical data, Moore predicted the doubling of the number of components on each chip by 1975. (Reproduced from reference[2])

In 1975, Moore revised his 1965 prediction to "the number of the transistors per chip doubles approximately every two years."[3] Moore's law is applicable to the capabilities of many digital electronic devices: processing speed, memory capacity, sensors and number and size of pixels in digital cameras.[4] It has also boosted the impact of digital electronics in almost every part of the world economy. Moore's law has been a driving force for the development of technology and guidance for social improvements in the late 20th and early 21st centuries.[5] Intel executive David House quoted "18 months" for the period for the doubling of the number of transistors per chip.[6] However, Moore's law is not a physical or natural law; it is an observation.[7] It is expected to be applicable until at least 2015 or 2020 according to sources in 2005.[8] However, slower growth is expected at the end of 2013 according to the 2010 update to the International Technology Roadmap for Semiconductors,[9] after which time it is predicted that the period of doubling the number of the transistors will be extended to every three years. However, as the lithographic techniques used for producing integrated circuits are limited by the wavelength at which they operate,[10] the rapid size shrinking of the traditional transistors will reach its physical limit in the near future.

As the traditional silicon-based electronic industry is approaching the end, new processes need to be developed in order to meet the ever increasing demands of faster, smaller and more environmentally friendly computing components. One promising alternative direction for the electronics industry is to replace the "top-down" lithographic approach with a "bottom-up" synthetic chemical approach which enables the manufacturing of nanoscale devices directly from their molecular constituents.[10] With the advantages of small size and self-

assembling abilities, nano devices based on molecules can lead to cheap fabrication using self-assembly techniques. Their structures can be tuned through synthetic chemistry and control of their electrical transport properties is possible due to the conformational flexibility of the molecular components.[11,12]

In 1974, Aviram and Ratner presented a theoretical study entitled "Molecular Rectifiers" in which they suggested that molecules could be used as rectifiers.[13] The specific molecule **1** has tetrathiafulvalene (TTF) as a donor (D) unit and tetracyanoquinodimethane (TCNQ) as an acceptor (A) unit connected by a σ-tunneling rigid alkane bridge (Fig. 1.2).

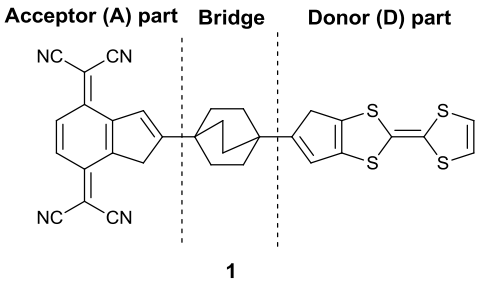

Fig. 1.2 Molecular structure of the rectifier designed by Aviram and Ratner. (Reproduced from reference[13])

It was proposed that molecule **1** would show potential electronic applications along its molecular axis when aligned between two electrodes. This early theoretical model pointed to molecules that may be designed to accomplish previously unattainable electronic functions. The later development of self-assembled monolayers (SAMs) and scanning probe microscopies (SPMs) provided the essential techniques for investigating electron transport through molecules. The field of molecular electronics has undergone rapid and intense study in recent decades. These efforts have been motivated by the expected advantages if molecular components were successfully assembled into microelectronic devices. For example, the flexibilities of molecular structures could present new electronic functions combined with lower cost for bulk manufacture compared to conventional semiconductors; and the dramatically shrinking size of the molecular components, compared to the current ones, may enable heightened capacities and faster performance.

Fig. 1.3 presents three primary features where molecular devices can be distinguished from conventional electronics. Even though the potential size of a molecular device could be as small as a single molecule, modern industry does not focus only on the ability to make devices

smaller, but also on assembling many devices simultaneously on each chip. From an economic viewpoint, enhanced parallel fabrication is equally important to the size of the device. The function sector of Fig. 1.3 is the key aspect which gives molecular electronics priority over conventional electronics.

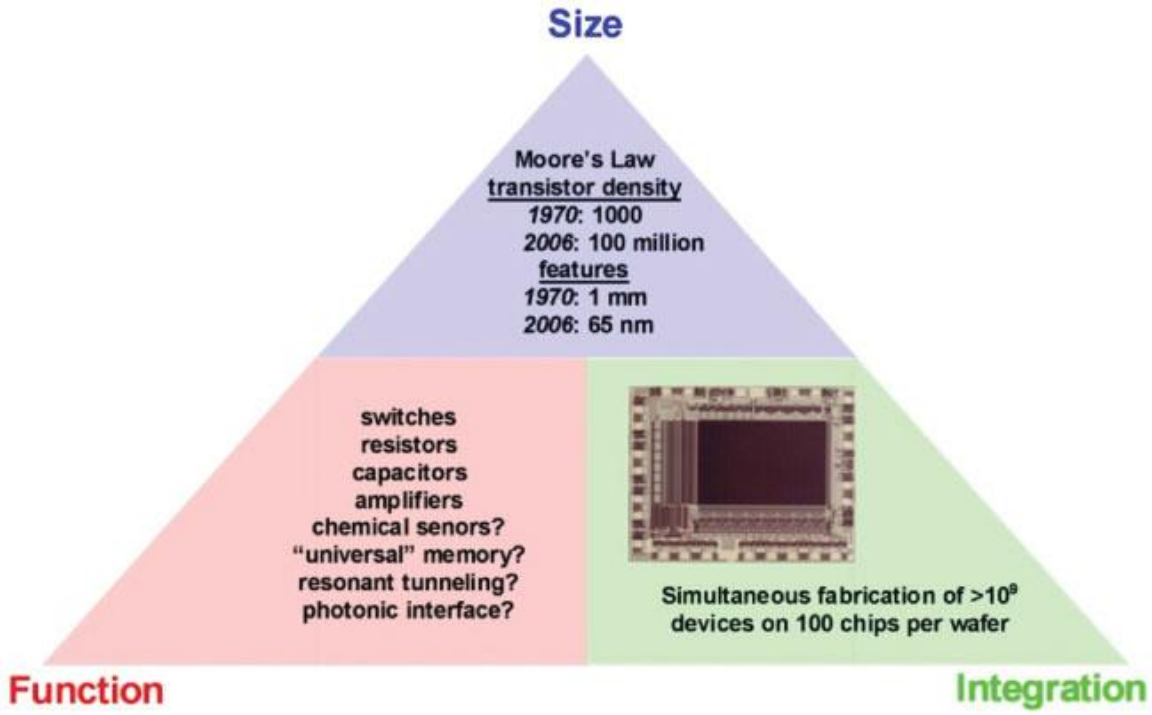

Fig. 1.3 Molecular electronics' "triangle of targets". (reproduce from reference[14])

1.2 Measuring Methods

Molecule-based devices offer the ability to control and measure the charge transport through the molecules. Accordingly, two types of molecular junctions can be distinguished, namely: many-molecule junctions and individual-molecule junctions. In the former case a molecular monolayer is usually trapped between two facing electrodes, which contain cross junctions[15], between liquid metal drop electrodes[16], or assembled in nanopores.[17] On the contrary, individual-molecule junctions comprise only a few molecules, or even a single molecule, trapped between two facing electrodes. For these systems, the key techniques are: scanning probe microscopy (scanning tunneling microscopy or conducting probe atomic force microscopy)[18], mechanically controllable break junctions[11], electrochemical deposition of nanogap electrodes[19] and electromigration breakdown methods[20].

1.2.1 Scanning Probe Microscopy Methods

Due to the development of scanning probe microscopy (SPM) in the 1980s, the study of single-molecule junctions became possible. SPM enables individual molecules on surfaces to be imaged and the molecule's electrical behaviour to be characterised using scanning tunneling spectroscopy (STS).[21-24]

1.2.1.1 Conducting Probe Atomic Force Microscopy (CP-AFM)

AFM techniques with the help of conducting probes have been used to measure electrostatic forces, charge distributions, voltage drops and resistances on sub-100 nm length scales[25]. These techniques enable detailed electrical characterization of materials as topographic imaging and electrical measurements are achieved simultaneously. A metal-coated conductive tip is used in this method to form a contact with the conductive substrate through the molecules. Current-voltage characteristics through an external circuit are recorded during the whole process.

A reliable method to measure the current-voltage *I(V)* characteristics of a metal/molecule/metal circuit was reported by Cui and Lindsay in 2001[26]. 1,8-Octanedithiol molecules were inserted into an octanethiol monolayer on a Au(111) substrate. One of the two terminal groups of the dithiol chemically bonded to the gold substrate leaving the other thiol group exposed on the top of the monolayer. The octanethiol molecules isolated the dithiol molecules from one another which enabled the formation of single-molecule junctions with the dithiols. The exposed thiol group was able to trap the floating gold nanoparticles in the suspension and an AFM probe could make contact with the individual particles bonded to the monolayer (Fig. 1.4A).

Five different families of curves were obtained from *I(V)* measurements through over 4000 nanoparticles. Fig. 1.4B shows the representative curves from each family. When divided by an appropriate integer, all the curves were found to be multiples of a fundamental curve (Fig. 1.4C). 4600 curves were shown to sharply peak at the integer values 1, 2, 3, 4 and 5 (Fig. 1.4D). The fundamental set of curves which contain more than 1000 curves was obtained by using a dithiol molecule to connect the gold nanoparticle to the underlying gold substrate. The other sets of curves were assigned to more than one dithiol molecule participating in forming the circuits.

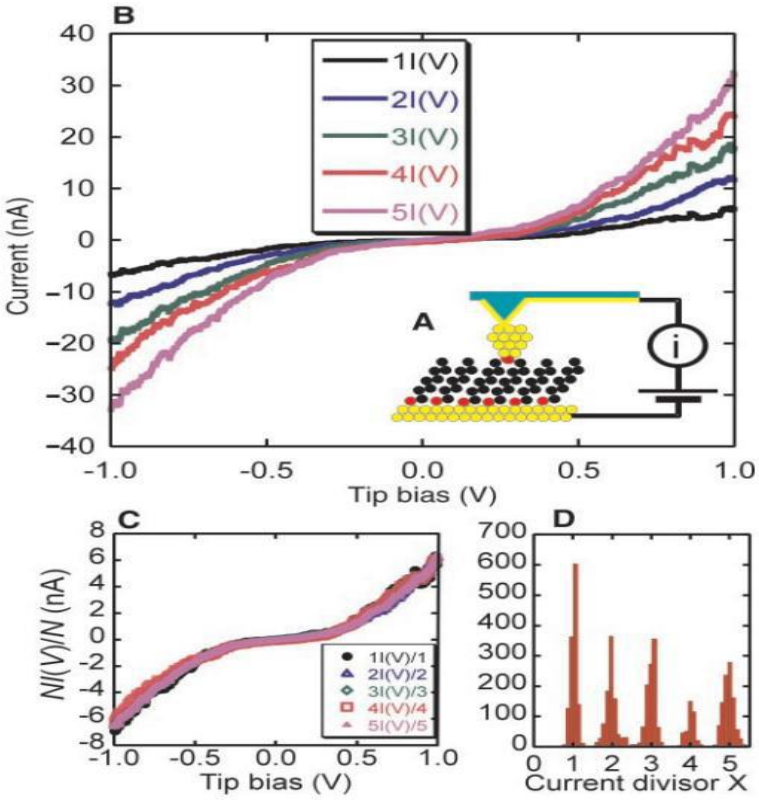

Fig. 1.4 (A) Schematic diagram of the experiment (sulfur atoms are shown in red). (B) *I(V)* curves measured with the apparatus shown in (A). These figures are labelled B, C and D. (C) Curves from (B) divided by an integer (*N*=1, 2, 3, 4 and 5). (D) Histogram of values of a divisor, X (a continuous parameter), chosen to minimize the variance between any one curve and the fundamental curve, *I(V)*. (Reproduced from reference[26])

In CP-AFM, the metal-coated tip gently approaches the molecules on the conducting substrate while the current-voltage characteristics of the circuit are recorded. Accordingly, this technique removes the cause of current reduction by the extra tunnelling gap, as occurs in the STM setup (which will be discussed later). However, the significantly larger size of the metal-coated conducting probe tip introduces a high degree of uncertainty in the numbers of the molecules being measured. Also the roughness and morphology of the bottom substrate need to be considered to estimate the number of molecules investigated. Very sensitive control of the tip loading force is also required in order to avoid applying excessive pressure to the molecular monolayers, as pressure may modify the structure and electronic properties of the monolayer.

1.2.1.2 Scanning Tunneling Microscopy (STM)

Gerd Binning and Heinrich Rohrer were award the Nobel Prize in Physics in 1986 for their discovery of Scanning Tunneling Microscopy (STM). In STM, a very sharp conductive tip

controlled by a piezoelectric effect is brought very close to the surface of the sample to be analysed and a bias voltage is applied between the tip and the surface, which allows electrons to tunnel through the space between them. While the current and height of the tip are kept constant, by recording the movement of the tip a surface image is formed.

STM-Break Junction

A break junction (BJ) technique based on STM (STM-BJ) was first described by Xu and Tao[27] by using an STM tip to move up and down very quickly on the metal electrode in the presence of sample molecules to gain contact with them. This method can quickly form thousands of individual molecular junctions (Fig. 1.5). The sample molecules in solution can bind to either the electrode substrate or the tip with anchor groups which are covalently attached at both ends of the molecules. The first step of this process is that the tip is driven down to the electrode substrate until it contacts the molecules that are attached there. During this process, some of the molecules can bind to the tip with their other anchoring group to form tip/molecule/substrate junctions (Fig. 1.5a). Then, the junctions are broken by retracting the tip. One or more junctions are broken successively as shown by a stepwise decrease in the current (Fig. 1.5b). This process is repeated until a large number (usually several thousands) of junctions have been created and measured. The histogram peaks generated from the conductance data are typically located around the integer multiples of a fundamental value which is assigned to the single-molecule conductance (Fig. 1.5c). As this technique enables large numbers of measurements in a very short time, robust statistical conductance data proves the formation of molecular junctions.[18,27-29]

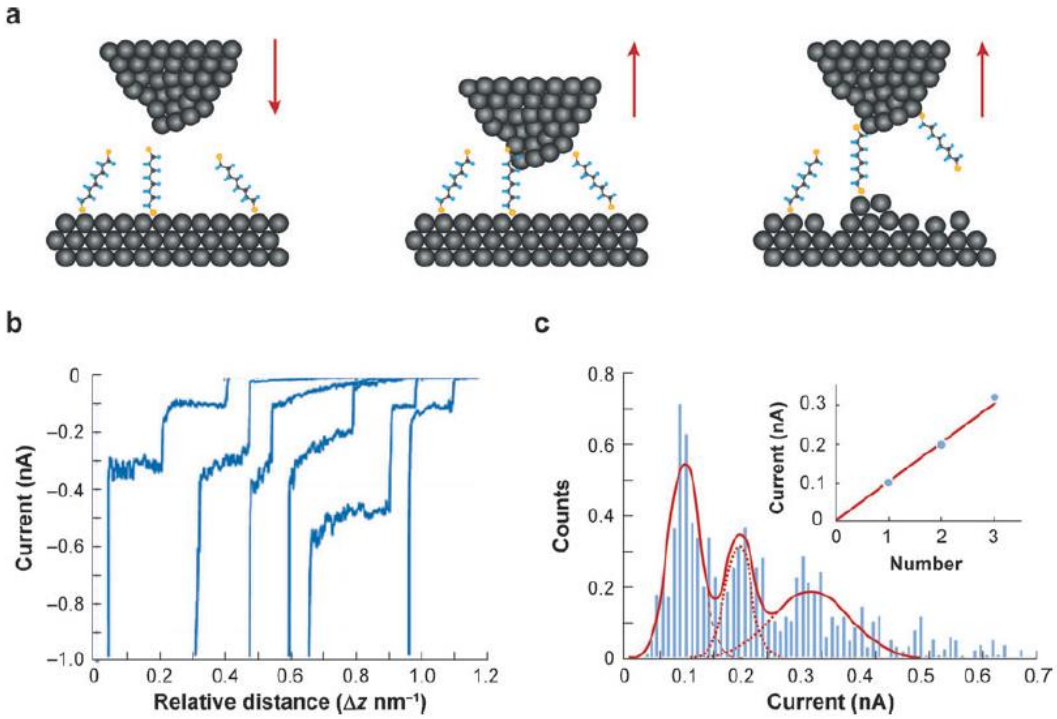

Fig. 1.5 (a) Scanning Tunneling Microscopy Break Junction (STM-BJ) process with 1,8-octanedithiol molecules. (b) The current (conductance) for viologen dithiol (N,N'-bis(6-thiohexyl)-4,4'-bipyridinium dibromide) recorded during the process discussed above. Bias voltage = −0.1 V. (c) Conductance histogram generated from thousands of junction breaks which shows the basic value and its integer multiples. (Reproduced from reference[29])

I(s) Method

In 2003, Haiss *et al.*[30] first reported the *I(s)* method by using a viologen derivative, namely dithiol (N,N'-bis(6-thiohexyl)-4,4'-bipyridinium diiodide (6V6) (**2**), as the molecule of interest. These molecules lie parallel to the surface and form a low-coverage phase on Au(111). As shown in Fig. 1.6, as soon as the STM tip was brought close enough to the substrate without contacting, the formation of stable molecular junctions between the tip and substrate was observed. The tip was then lifted while keeping the x-y position constant and the *I(s)* data was measured.

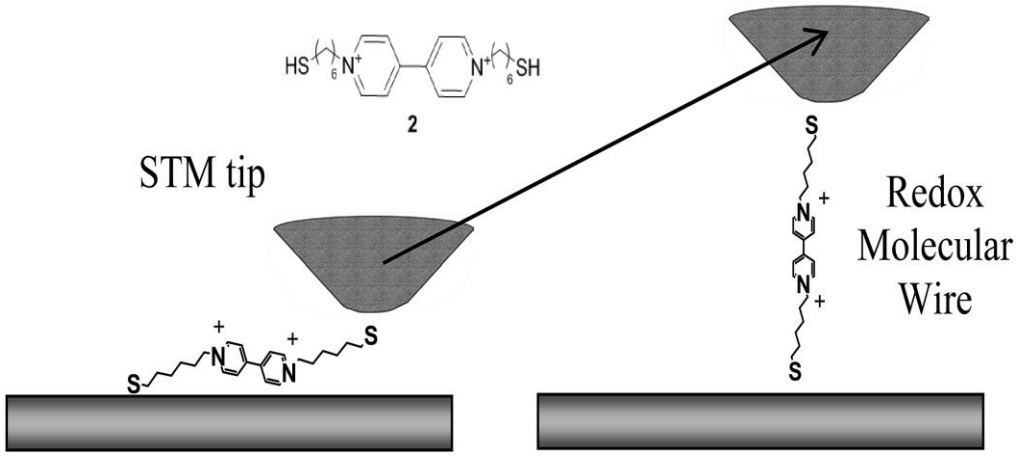

Fig. 1.6 Schematic diagram of the *I(s)* experiment. (Reproduced from reference[30])

Two different types of *I(s)* scan were recorded. One showed an exponential decrease of the tunneling current, while the other showed a slight decrease with a characteristic current plateau (I_W) (Fig. 1.7). The plateau is ascribed to the conductance of the molecular junction.

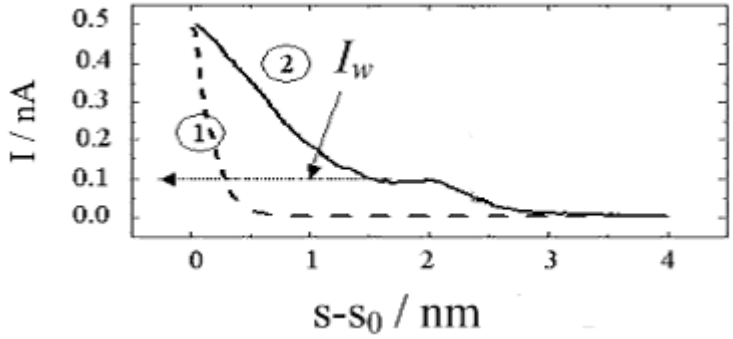

Fig. 1.7 Current decay curves [*I*(*s*) scans] for a 6V6 molecule (2) on a gold surface in air. (Reproduced from reference[30])

I(t) Method

A STM tip is set up at a certain distance from the substrate while the tunneling current as a function of time is recorded (Fig. 1.8a). No current jumps are observed when the tip is placed against clean gold surfaces or surfaces covered with monothiols. Significant current jumps appear when the tip is placed against a surface covered with alkanedithiol molecules. By analysing a large number of current jumps recorded at different locations on the substrate, a histogram of the distribution is shown in Fig 1.8c. The distribution presents a characteristic maximum from which single-molecule conductance can be calculated.

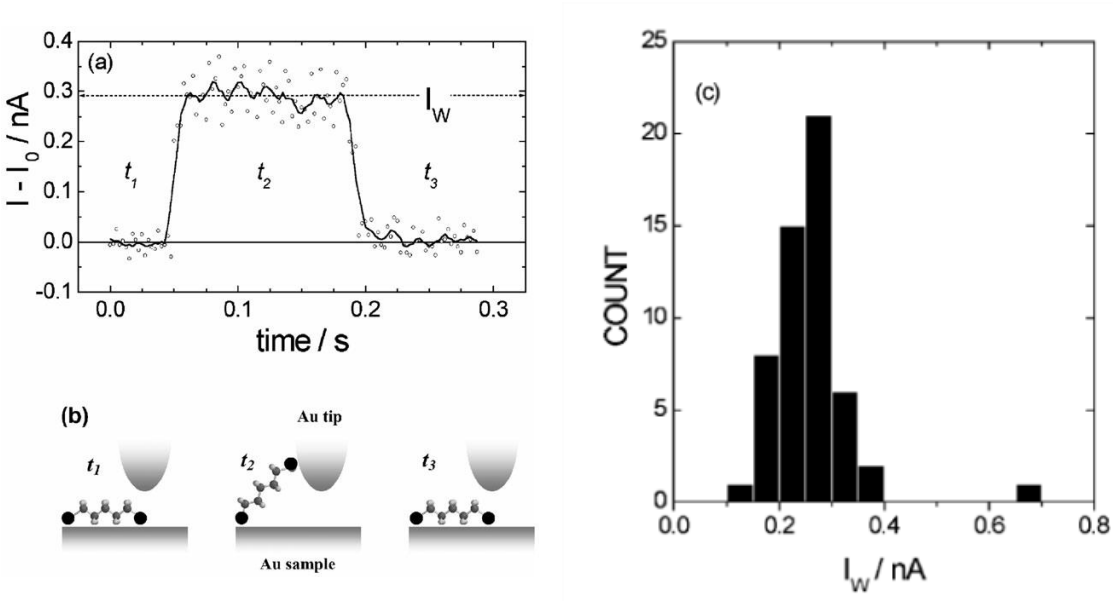

Figure 1.8 (a) Typical current jump recorded on a gold surface with a small concentration of 1,8-octanedithiol. (b) Schematic diagram of *I(t)* experiment. (c) Histogram of count distribution. (Reproduced from reference[31])

1.2.2 Mechanically Controllable Break Junctions (MCBJ)

One of the biggest challenges in molecular electronics is to create separated electrodes between which sample molecules can fit and be reproducibly measured. The MCBJ technique enables the precise and continuous mechanical adjustment of the nanogap between two electrodes.

A schematic standard MCBJ setup is shown in Fig. 1.9 (left). A very thin metallic wire (normally gold) is attached to a flexible substrate, which is called the bending substrate. In general, a notch is made in the middle of the wire. The bending substrate is fixed at both ends by counter supports. A stacked piezo which is controlled by a piezoelectric actuator or motor exerts a vertical force on the bending beam. As a result, the wire is first elongated at the notch and then fractures leaving two facing electrodes. The distance between the two facing electrodes can be controlled precisely by forcing or relaxing the stacked piezo. When applying a solution of sample molecules into the gap, one or more molecules may bridge the gap and the electronic properties of the molecule(s) can be measured.

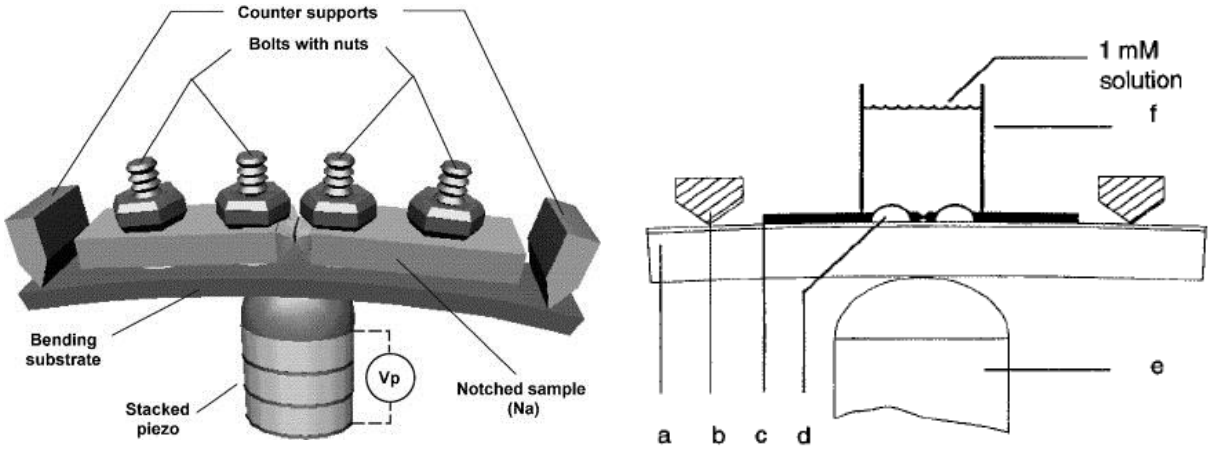

Fig. 1.9 Graphics of the MCBJ (left). (a) the bending beam, (b) the counter supports, (c) the notched gold wire, (d) the glue contacts, (e) the piezo element, and (f) the glass tube containing the solution of molecules to be measured (right). (Reproduced from reference[1,32])

There are many advantages to the MCBJ technique for single-molecule measurements. For example, due to its flexible configuration, it can be easily combined with other systems, such as a Raman spectrometer or high vacuum system. There is less likely to be contamination of the electrodes as they are freshly formed in the breaking process. It is also very suitable for single-molecule measurements when advanced lithography techniques can be used to bring the facing electrodes down to the molecular scale.

The high mechanical stability of the MCBJ setup distinguishes it from other techniques. As the electrodes are closely fixed to the substrate (approximately 0.5 mm by traditional fabrication and approximately 1 μm by lithographic fabrication), the length of the free standing part is much shorter than in a normal STM setup, which results in a very high resonance frequency. Moreover, the mechanical configuration of the MCBJ setup gives a very precise control of the electrodes. By pushing and pulling the rod vertically (ΔX), there is only a highly reduced horizontal displacement (ΔZ) of the electrodes.

The MCBJ technique was first used to study electron tunneling by Moreland in 1985[33]. Then Muller applied it to the study of quantum size conduction in metallic constrictions in 1992[34]. Reed *et al.*[1] first used MCBJ as the method to measure electronic conductance in single molecules in 1997. The experiment was conducted at room temperature (Fig. 1.9 right). Benzene-1,4-dithiol dissolved in 1 mM THF was used in this experiment. After the formation of two facing electrodes which were broken in the solution under argon, benzene-1,4-dithiol attached to the electrodes resulting in self-assembled mono-layers (SAMs) which were nearly perpendicular to the surface (Fig. 1.10). The solvent was allowed to evaporate and no further

preparation and cleaning were needed for the surface. The evaporation of the THF resulted in the change of dimensional stability of the break, thus the tips were withdrawn. Fig. 1.11 shows the displacement of the dithiol. The study presented a qualitative measurement of the conductance of a single molecule, which opened that gate of single-molecular electronics.

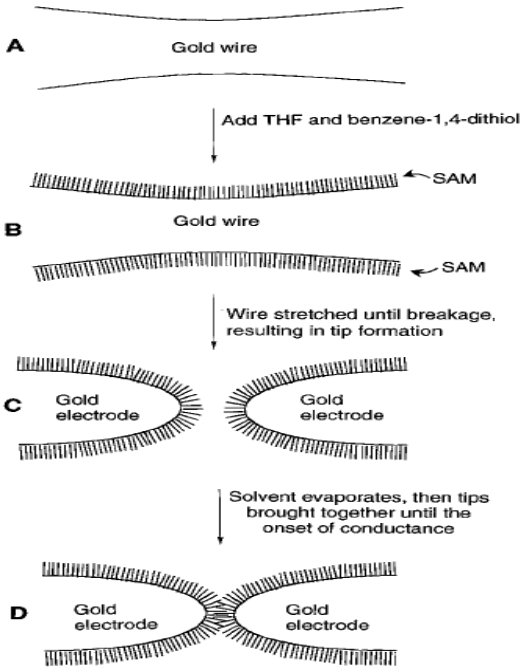

Fig. 1.10 MCBJ process: (A) gold wire (B) benzene-1,4-dithiol SAMs on gold (C) two facing electrodes covered with sample molecules (D) break junction formed. (Reproduced from reference[1])

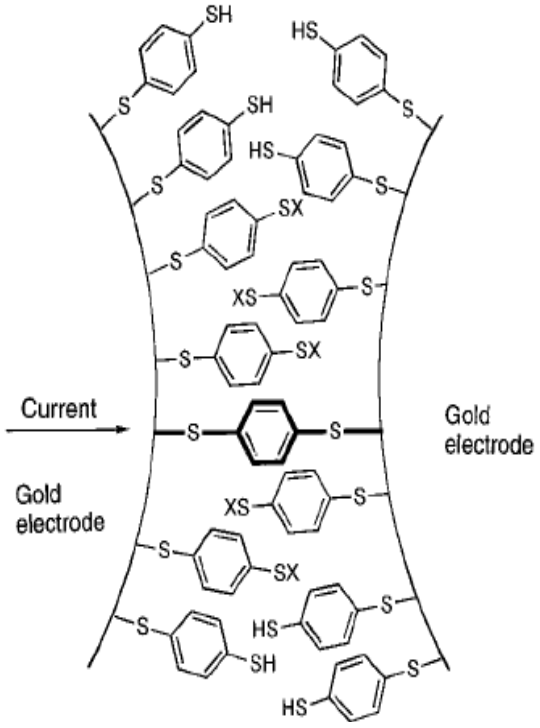

Fig. 1.11 The formation of the dithiolate bridge. End groups denoted as X can be either H or Au. (Reproduced from reference[1])

Conductance Measurements in Liquid

Due to the solvent effect, such as turbulence-induced noise, capacitive charging and molecular polymerization, electrical measurements carried out in solvent are more challenging than those conducted in a vacuum. Additionally, solvent molecules may also influence the intrinsic transport mechanisms. Gruter *et al.*[35] studied the influence of solvents on the electrical conductance of atomic contacts by introducing a liquid cell to the break junction setup. A variety of tunneling barrier heights with different solvents was observed. The electrical conductance of four conjugated molecules was determined and compared in a liquid environment by Huber *et al.*[36], as shown in Fig. 1.12. They found that the conductance of oligo(phenyleneethynylene)s (OPEs) (**4**, **5** and **6**) was slightly lower than that of oligo(phenylenevinylene) (OPV) (**3**) of similar molecular length. They also found that there was little difference between the conductance of

the OPE (**4**) and the two modified OPEs (**4** and **5**) with alkoxy side groups, which means the solubilizing side groups do not noticeably influence the conductance of the molecules. This was an important observation as longer OPE molecules require the presence of many long solubilizing side-chains (see Chapter 2).

In addition to the advantages of the MCBJ techniques, there are also disadvantages. Regarding the measurements, unlike STM, MCBJ techniques are not able to measure the force and surface morphology. The breaking process also presents some drawbacks. For example, the shape and atomic configurations of the electrodes are unknown. Nevertheless, MCBJ is a solid and fundamental technique especially in single-molecule measurements.

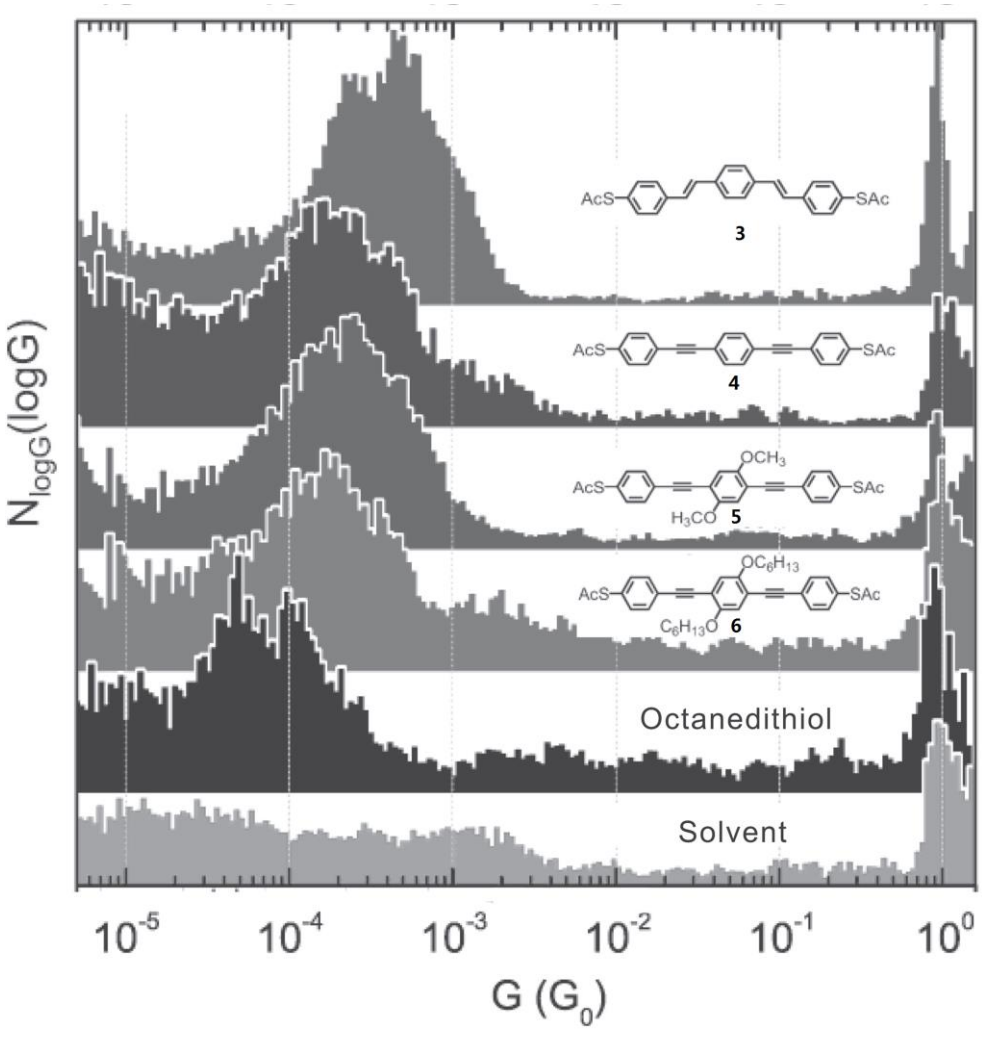

Fig. 1.12 Measurements of single molecule conductance with MCBJ in solution. (Reproduced from reference[36])

1.3 Functional Applications of Molecules

As discussed above, molecular systems exhibit great promise for electronic device applications. The following sections will discuss specific molecules and their applications in (single) molecular electronics.

1.3.1 Switching

Switching phenomena in molecules can lead to potential devices such as memory units, which are likely to be an economic application of molecular electronics. In the past decades, mainly light-triggered processes and redox-active systems have been reported for their switching abilities. Lörtscher *et al.*[37] demonstrated that by applying an external voltage stimulus, a single molecule of structure **7** connected to two symmetric leads in a two-terminal configuration can be reversibly and controllably switched between two distinct states. The intermolecular effect and contact effects were excluded by using the MCBJ technique under a very controlled environment. By studying model analogues it was deduced that the nitro group in molecule **7** contributed to the switching effect.

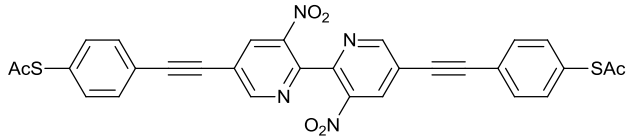

7

Fig. 1.13 Molecular structure of bipyridyl-dinitro oligo(phenyleneethynylene) dithiol (BPDN-DT) investigated in Lörtscher's work. (Reproduced from reference37)

Optoelectronic switching may be triggered by light stimulation. Light-induced conformational change in a molecule is one of the mechanisms of photo switching (Fig. 1.14). Dulik *et al.*[38] have demonstrated an optical one-way switching of photochromic dithienylethene from the conducting to the insulating state. Visible light was used to switch the molecule from a closed state to an open state with a corresponding increase of resistance, due to reduced π–conjugation through the molecule. However, the reverse process was not observed, which should occur upon a second illumination, due to the quenching of the photo-excited closing reaction. As the high density of states of the Au electrode overlaps with the HOMO level of the ring-open isomer, electrons were quickly transferred to the molecule which finally inhibits the ring-closure process. By applying a highly conductive organic top electrode, the quenching problem was solved and on-off state switching was observed (Fig. 1.14b).[39]

Kim *et al.*[40] carried out a systematic investigation of the two-way photo switching and the corresponding charge transport characteristics of single molecules. Electrical and optical measurements were reported on sulfur-free diarylethene molecules and MCBJs were used at low temperatures to measure the current-voltage characteristics. They found an unexpected behaviour of the current-dominating molecular orbital upon isomerization when the results were compared with the single-level transport model. They stated that both the side chains and end groups of the molecules are crucial to determine the charge transport mechanism of photo switching molecular junctions, as seen in Fig. 1.14. Single-molecule conductance increased for all the four compounds after the transformation from the open (Fig. 1.14d) to the closed state (Fig. 1.14e). As seen in Fig. 1.14e, the 4Py molecule presents the highest conductance. This configuration establishes a very direct link between the molecular π-system and the metallic surfaces which leads to a relatively large signal ratio of the conductance. (4-Pyridyl anchors will be used extensively in Chapters 2 and 3 of this thesis).

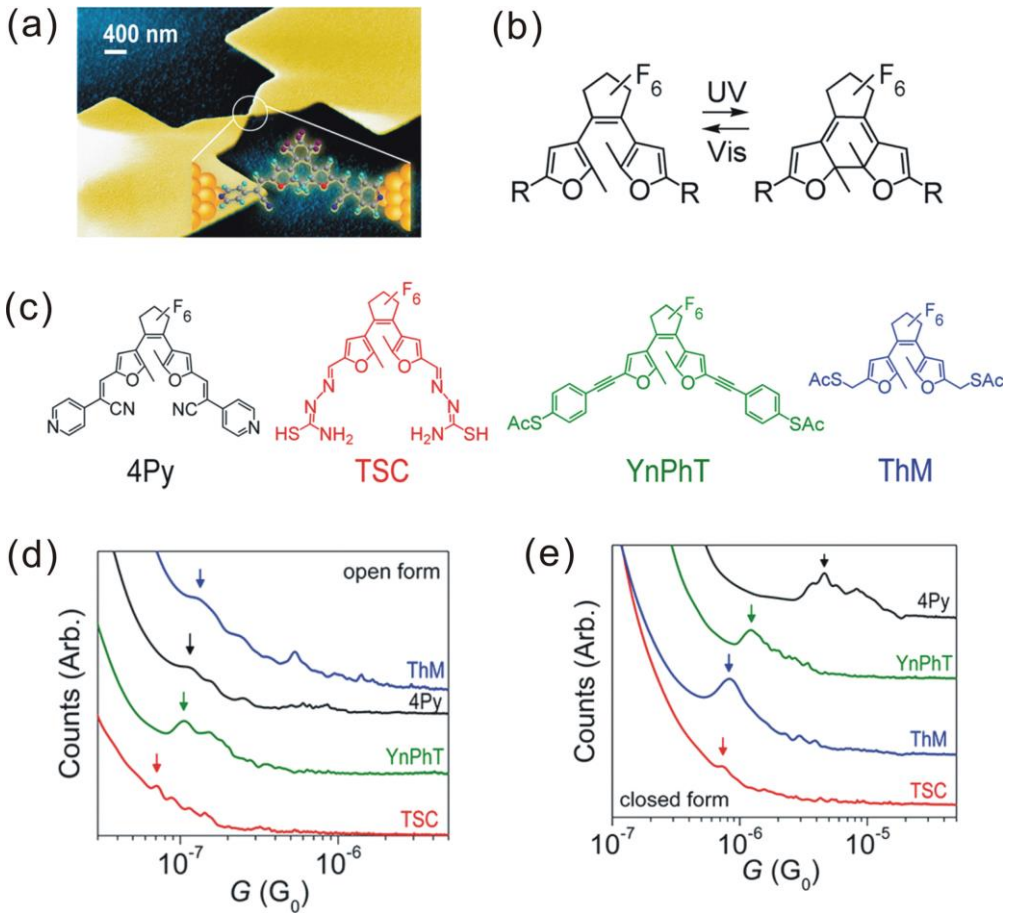

Fig. 1.14 (a) An illustration of an Au − 4Py − Au junction. (b) Sketches of open (left) and closed (right) forms of photochromic molecules (difurylethenes). (c) Structures of the four different molecules, 4Py, TSC, YnPhT, and ThM, respectively, (d,e) Conductance histograms of photochromic molecular junctions for open and closed forms of all four molecules. (Reproduced from reference[41])

Transport properties through molecules with redox centres were investigated by Schiffrin *et al.*[42] using STM techniques. The studied molecule **2** (as in Fig 1.6) is shown in Fig. 1.15. Molecules were assembled on the Au-substrate and Au nanoparticles were placed on top of the sulfur end groups to make contact with the STM tip. Scanning tunneling spectroscopy (STS) enabled the current characteristics through the molecular junction to be recorded while the redox state of the viologen subunits was controlled electrochemically without affecting the bias between the STM and the substrate. By oxidizing the viologen linkers from $V^{\bullet+}$ to their dicationic state V^{2+}, a decrease of the conductivity was observed.

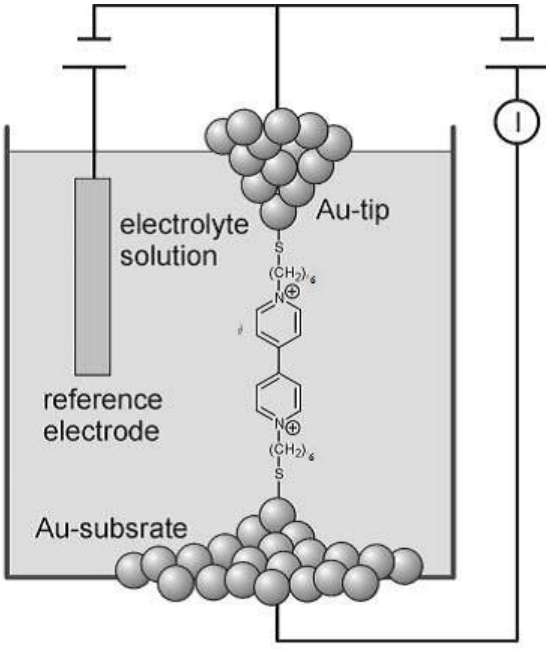

Fig. 1.15 A viologen derivative investigated in electrochemical STM setup. (Reproduced from reference[43])

Wandlowski *et al.*[44] have provided a more comprehensive investigation of viologen derivatives as electrochemical potential dependent structures. They have reported the self-assembly and redox properties of viologen derivatives on gold electrodes. Due to the electronic structure change after the electrochemical stimulation, the redox state dependent transport currents through single-molecule junctions revealed a sigmoidal potential dependence.

For the viologen derivatives above,[43,44] the functionalised junctions are based on the electronic population of the redox chromophore, which is separated from the electrodes by

rather insulating alkyl spacers. Additional new effects are expected when the redox chromophores are conjugatively linked to the electrodes. As displayed in Fig. 1.16, Hummelen *et al.*[45] have integrated anthraquinone subunits into a conjugated oligo(phenyleneethynylene) system with sulfur anchor group at both termini (**8**). The blue colour shows the electron delocalisation in the molecule system, and it can be seen that the central quinone part interrupts the conjugation, while the reduced hydroquinone dianion state (**9**) provides a fully conjugated pathway for the tunneling current.

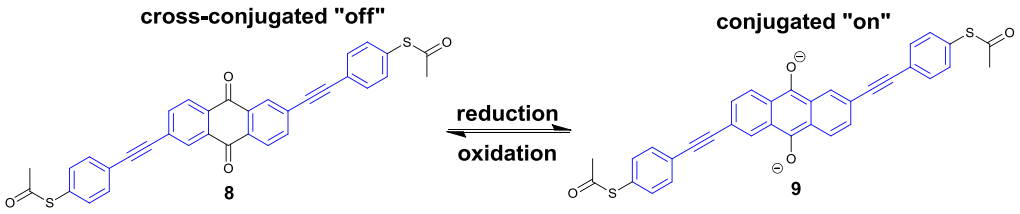

Fig. 1.16 "On" and "off" states of anthraquinone centred OPE molecules with sulfur anchoring groups.

A two-step, reversible, redox process with a semiquinone intermediate upon reduction to the hydroquinone dianion (**9**) was recorded by cyclic voltammetry (CV). The variation of the delocalization of the chromophore's π-system was supported by the considerable differences in the absorption spectra of the fully conjugated dianion state and the oxidized state. Moreover, molecular orbital calculations also supported the proposed switch.

Nielsen *et al.*[46] inserted an extended TTF moiety across an OPE backbone with two sulfur end groups (Fig. 1.17) based on the idea of electrochemically addressing the π-conjugation through a chromophore. The delocalization of the molecule is expected to be changed from linear-conjugated to cross-conjugated (i.e., quinoidal structure in the central ring) by a two-step oxidation of the dithiol-2-ylidene units with considerable changes in electron transport. However, to our knowledge, investigations based on this molecule as a redox-controllable switch have not been reported yet.

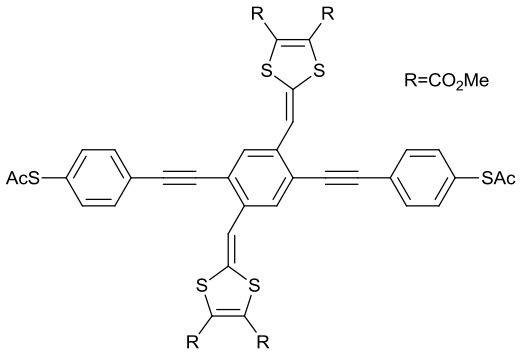

10

Fig. 1.17 Electrochemically triggered switch comprising an extended TTF derivative as a redox active central unit. (Reproduced from reference[46])

1.3.2 Rectification and Diodes

As noted in Section 1.1, the potential molecular rectifier **1** was designed in a theoretical paper by Aviram and Ratner in 1974 (Fig. 1.18).[13]

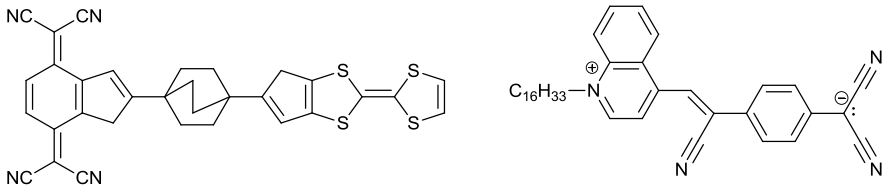

1 11

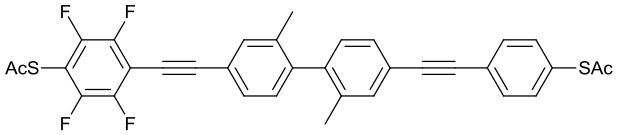

12

Fig. 1.18 Hypothetical molecular rectifier 1. Zwitterionic molecule 11 displays rectification assembled as a Langmuir-Blodgett monolayer between two electrodes. Prototype molecule 12 as a single-molecule rectifier.

To prevent the donor and acceptor units in **1** from interacting they need to be electronically separated by the σ-bridge. In a Gedanken experiment (Thought experiment), the molecule **1** was addressed between two metal electrodes. Electric current is predicted to pass at lower voltage from the acceptor to the donor rather than in the other direction. Calculation of the response of this molecule to an applied field predicted the rectification. To date this molecule has not been synthesised.

However, several experimental studies on the rectification of molecules have been reported. Molecule **11** with a zwitterionic ground state was investigated by Metzger *et al.* in 1999[47]. In a Langmuir-Blodgett film between two aluminium electrodes, monolayer of **11** displayed rectification ratios of up to 26:1. It was the first example of molecular based electronic rectification.

In 2005, Elbing *et al.*[48] reported the unsymmetrical compound **12** as a prototype single-molecule diode with thiolated termini and two weakly coupled π-systems with mutually shifted energy levels. Single molecules of **12** were addressed in a MCBJ setup and the *I(V)* traces displayed a weak diode-like behaviour with a rectification ratio of 1:5 at U = ±1.5 V. As the accepting-donating process is taken over by the reservoirs in the transport experiments based on molecular layers, the donor and acceptor properties are less important. However, at the single molecular scale, the D-A system represents a broken symmetry in the electronic transport, which is comparable with the principle of a semiconductor diode.

1.3.3 Molecular Wires

A wire is the simplest electronic component through which current can be transported between two points. At the molecular level wire-like behaviour is directly related to intramolecular electron-transfer (IET). Several kinds of molecules which share similar properties have been suggested as molecular wires. They should first be conductors of electrons or holes in order to allow passage of current through the wire. The techniques discussed above have been used to provide the current-voltage *I(V)* characteristics of molecular wires. Most of the efficient molecular wires are based on π-conjugated systems, including double or triple carbon-carbon bonds which can transport the electrons through their π-systems. A linear and restricted length molecular wire is optimal in order to contact the two components in the circuit[49].

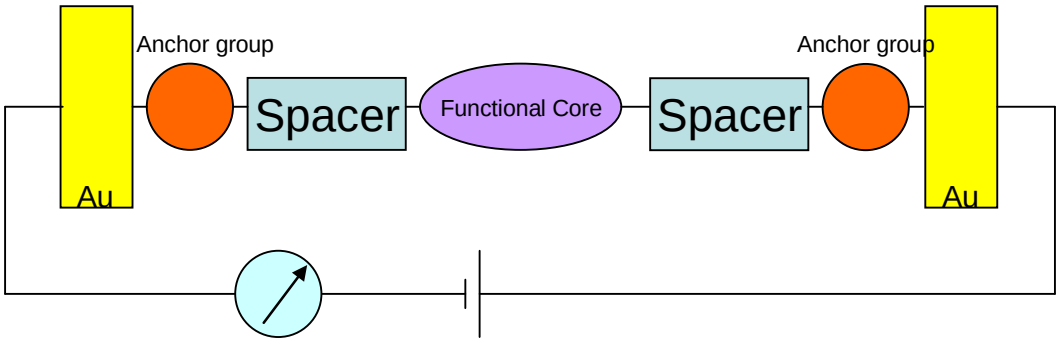

Fig. 1.19 Molecular wire model in a circuit

After the molecular wires are synthesised, key challenges are how to insert them into a circuit and how to measure their electrical properties. To facilitate this, anchoring groups are attached at both termini of the molecular wires, such as thiols, amines, cyanides, isocyanides or carboxylic acids.

One of the most important parameters is the bonding strength of the anchor group to the substrates. This determines the stability of the molecular junction and also affects the properties of the molecular wires. Sometimes it is hard to attach the anchor groups directly to the functional core, and thus the spacer units are included in the structure.

A comprehensive investigation of tolane-type single-molecular junctions with different anchor groups has recently been conducted in our group by Dr Murat Gulcur, in collaboration with Professor Wandlowski's group at the University of Berne[50]. Experimental measurements in Berne and theoretical calculations in Professor Lambert's group at the University of Lancaster explored the roles of anchor groups through a comparison of pyridyl, thiol, amino and cyano anchor groups (molecules **13-16**, respectively, Table 1.1). Both STM-BJ and MCBJ techniques were used.

Table 1.1 Chemical structure and the dominant conductance values from STM-BJ and MCBJ. (Reproduced from reference[50])

Structure	Conductance $\log(G/G_0)$ (STM-BJ)	Conductance $\mathrm{Log}(G/G_0)$ (MCBJ)
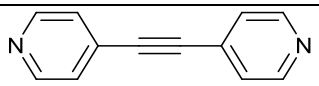 **13**	-3.3	-3.3
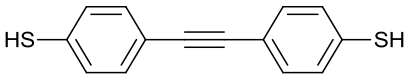 **14**	-2.7	-2.7
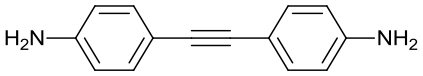 **15**	-3.1	-3.1
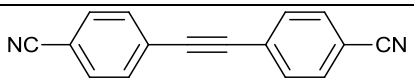 **16**	-4.6	-4.6

Fig. 1.20A shows two main feature of compound **13** (-Py), the high conductance peak (G_H) at 5.0 $\times 10^{-4}$ G_0, and the low conductance peak at 7.9 $\times 10^{-7}$ G_0. For compound **14** (-SH), the high conductance peak was found at 2.0 $\times 10^{-3}$ G_0 for both methods and a relatively weaker low

conductance peak was found at 1.0 $\times 10^{-5}$ G_0. As for compound **14**(-NH_2), the high conductance value is intermediate between the data of **14** (-SH) and **13** (-Py) at 7.9×10^{-4} G_0. A lower conductance peak for **15** (-NH_2) is also shown at 5.0×10^{-4} G_0. Fig. 1.20D shows **16** (-CN) presented the lowest conductance value among the four derivatives. A possible low-conductance feature could not be resolved due to masking by instrumental noise.

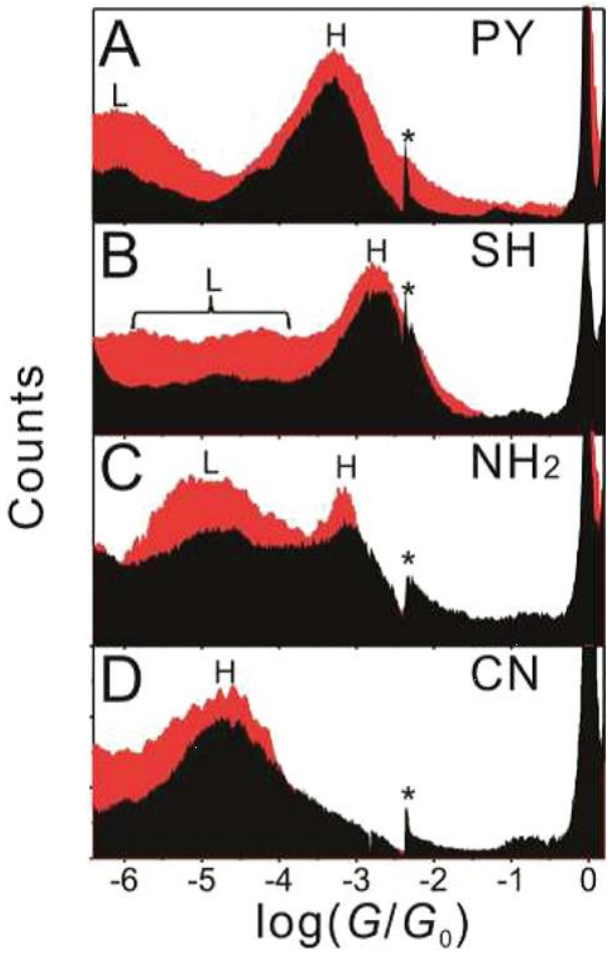

Fig. 1.20 Conductance histogram of compounds 13-16 (A) –Py (B) –SH (C) –NH_2 (D) –CN from STM-BJ (black) and MCBJ (red), * peak comes from the switch of the linear amplifier in STM-BJ. (Reproduced from reference[50])

According to the examples in Table 1 above, the anchor groups play a major role in determining the conductance values of molecular junctions. The trend of the conductance of the four molecules in Table 1.1 is -SH > -NH_2 > -Py> -CN in both experimental setups. The Durham-Berne study also establishes that the trend in the junction formation probability is –Py>-SH>-NH_2>-CN. Overall, according to binding geometry variation, anchoring stability and

junction formation probability, the -Py anchoring group is superior for tolane derivatives compared to the other anchoring groups studied.

1.3.3.1 Oligo(Aryleneethynylene)s (OAEs) and Oligo(Phenyleneethynylene)s (OPEs)

Oligo(aryleneethynylene)s (OAEs) have attracted considerable attention in the area of molecular electronics. OAEs have a cylindrical structure from which the backbones can gain extensive electron conjugation. Apart from that, the π-system is length persistent and a lack of *Z/E* isomerism of alkyne units (as observed in OPVs) makes OAEs much more popular. The general structure of OAEs is (-aryl-C≡C-)$_n$ where aryl groups are phenyl, thienyl, fluorenyl and pyridyl. Oligo(phenyleneethynylene)s (OPEs) are benchmark compounds for advanced materials applications[51].

Fig. 1.21 on the left shows the maximum conjugation of a three-ring OPE derivative, when all the rings are coplanar. When one of the phenyl rings twists, the conjugation is partly broken (right diagram). However, this is partly compensated for by the π electrons on the adjacent acetylene unit. In this way OPEs can retain extensive conjugation along the backbone.

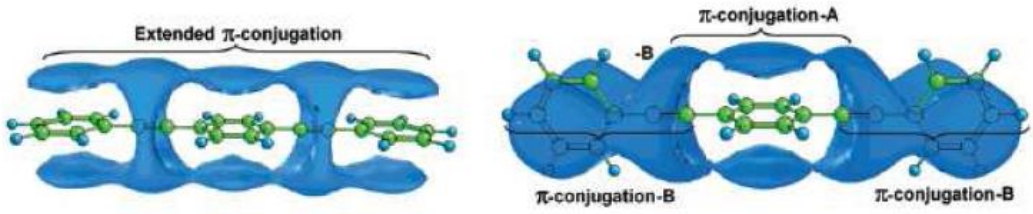

Fig. 1.21 Different conformations of π conjugated system of a three-ring OPE derivative. (Reproduced from reference[52])

1.3.3.2 Mono-Anchored Molecular Wires

Schönenberger *et al.* reported electron transport through π-π stacking of two OPEs assembling between two electrodes in 2008.[53] They studied a series of molecules with either two anchors (one at each end) or only one anchor (Fig. 1.22) by MCBJ techniques. They found that the height and the width of the histogram peaks for compounds **17-20** are very similar. The peak position for compound **18** is slightly reduced by a factor of approximately 2-3 in comparison to compound **17** which is due to nitrogen's weaker contact to gold compared to sulphur. However, a similar peak found for compound **19** was surprising. The only functional atom for formation of molecular junction is the "hidden" *ortho*-nitrogen in the pyridine ring, which would provide much less bonding to the electrode. On the contrary, the similar histogram showed that compound **19** had a similar property in the formation of molecular junctions as compounds **17** and **18**. Compound **20** had a similar histogram too. The evidence

points to a pair of molecules anchored in the junction through π-π stacking, with each molecule anchored at a different electrode. The shift of G_{peak} to lower values for **19** and **20** supported this claim, as non-covalent π-π stacking will give rise to weaker conjugation than is the case for **17** and **18** through a covalent pathway.

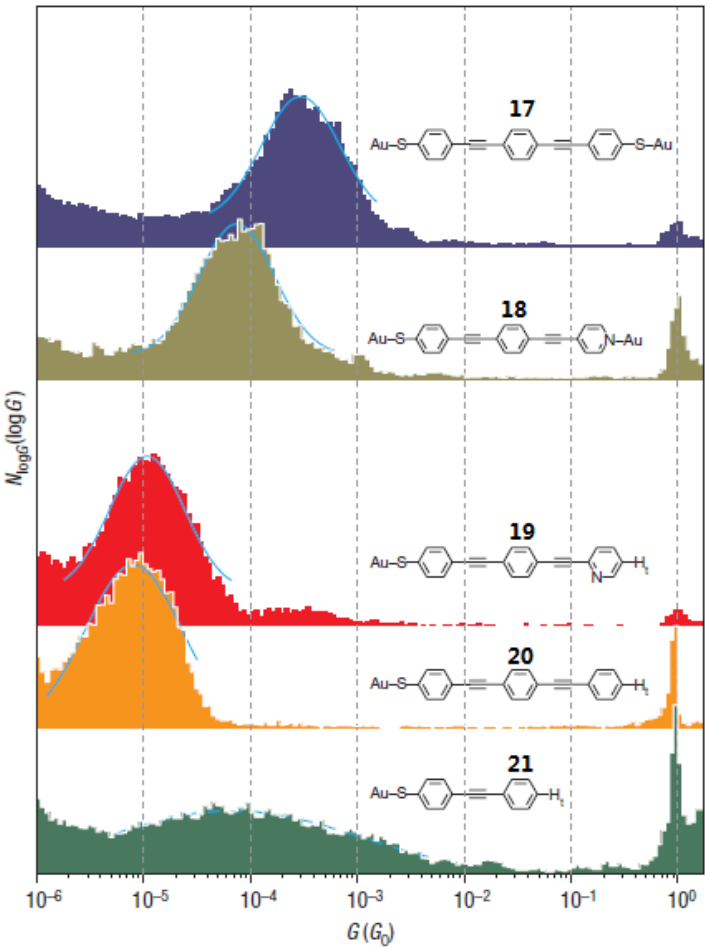

Fig. 1.22 Conductance histograms for molecules 17-21. (Reproduced from reference[53])

An extension of this work was conducted by our group, in collaboration with Professors Nichols and Higgins' group at Liverpool University, using the *I(s)* technique[54]. It was found that bulky *tert*-butyl substituents on the central phenyl rings of the OPE structures (Fig. 1.23) prevented the formation of π-π stacking. Also, for the first time, π-π stacking was clearly observed even for OPEs **22** with anchor groups at both ends. Moreover, even mono-anchored OPEs **24** and **25** could form single molecular junctions directly by π-electrons of the terminal phenyl rings interacting with one electrode with the thiolate anchor interacting with the other electrode.

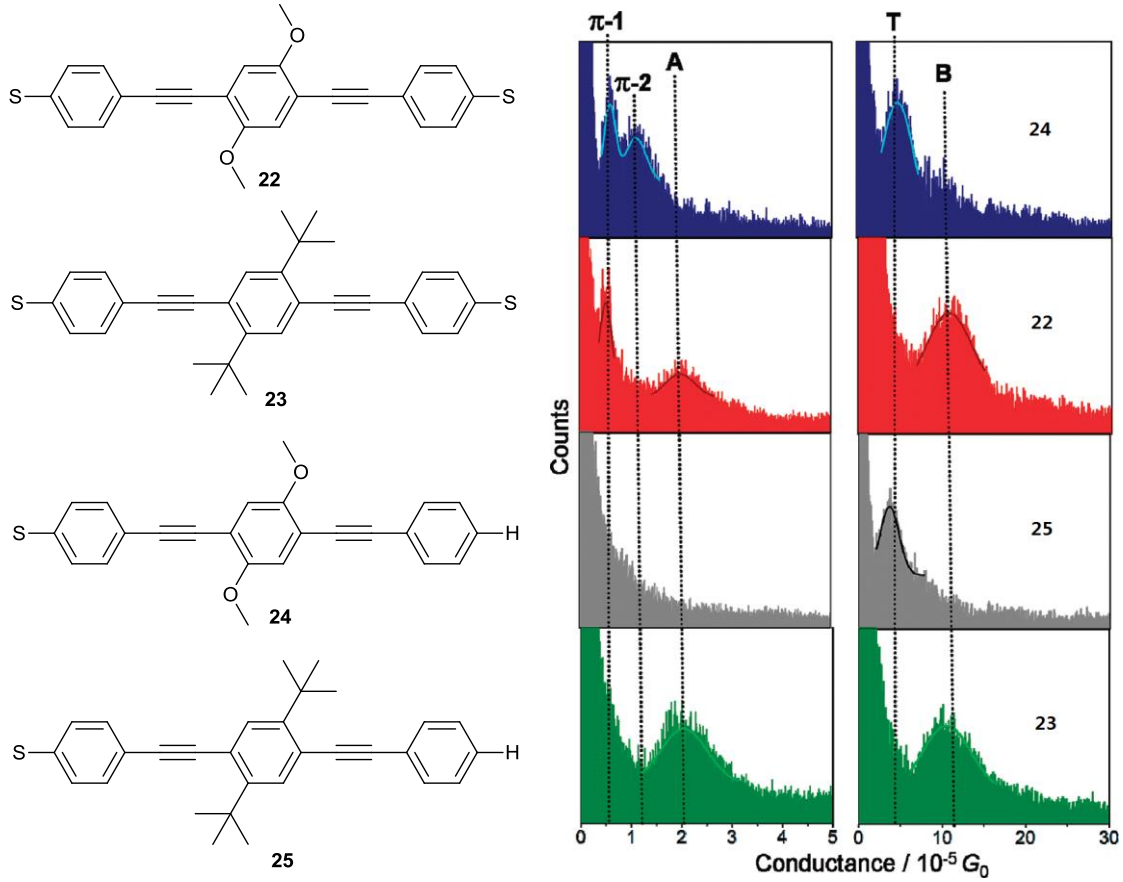

Fig. 1.23 Molecule structures and histograms for conductance. Left panel: low set point current (I_0=5 nA, and U_t = 0.6 V). Right panel: high set point current (I_0=60 nA, and U_t = 0.6 V). (Reproduced from reference[54])

A low current amplifier and a high current amplifier were both used for the measurements. The combination of these two amplifiers enabled the observation of either lower or higher conductance peaks so these measurements were with high sensitivity. The left panel shows the low current amplifier data. Compounds **22** and **24** show a peak labelled π-1 which is attributed to the formation of π-π stacking. As for compounds **23** and **25** with sterically blocking *tert*-butyl substituents, these π-peaks did not appear, providing confirmation that the π-peaks arose from intermolecular π-π stacking. However, the appearance of an additional peak labelled "T" for the mono-anchored compounds **24** and **25** was unexpected. From the break-off data (Fig. 1.24 left) this peak was consistent with the junction of a single molecule length. However, since these molecules only have one anchor group, it was inferred that the end phenyl group contacted the gold electrode directly. Illustrative configurations of the molecular junctions discussed above are shown in Fig. 1.24(right). (Mono-anchored molecular wires will be discussed further in Chapter 3.)

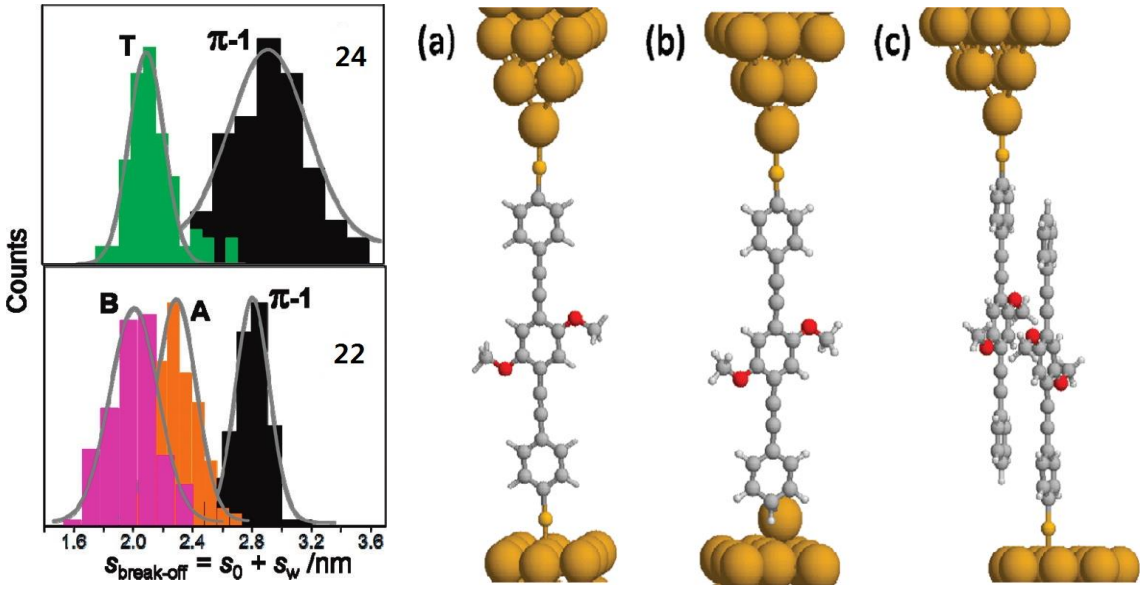

Fig. 1.24 (left) Break-off istance histograms for compounds 24 and 22. (right) Models of the considered junction configurations for the A peak of compound 22 (a), the T peak of compound 24 (b), and the π-1 peak of compound 22 (c). (Reproduced from reference[54])

In summary, ever since the first semiconductor was made in the 1900s, vigorous studies and exciting results have proved the benefits that the electronics industry brought to our daily life. Aviram and Ratner's prototype model of molecular rectification represents the beginning of an era in which the electronics industry moves to the molecular scale. The inventions of new techniques enabled the assembly and measurements of molecular devices. A large number of specifically designed molecules with specific functionalities have been studied as possible alternatives to the conventional silicon-based semiconductors. The central issue of molecular scale electronics always focuses on understanding the electron transport properties through single (or a few) molecules bridging two contract electrodes. Particularly, the effects of molecule-metal electrode contacts on electron transport are of central interest in this field. Many anchor groups have been tested,[50,55] although studies of the anchoring position are rather limited.[56-58] Additionally, there are still several other intriguing effects which control the conducting properties of molecular devices. In subsequent chapters of this thesis, I will present my research on the synthesis and characterisation of new molecules and studies of their electrical properties at the single-molecule level. The longer term aim is to develop new molecules which can be applied in functionalised molecular devices.

Chapter 2. Oligo(aryleneethynylene)s with Terminal Pyridyl Groups: Synthesis and Length Dependence of the Tunneling to Hopping Transition of Single-molecule Conductances

2.1 Introduction

As described in Chapter 1, synthetic chemistry has tailored organic molecules to achieve specific electronic functions, even at the single-molecule level.[43] Terminal anchor groups which have an affinity for gold are attached to the molecules to achieve the *in situ* assembly of metal/molecule/metal junctions.[29,59,60] The electrical conductance of these nanoscale junctions can be characterised using a range of techniques, notably, scanning tunneling microscopy (STM) conducting probe atomic force microscopy (CP-AFM), scanning tunneling microscopy break junctions (STM-BJs) and mechanically controlled break junctions (MCBJs).

Studies which aim to understand how charge transport mechanisms vary with changing the length of the molecular wire[61,62] have been very limited due to the challenges posed by the synthesis, rigorous purification and measurement of long molecules anchored between two electrodes. Two distinct charge transport mechanisms have been predicted theoretically and identified experimentally: coherent transport via tunneling or superexchange which dominates in short molecules, and incoherent thermally activated hopping in long molecules.[63] Choi *et al.* reported a series of oligophenyleneimine (OPI) molecules of length ca. 1.5-7 nm with an anchored thiol unit at one terminus and a phenyl unit at the other terminus. Contacting a monolayer of the molecules assembled on gold revealed a transition from tunneling to hopping at a molecular length of ca. 4-5 nm in junctions made of hundreds of molecules.[64] Fig. 2.1a shows the synthetic routes and the molecular structures of the ONI-p and ONI monolayers. The investigation was carried out using CP-AFM as shown in the inset to Fig. 2.1b. A clear transition in the length dependence of resistances is exhibited near 4 nm, which implies a change of transport mechanism. The resistances for long wires have much weaker length dependence than those for short molecules, which is expected for hopping transport (Fig. 2.1c). Single-molecule measurements were not reported in these studies.

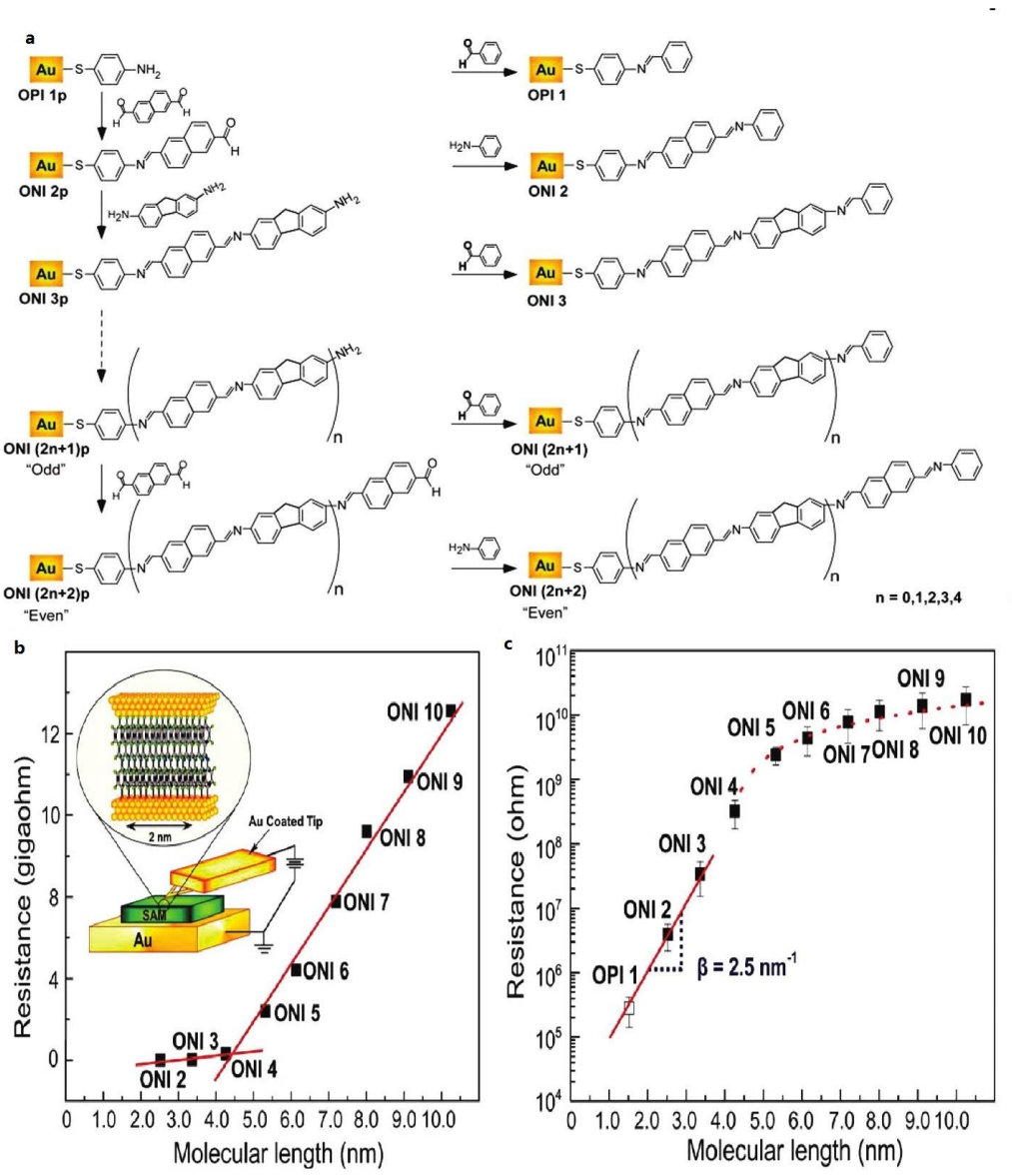

Fig. 2.1 a) Molecular structure and synthetic routes to ONI-p and ONI monolayers. b) A plot of R versus L for the Au/wire/Au junctions. b) Semilog plot of R versus L for the Au/wire/Au junctions. (Reproduced from reference.[64])

Hines *et al.* reported a transition from tunneling to hopping at a molecular length between 5.2 and 7.3 nm by means of STM-BJ measurements (at the single-molecule level) on four oligofluorene-based molecular wires terminated with thiols.[65] However, the transition could not be accurately identified as only four different molecular lengths were investigated.

We recognised that oligo(phenyleneethynylene) (OPE) derivatives are ideal candidates for studies on the correlation of conductance with molecular length. They are highly conjugated, rigid, rod-like molecules whose functional properties can be systematically tuned by chemical synthesis, which makes them a very important class of molecules in materials

chemistry and molecular electronics.[66,67] Short derivatives, typically OPE3 (3 refers to the number of phenyl rings in the backbone) systems, have been widely studied in metal/molecule/metal junctions,[36,68,69] but there are very few reports of transport studies through longer derivatives.[70] Lu *et al.* studied a series of OPEs of lengths ca. 1-5 nm with amino groups at both termini (Fig. 2.2a) and probed the charge transport mechanism in monolayers using STM-BJ and CP-AFM methods. A clear transition from tunneling to hopping was observed at a molecular length of ca. 2.75 nm (Fig. 2.2b).[71] Studies on related derivatives incorporating a ferrocene unit in the backbone, using the same contacting techniques, established that ferrocene enhanced the conductance in both the tunneling and hopping regimes.[72] Single-molecule measurements were not reported in these studies.

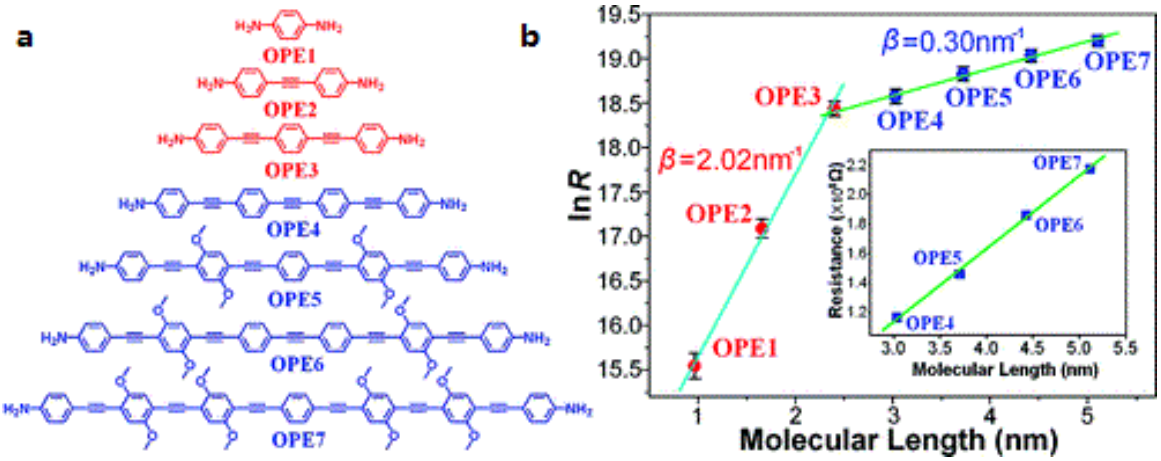

Fig. 2.2 a) Molecular structures studied in Lu's work. b) Semilog plot of R versus L for all of the Au/wire/Au junctions. (Reproduced from reference.[71])

Terminal 4-pyridyl (PY) units anchor molecules effectively to gold substrates and, unlike thiols,[73,74] they are stable under ambient conditions and no protecting group is needed.[27,75-77] As discussed in Chapter 1, it has been shown that for tolane derivatives pyridyl exhibits excellent anchoring performance with high conductance and 100% of molecular junctions formed.[50] Therefore, pyridyl units are used as anchors in the present series of molecules, in preference to amine or thiol analogs.

The motivation for this work is to study the length dependence of the single-molecule conductance of oligoaryleneethynylene (OAE) derivatives comprising OPE cores terminated at both ends with pyridyl groups. This study is clearly distinct from previous work on OPI[64] and OAE[71,72] derivatives, discussed above, which concerned monolayers comprising hundreds of molecules in closely packed arrangements. The benefit of single-molecule studies is that

artifacts arising from intermolecular interactions (e.g. π-π stacking) which are well-known in OAE derivatives (Chapter 1.3.3.2) are absent. We describe the synthesis and characterization of derivatives **OAE3**–**OAE9** of molecular length (i.e. intramolecular N…N distance) ca. 2-6 nm. The charge transport characteristics of these OAE derivatives in single-molecule junctions have been studied using the MCBJ technique in solution and under environmentally controlled conditions.

2.2 Synthesis

The OAE derivatives studied in this work are shown in Chart 2.1. The synthetic strategy uses iterative Pd-catalysed Sonogashira cross-coupling reactions[78] of new, linearly-conjugated phenyleneethynylene building blocks. The retrosynthetic disconnections of the molecules are based on: (i) commercial availability of starting materials; (ii) high yielding reactions; (iii) the synthesis of intermediate reagents which could be easily purified, thereby facilitating the final step to the target OAE derivatives.

Chart 2.1. Structures of the OAE derivatives studied in this work.

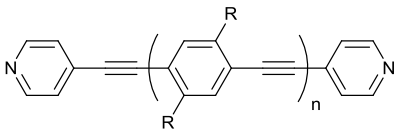

OAE3 a n = 1; R = H
b n = 1; R = OMe
OAE4 n = 2; R = OC_6H_{13}
OAE5 n = 3; R = OC_6H_{13}

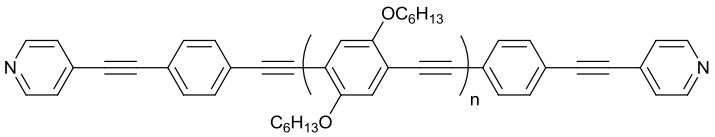

OAE6 n = 2
OAE7 n = 3

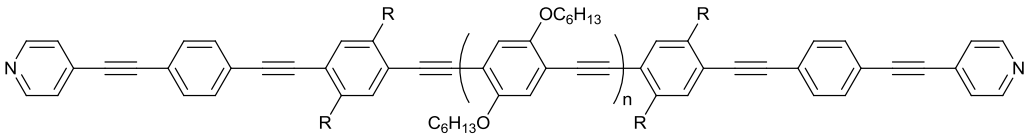

OAE8 a n = 2; R = H
b n = 2; R = OC_6H_{13}
OAE9 n = 3; R = OC_6H_{13}

OAE3a was synthesised by our former group member Dr. Murat Gulcur. The dimethoxy analogue **OAE3b** was synthesised to confirm that alkoxy substituents do not affect the conductance behaviour, as was reported previously for thiol terminated OPE3 analogs.[36] The synthetic route is as shown in Scheme 2.1.

Scheme 2.1 Synthesis of **OAE3b**

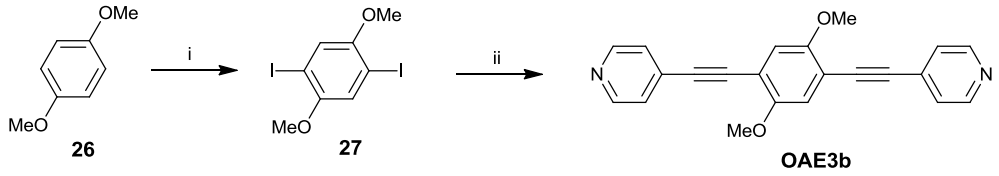

Reagents and conditions: (i) KIO_3, I_2, $AcOH/H_2O/H_2SO_4$, 18 h, 100 °C, 63%; (ii) 4-ethynylpyridine, $[Pd(PPh_3)_4]$, CuI, THF/Et_3N, 18 h, r.t., 30%.

Compound **27** was prepared by a modified literature procedure.[79] Sonogashira reaction was then conducted between compound **27** and 4-ethynylpyridine to give **OAE3b** in 30% yield.

For the synthesis of longer OAEs, a key aspect of our strategy was the use of 2-hydroxypropyl protecting groups[80] for the intermediate terminal alkynes, e.g. compounds **30** and **33** (Scheme 2.2). A benefit of this protecting group (compared to trialkylsilyl, which is more commonly used)[28] is that its high polarity facilitates the separation of any unreacted starting material or byproducts which do not contain this unit. Deprotection with loss of acetone is easily accomplished using sodium hydroxide in toluene.

Scheme 2.2 Synthesis of **OAE4**

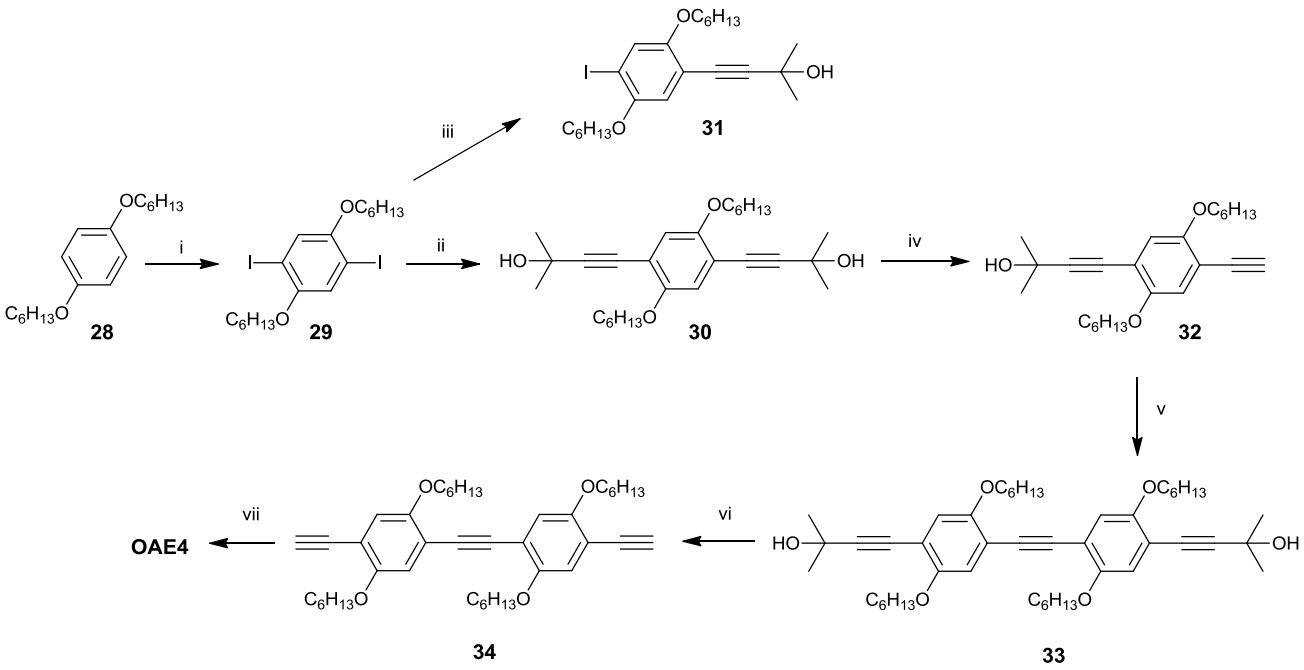

Reagents and conditions: (i) KIO_3, I_2, $AcOH/H_2O/H_2SO_4$, 24 h, 100 °C, 74%; (ii) 2-methyl-3-butyn-2-ol, $[Pd(PPh_3)_2Cl_2]$, CuI, THF/Et_3N, 20 h, r.t., 95%; (iii) 2-methyl-3-butyn-2-ol, $[Pd(PPh_3)_4]$, CuI, THF/Et_3N, 8 h, r.t., 45%; (iv) NaOH, toluene, 6 h, 70 ^oC; (v) **31**, $[Pd(PPh_3)_4]$, CuI, THF/Et_3N, 18 h, 50 ^oC, 95%; (vi) NaOH, toluene, 22 h, 100 ^oC, 36%; (vii) 4-iodopyridine, $[Pd(PPh_3)_4]$, CuI, THF/Et_3N, 23 h, r.t., 86%.

By controlling the number of molar equivalents of the starting material 2-methyl-3-butyn-2-ol, the reaction successfully produced primarily the di-coupled product **30** (by applying 2.2 equiv. of 2-methyl-3-butyn-2-ol) or the mono-coupled product **31** (by applying 0.95 equiv. of 2-methyl-3-butyn-2-ol). A notable feature of the deprotection reactions is that for bis-protected derivatives **30** and **33**, the major product can be exclusively mono-deprotected (**30→32**) or bis-deprotected (**33→34**) depending on the temperature and the length of time of the reaction. **OAE4** was obtained by coupling compound **34** with 4-iodopyridine which gave a yield of 86%.

By simply adding sodium hydroxide to a solution of compound **30** in toluene and stirring at 100 ^oC for 12 h, the bis-deprotected product **35** was obtained in 82% yield. Subsequent di-coupling of **35** with **31** gave the trimer **36**. Bis-deprotection was then conducted at 100 ^oC to give the intermediate **37** in 70% yield. Intermediates **37** and **34** were repeatedly used as central building blocks for the longer derivatives. Bis-coupling between intermediate **37** and 4-iodopyridine gave the final product **OAE5** with a yield of 68% (Scheme 2.3)

Scheme 2.3. Synthesis of **OAE5**

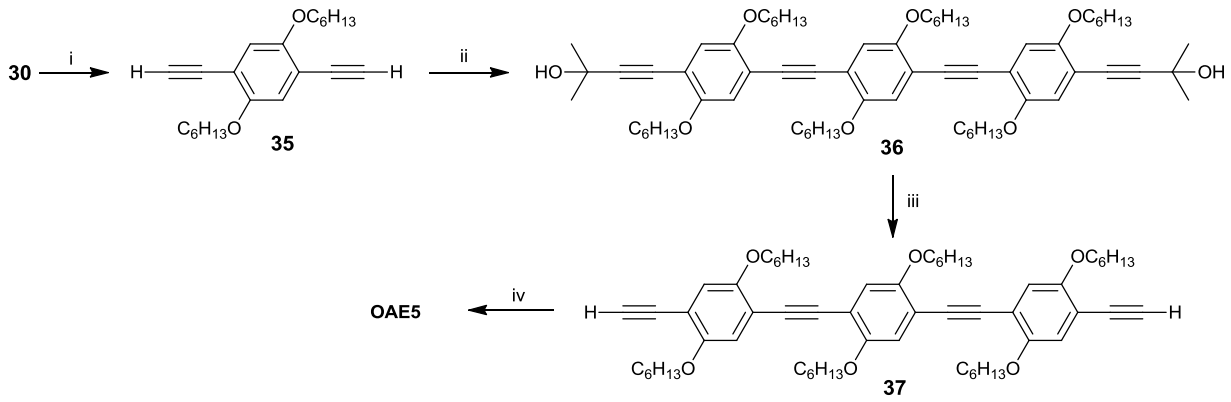

Reagents and conditions: (i) NaOH, toluene, 12 h, 100 °C, 82%; (ii) **31**, [Pd(PPh$_3$)$_4$], CuI, THF/Et$_3$N, 18 h, r.t., 47%; (iii) NaOH, toluene, 23 h, 100 °C, 70%; (iv) 4-iodopyridine, [Pd(PPh$_3$)$_4$], CuI, THF/Et$_3$N, 20 h, r.t., 68%.

For the synthesis of **OAE6** (Scheme 2.4), compound **38** was reacted with 0.95 equiv. of 2-methyl-3-butyn-2-ol under Sonogashira condition to give compound **40**. Bis-deprotection then followed to yield intermediate **41** in 60% yields. The final product **OAE6** was then produced in 68% yield by two-fold reaction of compound **41** and 4-iodopyridine.

Scheme 2.4 Synthesis of **OAE6**

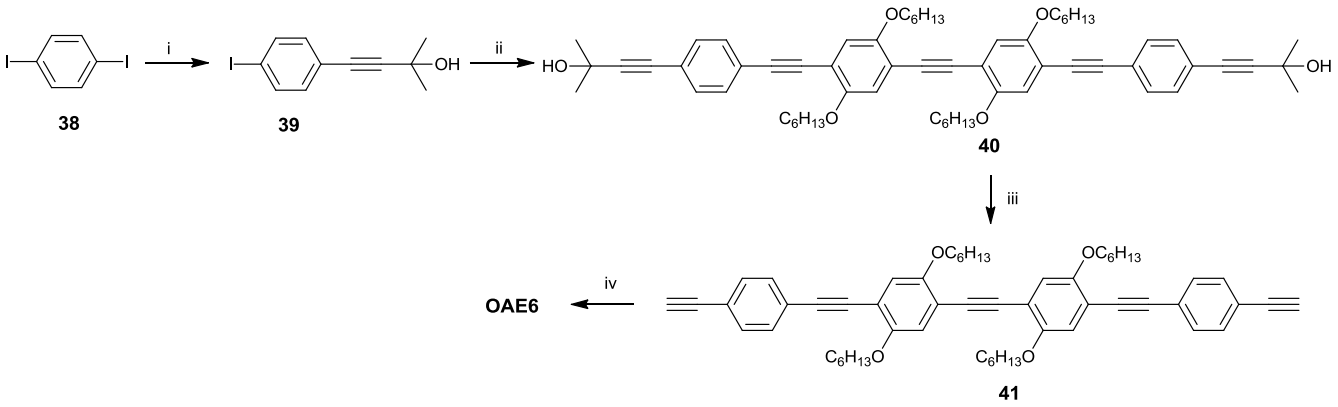

Reagents and conditions: (i) 2-methyl-3-butyn-2-ol, [Pd(PPh$_3$)$_4$], CuI, THF/Et$_3$N, 5 h, r.t., 46%; (ii) **34**, [Pd(PPh$_3$)$_4$], CuI, THF/Et$_3$N, 20 h, r.t., 87%; (iii) NaOH, toluene, 25 h, 100 °C, 60%; (iv) 4-iodopyridine, [Pd(PPh$_3$)$_4$], CuI, THF/Et$_3$N, 15 h, r.t., 68%.

The reaction between compound **38** and 0.95 equiv. of 4-ethynylpridine under Sonogashira condition gave compound **42** in 33% yield. Compound **42** was then di-coupled onto the intermediate **37** to give the final product **OAE7** with a yield of 67% (Scheme 2.5).

Scheme 2.5 Synthesis of **OAE7**

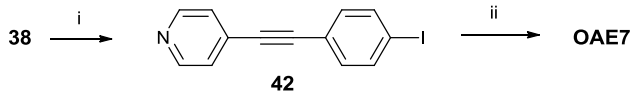

Reagents and conditions: (i) 4-ethynylpyridine, [$Pd(PPh_3)_4$], CuI, THF/Et_3N, 8 h, r.t., 33%; (ii) **37**, **[**$Pd(PPh_3)_4$], CuI, THF/Et_3N, 20 h, r.t., 67%.

Compounds **41** and **42** were reacted under Sonogashira conditions to give a bright yellow solid **OAE8a** (Scheme 2.6). However, as the solubility of **OAE8a** was so low, it could not be purified to the required level for single-molecule measurements. NMR spectra could not be obtained; a mass spectrum was consistent with its formation, and an X-ray crystal structure was obtained (which will be discussed later).

Scheme 2.6 Synthesis of **OAE8a**

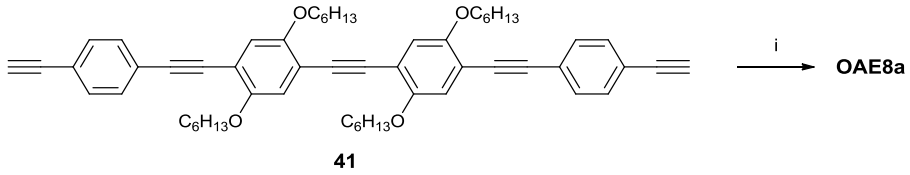

Reagents and conditions: (i) **42**, [$Pd(PPh_3)_4$], CuI, THF/Et_3N, 16h, r.t..

To obtain a soluble OAE8 derivative, four extra hexyloxy sidechains were attached to the backbone which finally gave **OAE8b** in 35% yield from **42** (Scheme 2.7). The ^1H NMR spectra of **OAE8b** established a high level of purity.

Scheme 2.7 Synthesis of OAE8b

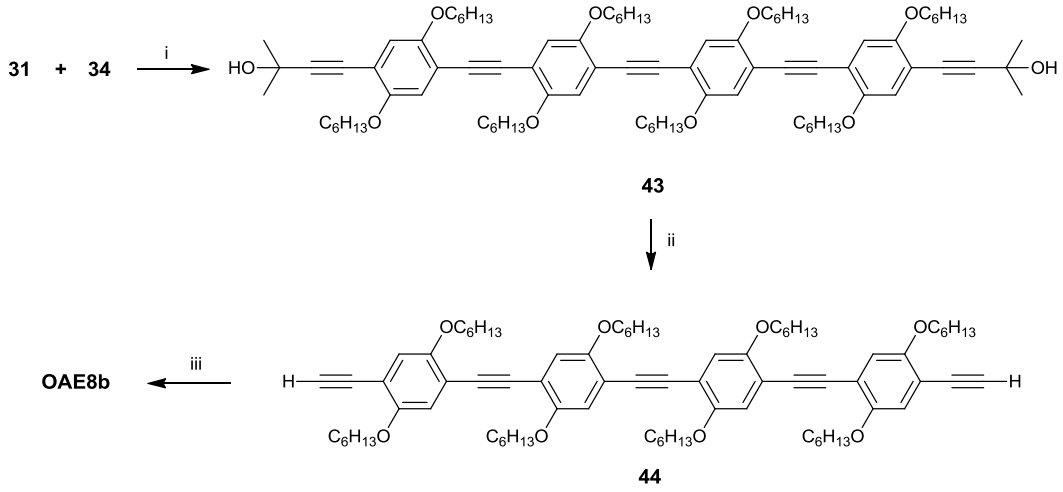

Reagents and conditions: (i) [$Pd(PPh_3)_4$], CuI, THF/Et_3N, 24 h, 50 ^oC, 78%; (ii) NaOH, toluene, 20 h, 100 ^oC, 80%; (iii) **42,** [$Pd(PPh_3)_4$], CuI, THF/Et_3N, 21 h, r.t., 35%.

The final target compound in the series was **OAE9** (Scheme 2.8). Standard conditions for reaction of **34** and **42** gave the mono-coupled product **45** in 60% yield. This was then reacted with compound **29** to give **OAE9** with a yield of 21%. A trend throughout this OAE series is that as the molecules get longer, it becomes harder to purify the compounds.

Scheme 2.8 Synthesis of OAE9

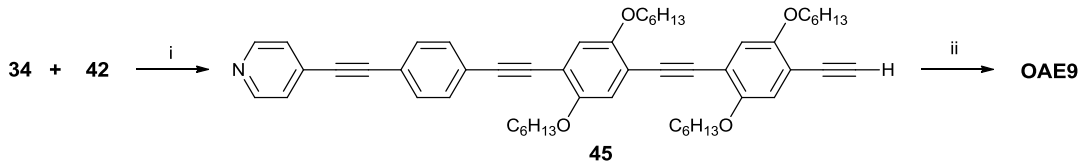

Reagents and conditions: (i) $[Pd(PPh_3)_4]$, CuI, THF/Et_3N, 18 h, r.t., 60%; (ii) **29**, $[Pd(PPh_3)_4]$, CuI, THF/Et_3N, 15 h, r.t., 21%.

2.3 Optical Properties

The solution UV-Vis absorption spectra of compounds **OAE3-OAE9** in dichloromethane solution establish that as the length of the molecules increases, the wavelength of the lower energy band increases (Table 2.1 and Fig. 2.3). However, as expected, the red shifts of the λ_{max} values are not linearly proportional to the increase in the molecular length. The presence of alkoxy substituents also contributes to a red shift. This is clearly seen in a comparison of derivatives **OAE3a** and **OAE3b**, which have the same backbone, yet very different absorption profiles. This effect has been reported previously for short OPE derivatives with terminal hydrogen atoms[81] and terminal thioacetyl units.[36] A similar increase of λ_{max} with increasing conjugation length has been observed in other aryleneethynylene oligomers.[82,83] These data establish that for **OAE3-OAE9** there is extended π-electron conjugation throughout the backbone and the saturation length has not been reached in the present series.

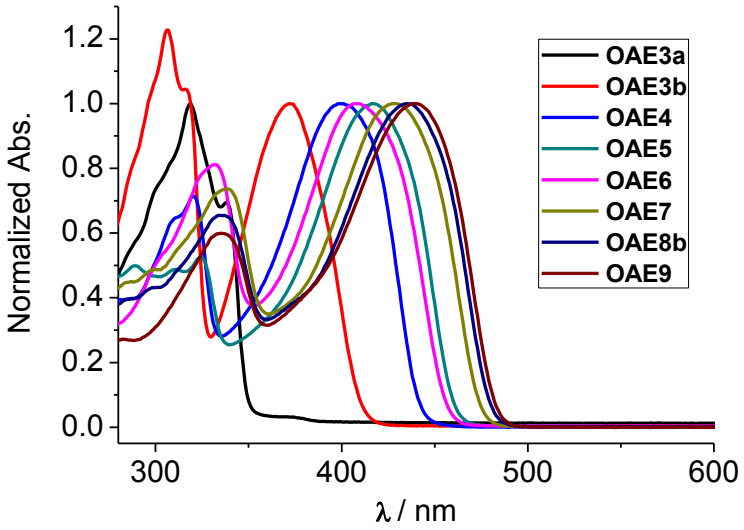

Fig. 2.3 UV-Vis absorption spectra for OAE3-OAE9 in dichloromethane solution, normalized to the lower energy band.

2.4 X-ray Molecular Structures

The structures of **OAE4**, **OAE5**, **OAE7**·CH_2Cl_2·3EtOH and **OAE8a**·2EtOAc were determined by single-crystal X-ray diffraction by Dr Andrei S. Batsanov. The text in this Section is adapted from a draft written by Dr. Batsanov.

Relevant previous structures. X-ray crystal structures of long OAE molecules are very rare. A search of the Cambridge Crystallographic Data Base on 30 August 2013 revealed only four X-ray crystal structures of OPE derivatives comprising five phenyl rings,[84-86] and no structures with more than five rings. Therefore, to our knowledge, the crystal structures of **OAE7** and **OAE8a** are unprecedented.

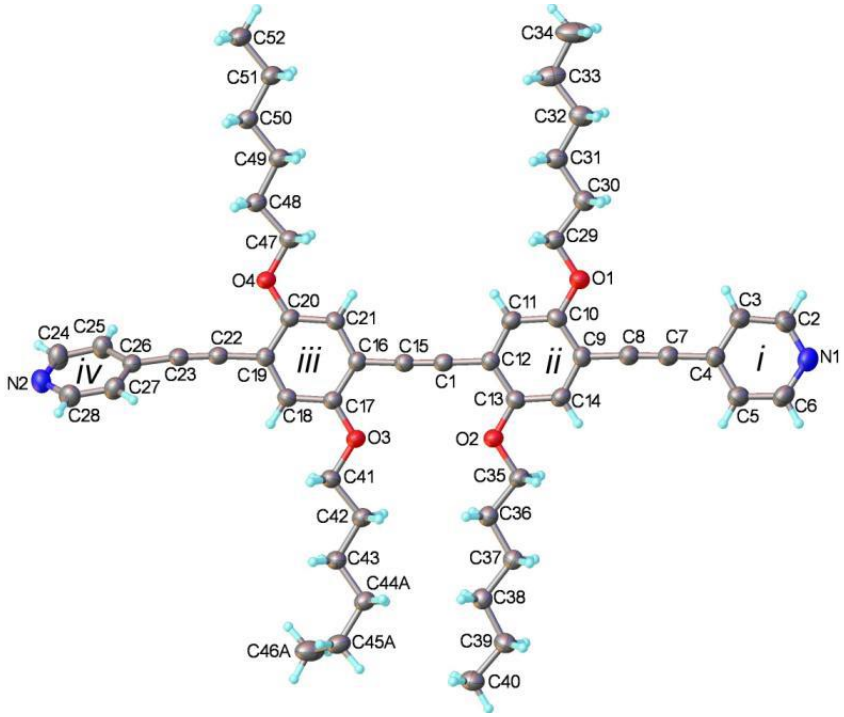

Fig. 2.4 Molecular structure of OAE4. N(1)…N(2) distance is 2.33 nm. Dihedral angles between rings (°): *i/ii* 6.7, *ii/iii* 2.8, *iii/iv* 60.5°.

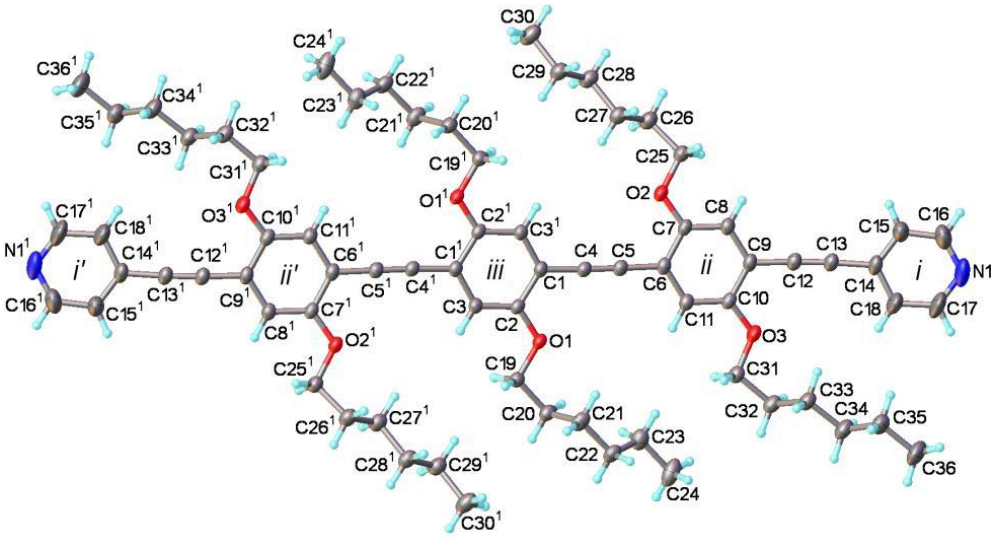

(a)

(b)

Fig. 2.5 (a) Molecular structure of OAE5. (b) conformation of the arene-ethyne rod. Intramolecular N…N distance is 3.00 nm.

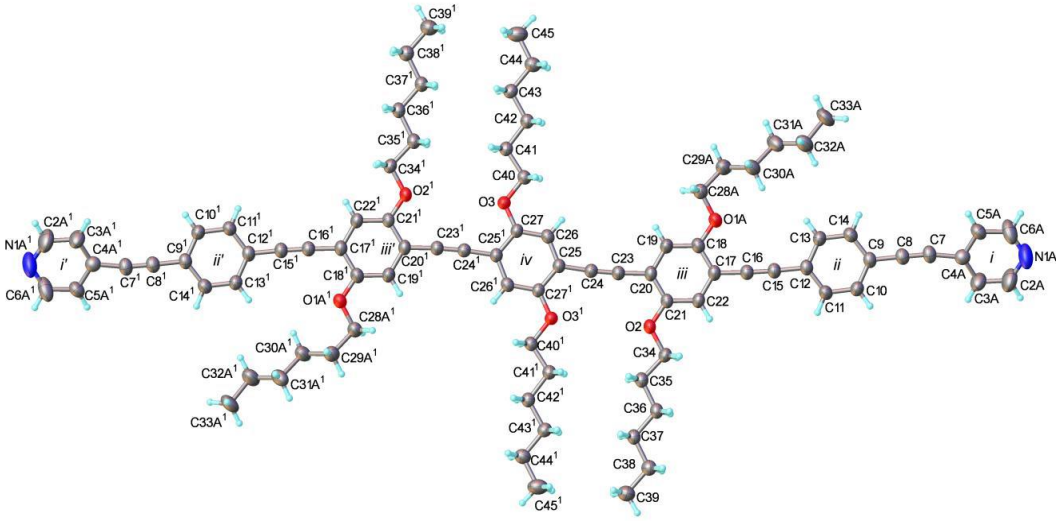

Fig. 2.6 Molecular structure of OAE7. Intramolecular N…N distance is 4.37 nm.

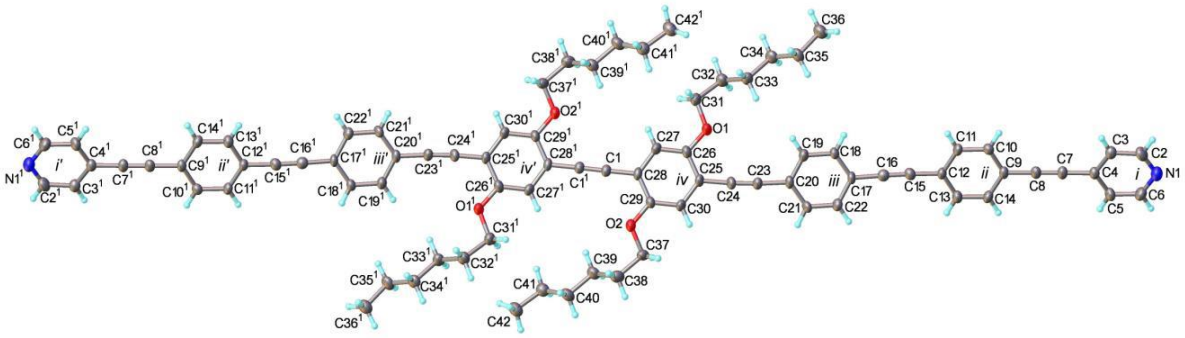

Fig. 2.7 Molecular structure of OAE8a. Intramolecular N…N distance is 5.07 nm.

Rod conformation. The molecule of **OAE4** (Fig. 2.4) has no crystallographic symmetry. Most of the backbone is linear and planar, but Py ring *iv* is twisted and its C(26)…N(2) axis is tilted by *ca* 16° from the rest of the rod. Other molecules have crystallographic inversion centers. In **OAE5** (Fig. 2.5a) the rod is S-shaped (Fig. 2.5b), with folding angles *i/ii* 10.1**°** *ii/iii* 4.2**°** and *i/iii* 14.3**°** but no appreciable twist. In **OAE7** (Fig. 2.6), inter-ring twists *ii/iii* 5.1**°** and *iii/iv* 1.3**°** are small, *i/ii* is somewhat larger, 20.4° and 18.0° for the two alternative positions. In **OAE8a** (Fig. 2.7) symmetrically independent rings, *i* to *iv*, show incremental screw-like twists, as indicated by the interplanar angles *i/ii* 9.7**°**, *i/iii* 22.0**°**, *i/iv* 40.0**°**. Similar rod conformations and variable twist angles have been reported previously for other OAE derivatives comprising five aryl rings in the backbone,[84-86] No general trends in conformation or twist angles can be extracted from the literature crystallographic data for OAEs or from the data for the present series. It is apparent that subtle crystal packing forces, including interactions between side-

chains, largely dictate the details of the backbone conformations and the longer-range ordering in the solid-state.

Conformation of the side-chains. In **OAE4** all the alkoxy side-chains adopt all-*trans* conformations and therefore are nearly coplanar with the arene rings, except for the C(44)C(45)C(46) fragment which is disordered between two opposite *gauche* conformations in 0.7:0.3 ratio. In **OAE5** and **OAE8a** all the side-chains have *gauche* conformation of the O-C-C-C fragment and therefore are slightly non-coplanar with the rings. The rest of the chains adopt all-*trans* conformations, except one chain in **OAE5** which is also *gauche* around the C(21)-C(22) bond. In **OAE7,** two independent side-chains adopt all-*trans* conformations and the third one is disordered (in a 3:1 ratio) between two alternative positions with opposite *gauche* conformations of the O-C-C-C fragment.

Crystal packing. In **OAE4** and **OAE5**, parallel molecules are stacked with a lateral slanting, so that the rod of one molecule is sandwiched between side-chains of two adjacent ones (as illustrated in Fig. 2.8 for **OAE5**). Molecules of adjacent stacks loosely contact via their pyridyl groups to form infinite zig-zagged chains (Fig. 2.9), which are effectively insulated from one another by alkyl groups, but in neither case is there any distinct type stacking of arene rings.

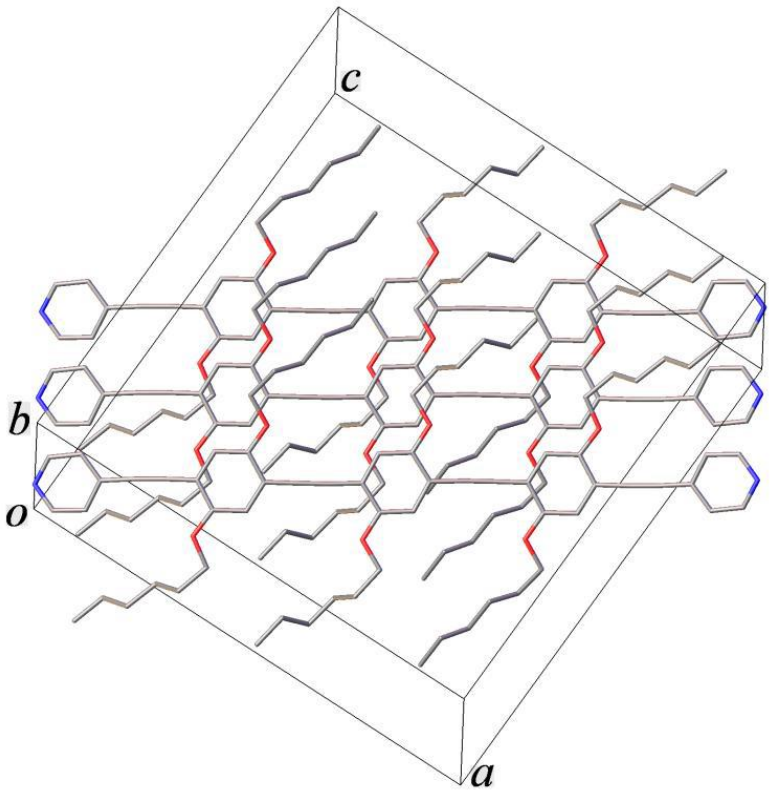

Fig. 2.8 Intercalation of alkyl chains and arene-ethyne rods in the structure of OAE5.

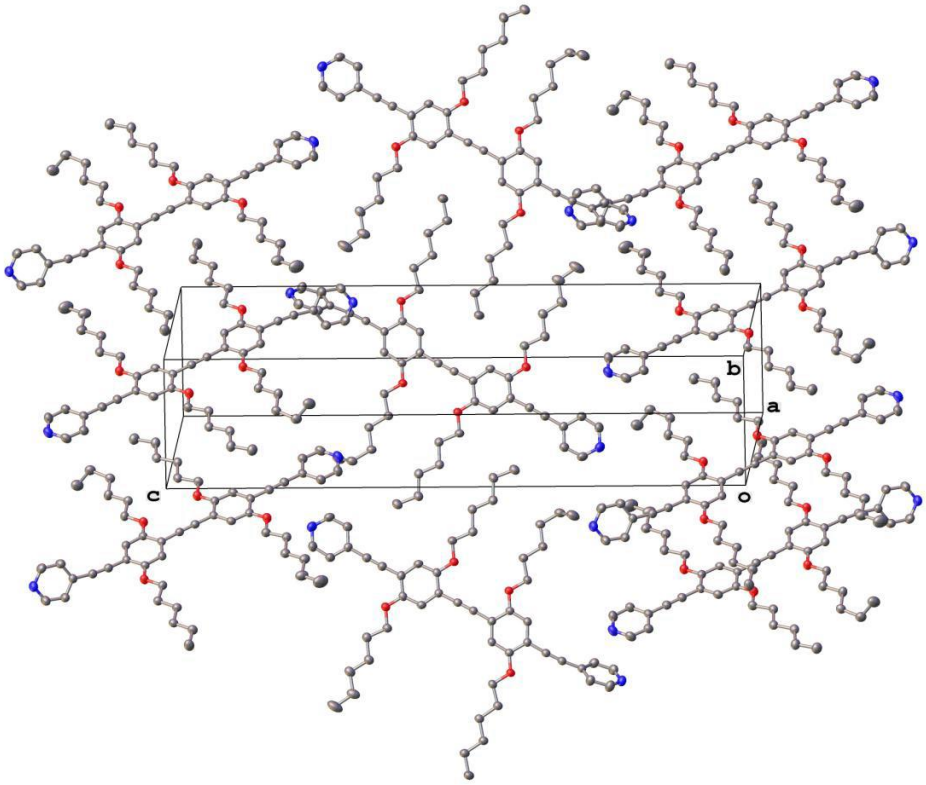

Fig. 2.9 Crystal packing of OAE4

2.5 Conductance Measurements

The transport characteristics of the OAE derivatives were obtained and analysed in Prof. Thomas Wandlowski's group at the University of Bern. The present author contributed to analysing and explaining the data presented in this section. The charge transport characteristics of the derivatives **OAE3**-**OAE9** in single molecular junctions were investigated using the mechanically controlled break junction (MCBJ) technique. Key parameters are listed in Table 2.1. Molecular junctions were formed by opening and closing a nanogap between two gold electrodes in a solution of 1,3,5-trimethylbenzene (TMB) and tetrahydrofuran (THF), 4:1 (v/v), containing typically 0.1 mM of the target molecules. The detailed experimental setup will be described in the experimental session in Chapter 7.

Table 2.1 Characteristic parameters of the UV/Vis absorption and transport measurements

Molecule	λ_{max}/nm[a]	L/nm[b]	G^*/G_0 1D[c]	G/G_0 2D[d]	Δz*e	z*[f]	JFP/%[g]
OAE3a	319	1.6	$10^{-4.5}$	$10^{-5.0}$ - $10^{-4.0}$	1.08	1.58	100
OAE3b	306, 372	1.6	$10^{-4.5}$	$10^{-5.0}$ - $10^{-4.0}$	1.00	1.50	100
OAE4	320, 401	2.3	$10^{-5.5}$	$10^{-6.0}$ - $10^{-5.0}$	1.88	2.38	100
OAE5	324, 417	3.0	10-6.7	$10^{-7.0}$ - $10^{-6.2}$	1.92	2.42	71
OAE6	331, 409	3.7	$10^{-6.8}$	$10^{-7.3}$ - 10^{-6}	2.22	2.72	18
OAE7	339, 428	4.4	$10^{-6.9}$	$10^{-7.0}$ - $10^{-6.5}$	2.31	2.81	18
OAE8b	335, 435	5.1	$10^{-6.8}$	$10^{-7.2}$ - 10^{-6}	1.78	2.28	20
OAE9	335, 439	5.8	$10^{-6.9}$	$10^{-7.5}$ - 10^{-6}	1.36	1.86	17

[a] Maxima of the characteristic UV-Vis absorption in CH_2Cl_2 solution; [b]molecular length L, which is defined as the distance between the centre of the nitrogen anchor atom at one end of a fully extended isolated molecule to the centre of the anchor atom at the other end. The lengths of the molecules were calculated by ACD/ChemSketch and are in very close agreement with the N…N distances obtained by single-crystal X-ray diffraction for **OAE4, 5, 7** and **8a** (see Section 2.4). [c] Most probable molecular junction conductance as estimated from Gaussian fits to the experimentally obtained 1D conductance histograms. [d]Conductance range of molecular junctions extracted from the 2D conductance vs. relative displacement histograms. [e] Δz* as most probable relative junction elongation (displacement); [f]z* = Δz* + 0.5 as absolute junction elongation (displacement), [g]JFP is the junction formation probability.

Fig. 2.10 displays typical conductance (G) versus distance (Δz) stretching traces, as plotted in a semilogarithmic scale, and recorded for 0.1 mM **OAE4** or **OAE7** in TMB/THF using the MCBJ technique. For reference, two traces (black curves) represent the OAE-free solution, which reveal classical tunneling characteristics, i.e. an exponential decrease of the conductance upon junction elongation. The traces recorded for **OAE4** and **OAE7**, which are characteristic representatives of this OAE family, are more complex. After the formation of the contact between the two gold leads, the nanoscale constriction was stretched with a typical rate of 2 nm s^{-1}. All curves show initially a step-like decrease of the conductance from 10 G_0 up to 1 G_0, with $G_0 = 2e^2/h$ being the fundamental quantum conductance. Opening the gap results in an elongation of the gold-gold junction and decreases the number of gold atoms in the constriction, which causes the conductance to change up to 1 G_0, where the contact between the two gold leads in the MCBJ consists of only one gold atom. Subsequently, an abrupt

decrease of the conductance over several orders of magnitude up to 10^{-5} G_0 occurs, which is assigned to the "jump out of atomic contact".[87] The gold-gold contact breaks, and OAE molecules from the solution, or already adsorbed at one of the two metal leads, bridge the gap. This process is reflected in additional features in the $\log(G/G_0)$ vs. Δz stretching traces. The examples plotted in Fig. 2.10 show well-developed plateaus at $G < 10^{-5}G_0$. These plateaus represent stable "electrode/OAE/electrode" molecular junctions. These traces show a distinct monotonic decrease in the conductance with stretching distance. Upon further pulling, a second decrease in conductance occurs, which is assigned to the rupture of the contact between the molecular wire and the gold leads.[69,88] The conductance finally reaches the noise level of $G \leq 10^{-8}G_0$ upon the complete breaking of the molecular junction. We note that the plateau length increases with molecular length L as illustrated in Fig. 2.10 for **OAE4** and **OEA7** as typical examples. We also observed that rupture of the molecular junction is less steep for junctions formed with the longer OAE molecules. The overall shape of the stretching traces as recorded for each molecule is qualitatively similar, but varies in detail. Therefore, a careful statistical analysis of a large number of individual traces was required to extract representative results.

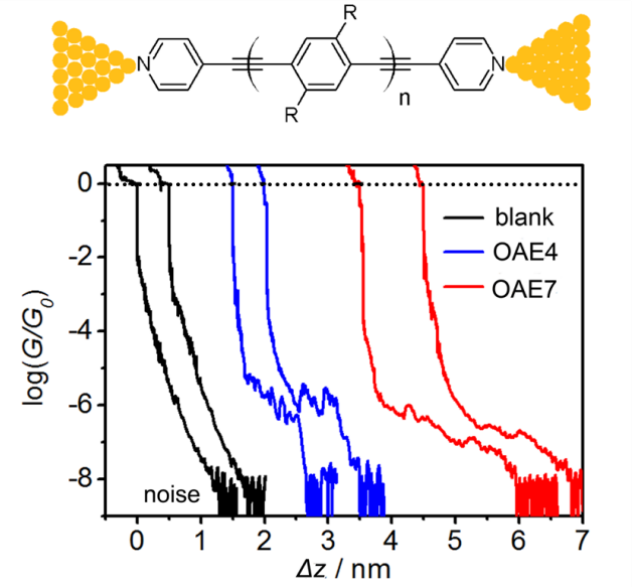

Fig. 2.10 Typical conductance vs. distances traces recorded in TMB/THF in the absence (black lines) and in the presence of 0.1 mM OAE4 (blue lines) or OAE7 (red lines) in a MCBJ setup at 0.10 V bias voltage, stretching rate 2 nm s^{-1}.

Several thousands of individual conductance versus relative displacement traces (G vs. Δz) were recorded and analysed further by constructing all-data-point histograms without any

data selection to extract statistically significant results from the different junction configurations. Fig. 2.4 displays the corresponding one-dimensional (1D) histograms of eight OAEs in a semilogarithmic scale as constructed from 2000 experimental conductance versus distance traces for each compound. The sharp peaks around 1 G_0 represent the conductance of a single atom gold–gold contact. The prominent peaks between 10^{-7} G_0 < G/G_0 < 10^{-4} G_0 represent molecular features. The 1D histograms reveal one pronounced molecular feature for each OAE derivative. The conductance peaks at $G < 10^{-7.5}$ G_0, which were also observed in OAE-free solutions, are caused by instrumental noise.[50,89] The statistically most probable conductances of molecular junctions formed by the respective OAEs as trapped between two gold contacts were obtained by fitting Gaussians to the characteristic maxima in the conductance histograms. The results are compiled in Table 2.1. The data presented in Fig. 2.10 and 2.11 are summarised in Fig. 2.12. We note that rather similar conductance values were found for molecular concentrations ranging between 10^{-6} M up to 10^{-4} M, which supports their assignment to single molecular junction conductances. The single molecular junction conductances decrease with increasing molecular length L from $10^{-4.5}$ G_0 for **OAE3** to $10^{-6.7}$ G_0 for **OAE5**, by three orders of magnitude. However, this trend levels off for longer molecular wires. The junction conductances of **OAE5** to **OAE9** reveal rather small changes spanning from $10^{-6.7}$ to $10^{-6.9}$ G_0, respectively. We also note that the width of the molecular conductance features increases with molecular length, which most probably reflects the increasing number of molecular conformations in the nanoscale junctions.

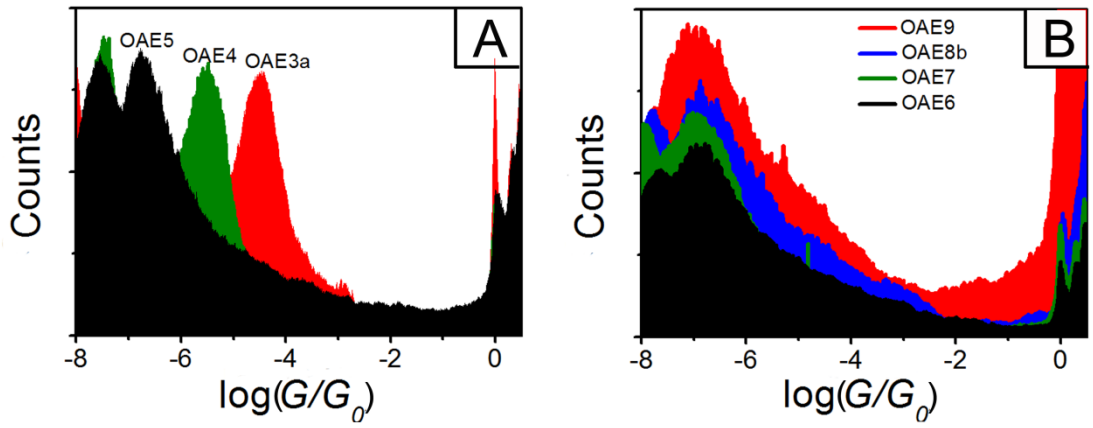

Fig. 2.11 All-data point 1D conductance histograms of OAE-derivatives as constructed from 2000 individual conductance vs. relative distance traces as plotted in Fig. 2.12.

The above analysis was extended by constructing two-dimensional (2D) conductance vs. relative displacement Δz histograms. Fig. 2.12A and B show typical results for **OAE4** and **OAE7**. The 2D conductance histograms were obtained as follows.[90,91] First all the individual conductance traces were normalised to a common distance scale by assigning the relative displacement $\Delta z = 0$ at $G = 0.7\ G_0$. This procedure is justified by the sharp drop in conductance around 1 G_0. The conductance versus relative displacement histogram was then constructed by counting the occurrences of [log(G/G_0), Δz] pairs in a 2D field. The 2D histograms of **OAE4** and **OAE7** show features of gold quantum contacts around $G \geq 1G_0$ and a second cloud-like pattern in [0.5 nm < Δz < 1.8 nm, $10^{-6.2}\ G_0 < G < 10^{-4.8}\ G_0$] centred at $G = 10^{-5.5}\ G_0$ (**OAE4**) and in [0.5 nm < Δz < 2.2 nm, $10^{-7.0}\ G_0 < G < 10^{-6.5}\ G_0$] centred at $G = 10^{-6.9}\ G_0$ (**OAE7**). We attribute the latter to the formation of single-molecule junctions. The corresponding characteristic conductance data are rather close to the positions of conductance peaks in the 1D histograms. Similar conclusions were also obtained for the other OAE derivatives. We also note that all 2D conductance histograms reveal a small but distinct decrease of the single junction conductance G with increasing displacement Δz. The corresponding intervals are given in Table 2.1 for all the compounds investigated. The data cloud below $10^{-7.5}\ G_0$ represents the noise level.

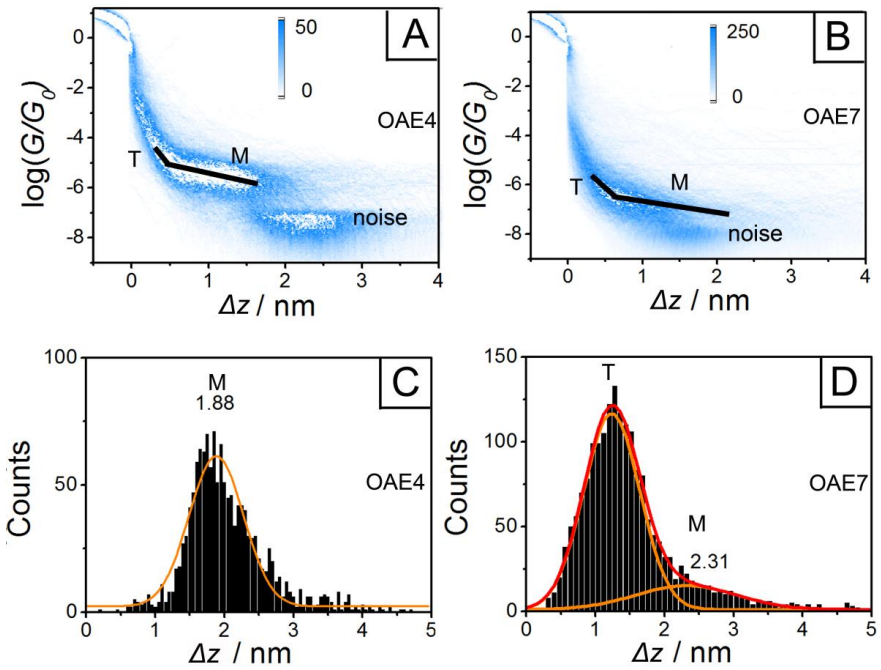

Fig. 2.12 (A,B) 2D conductance-relative-displacement histograms from MCBJ-BJ experiments for OAE4 (A) and OAE7 (B). (C,D) Relative displacement (Δz) distribution from MCBJ-BJ experiments for OAE4 (C) and OAE7 (D). The relative displacement histograms are obtained from conductance traces between 0.1 G_0 and $10^{-7}\ G_0$. The envelope traces represent Gaussian fits to the molecular junction contribution and to direct tunneling, labelled as M and T, respectively.

The characteristic relative stretching distance Δz was estimated from the distance of breaking the gold-gold contact (set as 0.07 G_0) up to the conductance range of the molecular plateau under study. The characteristic most probable lengths z^* were extracted from fitting Gaussians to the length distribution histograms (see Table 2.1). For **OAE3** and **OAE4**, the probability of forming molecular junctions is almost 100%. We note that a second, molecular-junction related feature M2 is observed for **OAE3a** around $10^{-7}G_0$ (Fig. 2.13A). This feature corresponds to a low conductance state, which most probably is related to the stacking of molecules in the junction.[53] The longer molecular wires did not show this feature, which could be related to the detection limit of the experimental setup or the existence of hexyloxy side chains, which could hinder the formation of molecular stacks in the nanoscale junction.

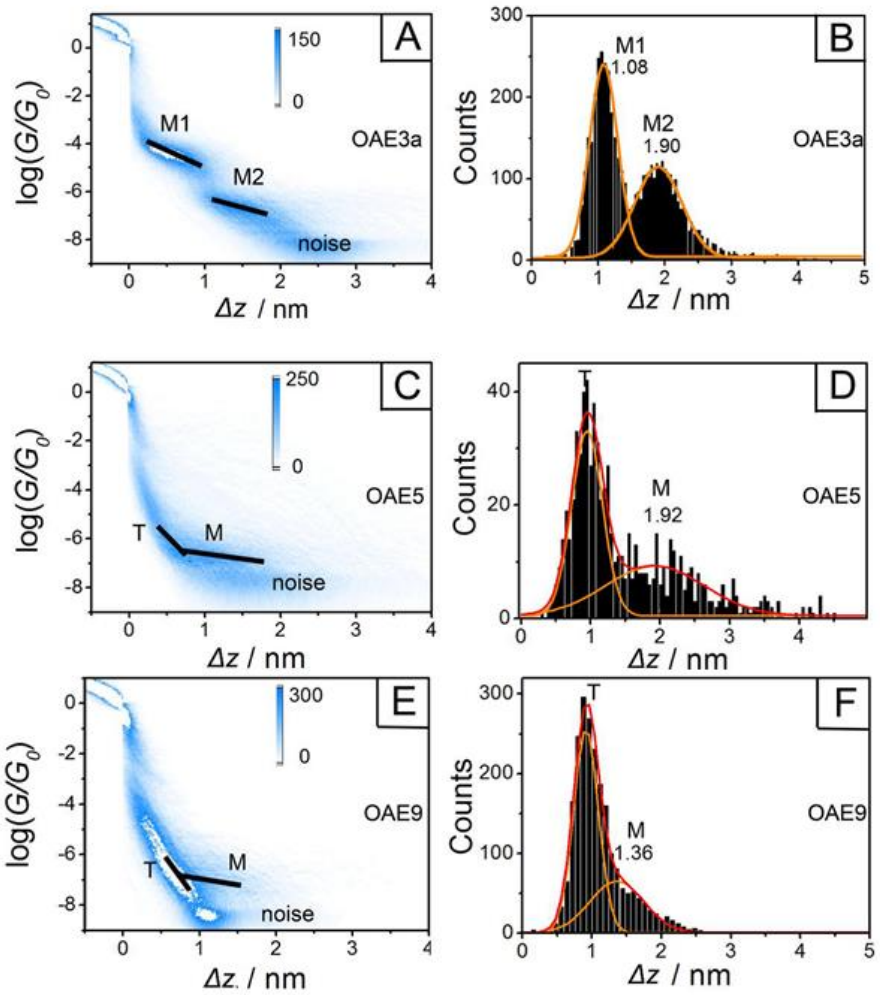

Fig. 2.13 2D conductance-relative-displacement histograms from MCBJ-BJ experiments for OAE3a (A), OAE5 (C) and OAE9 (E). Relative displacement (*z*) distribution from MCBJ-BJ experiments for OAE3a (B), OAE5 (D) and OAE9 (F). The relative displacement histograms are obtained from conductance traces between 0.1 G_0 and 10^{-7} G_0. The envelope traces represent Gaussian fits to distributions originating from molecular junctions (M) and direct tunneling (T).

Analysing the evolution of a molecular junction upon stretching provides additional information about the stability and junction formation probability. We constructed relative displacement (Δz) histograms[50] by calculating the displacement from the relative zero position at 0.7 G_0 to the end of the molecular conductance region, just before the onset of the noise level. Fig. 2.12C,D displays characteristic displacement histograms of **OAE4** and **OAE7**. The plot of **OAE4** reveals a uniform normal distribution with a well-defined maximum. No stretching traces shorter than 1.2 nm were observed, indicating that no significant contribution due to direct tunneling (T) through the solution exists. Therefore, we conclude that the molecular junction formation probability of **OAE4** approaches 100%. The single maximum in Fig. 2.12C represents the most probable relative characteristic stretching distance $\Delta z^* = 1.88$ nm, which may be considered as a measure of the most probable characteristic plateau length of an **OAE4** molecular junction. The most probable absolute displacement z^* in an experimental molecular junction formed between two gold tips and **OAE4** was obtained by adding the snap-back distance Δz_{corr} to the relative displacement: $z^* = \Delta z^* + \Delta z_{corr}$. Based on previous Bern-Durham work with pyridyl-terminated tolane,[50] $\Delta z_{corr} = (0.5 \pm 0.1)$ nm was used, which leads to $z^* = 2.38$ nm for **OAE4**. (This value is close to the molecular length L of **OAE4**.)Similar trends were found with **OAE3** (c.f. data in Table 2.1).

The 1D displacement histograms of the longer OAEs are more complex. Fig. 2.12D illustrates data of **OAE7** as an example. In addition to a well-developed molecular feature with a maximum at $\Delta z^* = 2.31$ nm, which gives $z^* = 2.81$ nm as the most probable absolute displacement, we observed a second peak with a maximum around 1.2 nm. This peak originates from an increasing number of individual conductances versus distance traces without the formation of a molecular junction. In other words, it represents contributions from direct tunneling. The area ratio between the molecular contribution and the total data density in the histogram plotted in Fig. 2.12D leads to a junction formation probability of 18% for **OAE7**. A similar analysis of the experiments with **OAE6** to **OAE9** reveals the following trends: (i) The molecular junctions break prior to a fully extended configuration; (ii) the molecular features in the 1D displacement histograms broaden; and (iii) the junction formation probability decreases considerably with increasing molecular length L. These observations demonstrate that the larger number of molecular conformations and/or the increasing number of hexyloxy sidechains of the longer OAEs appear to hamper the formation of stable (single) molecular junctions. Changes in the molecular structure near the pyridyl binding site may play a role. For **OAE3**-**OAE5**, the phenyl rings adjacent to the pyridyls are disubstituted

with alkoxy groups, whereas for **OAE6**-**OAE9** these rings are unsubstituted. The latter might strengthen the π-interaction of the molecule with the gold substrate, and therefore, an additional energy might be needed to lift the respective OAEs from the substrate surface. This extra energy threshold might not always be reached so that the percentage of stretching events that are unsuccessful (no molecular junctions being formed) is larger, which leads to a lower junction formation probability. This process could be addressed in future by molecular dynamics simulations in combination with electromechanical force-distance and conductance-distance measurements.

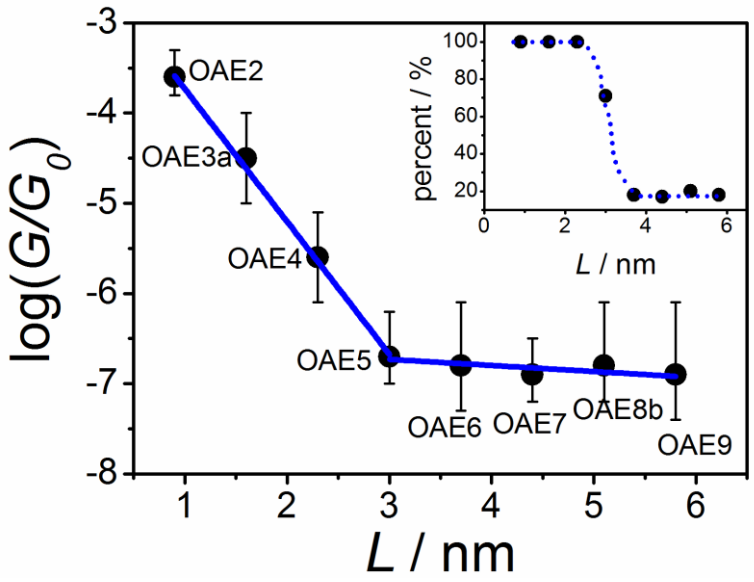

Fig. 2.14 Semilogarithmic plot of the most probable single-molecule junction conductances (individual data points as obtained from the analysis of the 1D conductance histograms) and of the conductance range (bare symbols as extracted from the analysis of the 2D conductance histograms) in units of log(G/G$_0$) versus the molecular length for a family of pyridyl-terminated OAE derivatives. The inset represents the junction formation probability (JFP) dependent on the molecular length L. All numerical data are compiled in Table 2.1

Fig. 2.14 displays the dependence of the most probable single junction conductances of **OAE3-9** on molecular length L. For the shorter molecules, from **OAE3** to **OAE5**, the conductance decreases exponentially according to eq 1

$$G = G_c e^{-\beta L} \quad (1)$$

with an attenuation constant β = (3.3 ± 0.1) nm^{-1} and a contact conductance per pyridyl terminating group, G_c = (0.54 ± 0.07) µS at L = 0, which leads to a contact resistance $R_c = 1/G_c$ = (1850 ± 232) kΩ. Similar values of β were reported for other rigid-rodlike single molecular wires or assembled monolayers, such as dithiol-terminated OPEs (3.4 ± 0.1 nm^{-1}),[69]

oligophenyleneimines (OPI, β = 3.0 nm^{-1}),[64] oligophenylenedithiols (PP, β = (3.5–5.0) nm^{-1}),[92,93] or pyridyl-terminated oligoynes (OY, β = (3.1 ± 0.4) nm^{-1}).[94] Smaller values of β were reported for OPEs with amine anchoring groups (OPE, β = 2.0 nm^{-1}),[71] oligoflorenes (OF, β = (2.06 ± 0.09 nm^{-1})),[65] oligophenylenevinylenes (OPV, β = (1.7–1.8) nm^{-1}),[88,95] oligothiophenes (OT, β = ~1 nm^{-1}),[96] and for metal-porphyrin containing molecular wires (P, β ≪ 0.1 nm^{-1}).[97]

The contact resistance R_c = 1850 kΩ per pyridyl anchoring group **for OAE3-9** is larger than R_c = 205 kΩ, which is the corresponding value for pyridyl-terminated oligoynes.[94] A similar trend is observed with the dithiol-terminated OPEs (40 kΩ)[69] and oligoynes (~3.2 kΩ).[94] These data demonstrate that the values are not only determined by the molecular anchoring site but also by the coupling of the anchor group to the wire backbone.

Comparing the results of the single-molecule conductance measurements for the short OAE derivatives with the literature data above, and, in particular, with results reported for pyridyl-terminated oligoynes[94] and thiol-terminated OPEs,[69] as well as the excellent fit of eq 1 to the experimental data, demonstrates that electron transport across the **OAE3-OAE5** wires is controlled by coherent transport via tunneling or superexchange.

The longer derivatives **OAE6-OAE9** behave differently. The most probable single junction conductances are still exponentially dependent on molecular length L. However, the fit of eq 1 to the experimental data gives an attenuation constant β = (0.16 ± 0.08) nm^{-1}, which is significantly smaller as compared to β = (3.3 ± 0.01) nm^{-1} of the shorter OAEs. Similar small β values were reported for longer amine-terminated OPEs (β ~ 0.3 nm^{-1}),[71] thiol-terminated oligofluorenes (β ≪ 0.1 nm^{-1}),[65] and longer oligophenylenimines (β ~ 0.9 nm^{-1}).[61] Comparing these results suggests that transport through the longer pyridyl-terminated OAEs occurs by a thermally activated hopping mechanism.[63] Transition from tunneling to hopping was found at a molecular length of ~3 nm for the present series.

As stated in Section 2.1, single-molecule studies of length dependence have not been reported previously for OAE systems. CP-AFM experiments which involve contacting hundreds of molecules within self-assembled monolayers, revealed the transition from tunneling to hopping at a molecular length of ca. 2.75 nm for a series of amine-terminated OPEs[71] and ca. 4 nm for thiol-anchored oligophenyleneimines.[64] Single-molecule conductance experiments employing the STM-BJ techniques reported characteristic transition lengths of 5.6-6.8 nm for polythiophenes[98] and 5.2-7.3 nm for oligofluorene-based molecular wires,[65] both terminated with thiol anchors. We note that, for the oligofluorene series, the experiments are very limited

within the length range investigated. This comparison demonstrates convincingly that the transition length from tunneling to transport controlled by hopping depends critically on the structure of the molecular backbone. However, the existing limited database of single-molecular junction studies does not yet allow general trends to be extracted. For future work, comparative studies on molecular wires not only of known and tunable length, but also with controlled molecular conformation, are essential to achieve this goal.

2.6 Conclusions

A new family of linear OAE derivatives has been synthesised, using iterative Sonogashira cross-coupling reactions, with terminal 4-pyridyl anchor groups and molecular lengths (N…N distance) of ca. 2-6 nm. The charge transport properties of these molecular wires have been characterised by MCBJ experiments. Single-molecule junction conductance measurements reveal a transition from coherent transport via tunneling, which dominates in shorter molecules, to incoherent hopping in longer molecules. The transition occurs at a molecular length L ~ 3.0 nm and for conductances below $10^{-6.5}$ G_0. Increasing the molecular length L leads also to a reduction of the probability for molecular junction formation from 100% to values below 20%. This trend is attributed to the larger number of molecular conformations and the increasing number of hexyloxy sidechains, which appear to hamper the formation of stable OAE type (single) molecular junctions. A comparison of our data with literature data for other oligomer systems establishes that the details of the tunneling-to-hopping transition depend on the nature of the molecular wire backbone as well as its coupling to the respective anchoring sites. This work represents the first studies on length dependence of conductance of OAE derivatives at the single-molecule level. However, unambiguous and more general correlations between structure and transport characteristics cannot yet be established due to the limited number of reliable single junction conductance studies with long molecular wires of well-defined structure, in particular, molecular conformation. This topic comprises a major challenge for future synthesis, measurements and theory in molecular electronics.

Chapter 3. Pyridyl Anchored OAE3 Molecular Wires

3.1 Introduction

Single molecular conduction measurements are mostly studied in terms of a nonresonant tunneling process in which the molecule acts as a tunneling barrier.[60,99,100] Accordingly, the main characters that define the efficiency of the charge transport are the width and height of the energy barrier, and the electronic coupling between the electrodes and the molecule. Conductance through a single molecule then depends exponentially on the length of the electron pathway; this has been observed in many experiments.[60,71,72,99-101] However, a substantial parameter, Quantum Interference (QI), is disregarded in this simple tunneling picture which can strongly influence transport at the molecular scale. QI effects in molecular electronics were first considered in 1988,[102] and these effects have attracted increasing theoretical[103-105] and experimental[89,106,107] interests. Theorists predict that, in single molecule systems, large conductance modulations should accompany quantum interference. For instance, a benzene ring bonded with two electrodes through a *meta*-configuration should have a conductance which is 5 orders of magnitude lower than that of a *para*-configuration.[106]

Solomon *et al.* pointed out that a large dip in the electron transmission probability has been shown for cross-conjugated molecules due to interference between electron transport pathways in energetic space.[106,107] They studied a series of comparable molecules as shown in Fig. 3.1. Unexpectedly, for both fully conjugated molecules **46** and **47**, they found there is a 6 orders of magnitude difference in the transmission at the Fermi energy. Close to the Fermi energy, the transmission in **46** resembles that in **48** where the conjugation is broken by replacing the double bond with saturated carbons throughout the backbone. They also noted potential applications for this kind of molecules according to the dramatic current-voltage features shown in Fig. 3.1. The current through **46** increases by 5 orders of magnitude over the range considered and in particular, between 1.5 and 2.0 V, there is a 2 orders of magnitude increase, suggesting they are candidates for a molecular switch.

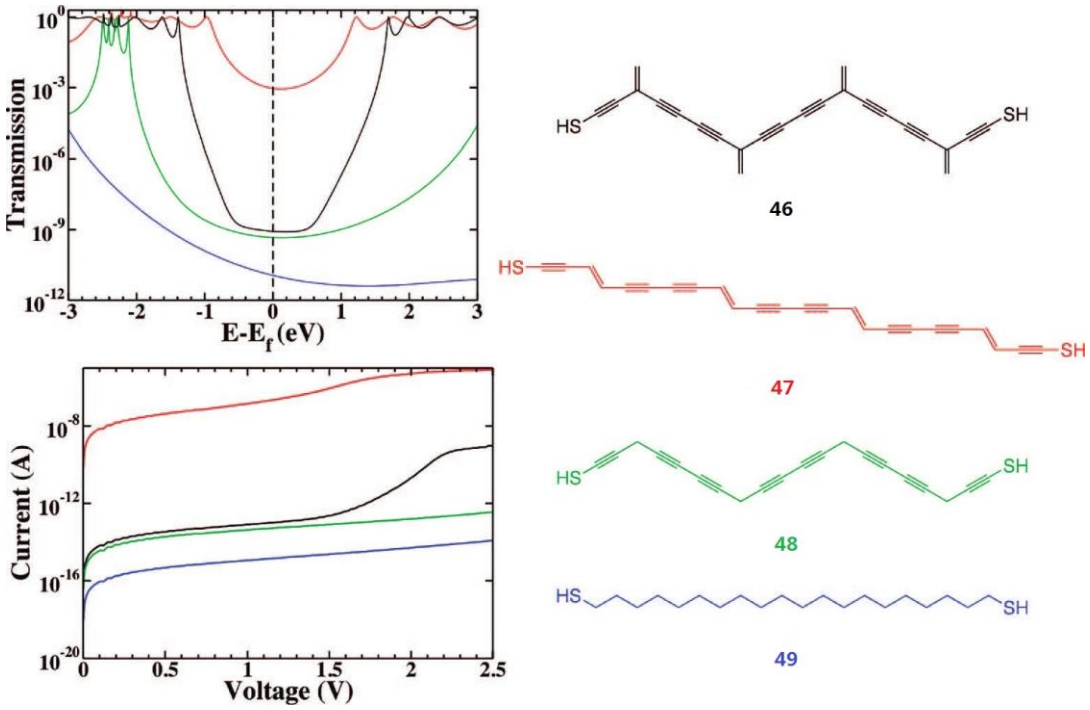

Fig. 3.1 Zero bias transmission as a function of energy, and current as a function of voltage, for a group of comparable molecules, illustrating the unusual transport characteristics of a cross-conjugated system. Specifically, an extended cross-conjugated molecule (46) is compared with its linearly conjugated counterpart (47) and with a partially conjugated (48) and a saturated (49) system of a similar length. (Reproduced from reference[107]).

Following their previous work, the authors studied the hypothetical system shown in Fig. 3.2 and calculated that the conductance through the "short" system is much lower than that through the "long" system. The difference in conjugation between the two paths in Fig. 3.2 causes the critical difference in conductance.[108]

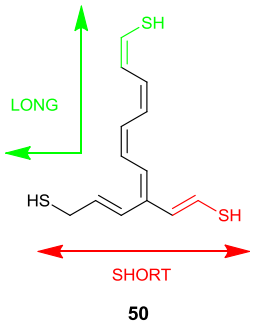

Fig. 3.2 The "long" and "short" pathways are defined as two different methods of attaching the molecule to two gold electrodes. In both cases one electrode is attached to the thiol group shown in black; the long system utilizes the vinylthiol shown in green, and the short system uses the vinylthiol shown in red. (Reproduced from reference[108])

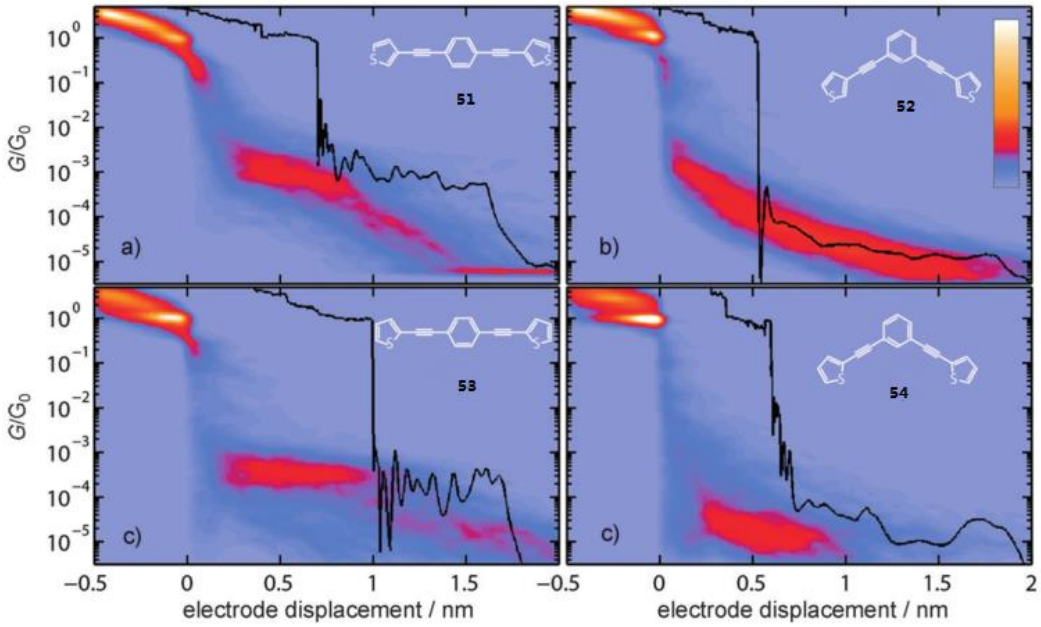

Fig. 3.3 Two-dimensional trace histograms constructed from 500 consecutive breaking traces taken at ambient conditions and 0.1 V bias for junctions exposed to a 1 mM solution of a) 51, b) 52, c) 53, and d) 54 in chloroform. Regions of high counts represent the most probable breaking behaviour of the contact. The black curves are examples of individual breaking traces. (Reproduced from reference[109])

Very recently, Arroyo *et al.*[109] studied a series of molecules with a benzene ring as the central unit of a series of OAE molecules to which thienyl anchoring units are connected either in *para*- or *meta*-configurations (Fig. 3.3). They observed in MCBJ experiments that the conductances through *meta*-coupled molecules **52** and **54** are at least one order of magnitude lower than through the *para*-coupled analogues **51** and **53**. In the two-dimensional trace histograms, the high counts of **52** are in the 10^{-5} G_0 region, whereas the conductance for **54** approaches the limit of the resolution of the setup. They ascribed this difference to constructive QI in *para*-coupled molecules, whereas destructive QI occurs in *meta*-coupled molecules.

Mayor *et al.* reported by measuring single molecular conductances of two molecules **55** and **56** with acetyl protected thiol anchor groups in *meta* and *para* positions respectively (Fig. 3.4), the currents for **55** were about 10 nA at U= 1 V, almost two orders of magnitude lower than the values of **56** under similar conditions.[58]

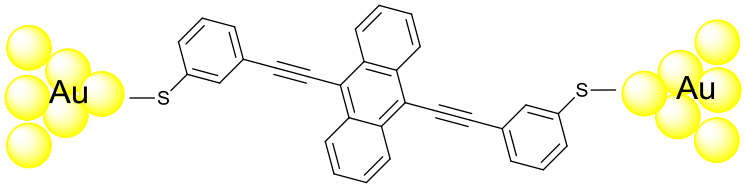

55

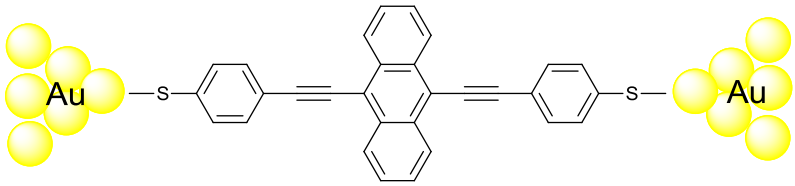

56

Fig. 3.4 Molecular structures of molecules studied in Mayor's work. (Reproduced from reference[58])

Aradhya *et al.* compared the conducting *para*-terminated 4,4'-di-(methylthio)stilbene **57** and moderately conducting 1,2-bis(4-(methylthio)phenyl)ethane **58** to that of insulating *meta*-terminated 3,3'-di(methylthio)stilbene **59** in single molecule junctions (Fig. 3.5).[110] Both the stilbene derivatives have similar mechanical stability in the junctions, but the electronic properties are different. The *para*-linker groups behave as typical electro-mechano contacts, whereas the *meta*-linker groups only act as mechanical contacts with a destructive conductance.

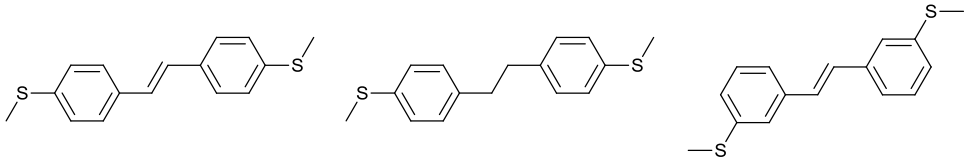

57 58 59

Fig. 3.5 Molecular structures of molecules studied in Aradhya's work. (Reproduced from reference[110])

Inspired by the above reports, in the present work with the aim to study the effects of QI on charge transfer through a single benzene ring and to gain knowledge of junction formation geometry toward the change of intramolecular charge transfer, a series of OAE molecules was specifically designed, as shown in Scheme 3.1. The central core of each molecule is a benzene ring with ethynylpyridyl linkers connected either in *para*- or *meta*-configurations. The position of the nitrogen in the anchor unit was also varied (*ortho*, *meta* or *para*) in order to explore the effects of anchoring geometry and charge transfer at the pyridyl-gold interface. Molecules with substituents on the central benzene ring were also synthesised

to study the robustness of junction formation. To further explore the role that the pyridyl nitrogen plays in the anchoring process and assess the influences of π-stacking effects, unsymmetrical molecules with only one pyridyl anchor group were also studied (Scheme 3.1).

3.2 Synthesis

The synthesis of the symmetrical molecules uses Pd-catalysed Sonogashira cross-coupling reactions[78] of various ethynylpyridine building blocks (Scheme 3.1). The reactions were shielded from direct light due to the light sensitivity of ethynylpyridine derivatives. The symmetrical molecules (groups 1, 2 and 3) were synthesised from the commercially available di-iodoarene and ethynylpyridine, respectively, under standard Sonogashira conditions. To obtain **63** iodination of 1,2,4,5-tetramethoxylbenzene (**62**)[111] was first conducted according to the literature procedure[111] which was "*n*-BuLi was added to the solution of **62** at r.t. and iodine was added after 48 hours." However, a black residue which could not be identified was found after attempted purification. Alternative conditions were tried by varying the temperature and length of the lithiation process and we found the optimised condition which converted 1,2,4,5-tetramethoxylbenzene to the diiodo derivative **63** with a high yield of 88% (conditions as specified in the Experimental). **63** was then reacted with 4-ethynylpyridine, as below, to give **p-p-p (4OMe)** in 65% yield. Unsymmetrical molecules (group 4) were synthesised by reacting compound **42** with different ethynylpyridine isomers under Sonogashira conditions.

Scheme 3.1 Synthetic scheme for the molecules studied.

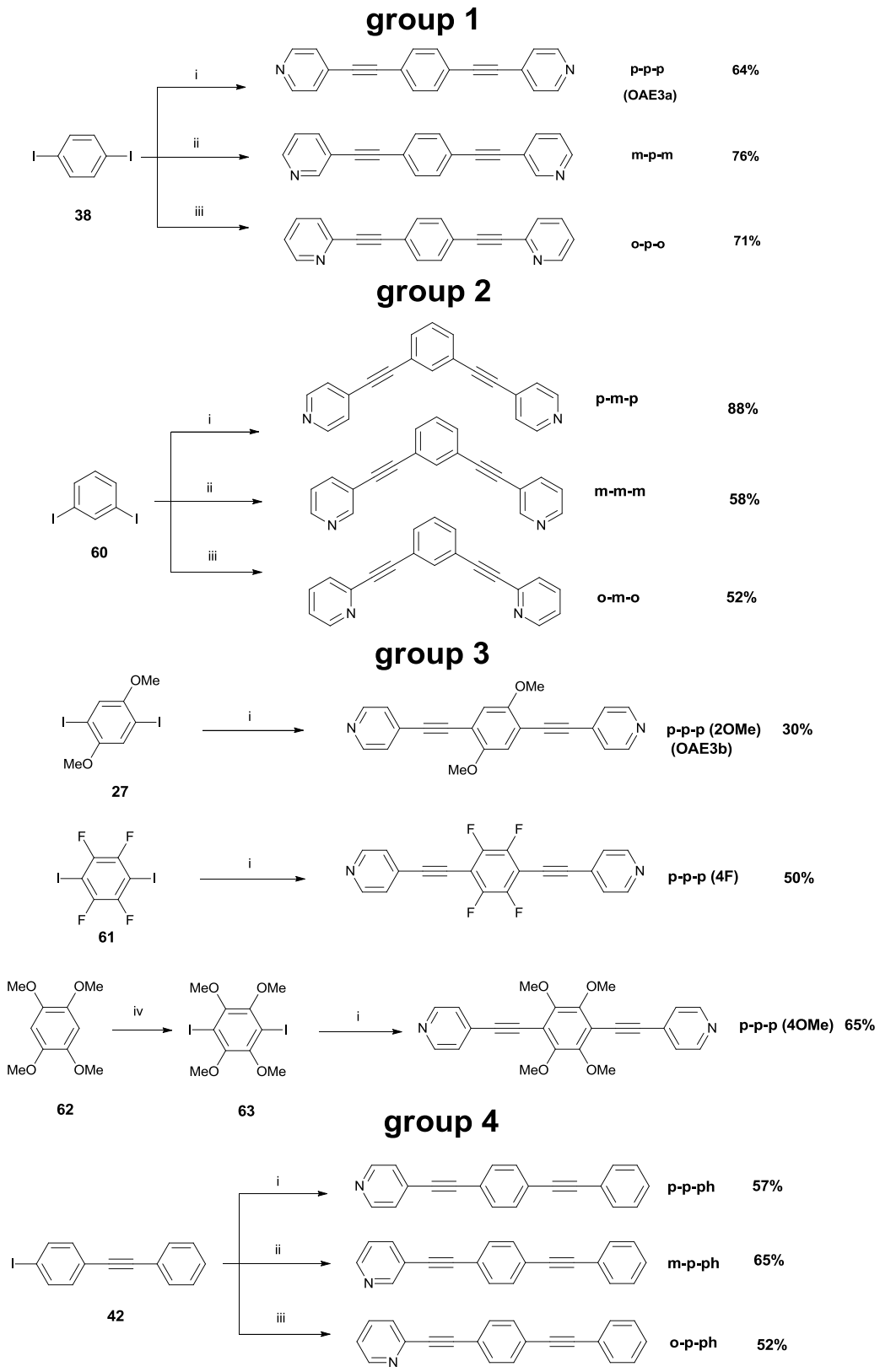

Reagents and conditions: (i) 4-ethynylpyridine, $[Pd(PPh_3)_4]$, CuI, THF/ Et_3N; (ii) 3-ethynylpyridine, $[Pd(PPh_3)_4]$, CuI, THF/ Et_3N; (iii) 2-ethynylpyridine, $[Pd(PPh_3)_4]$, CuI, THF/ Et_3N; (iv) *n*-BuLi, I_2, THF, 12 h, -78 ^{o}C, 88%.

3.3 Optical Properties

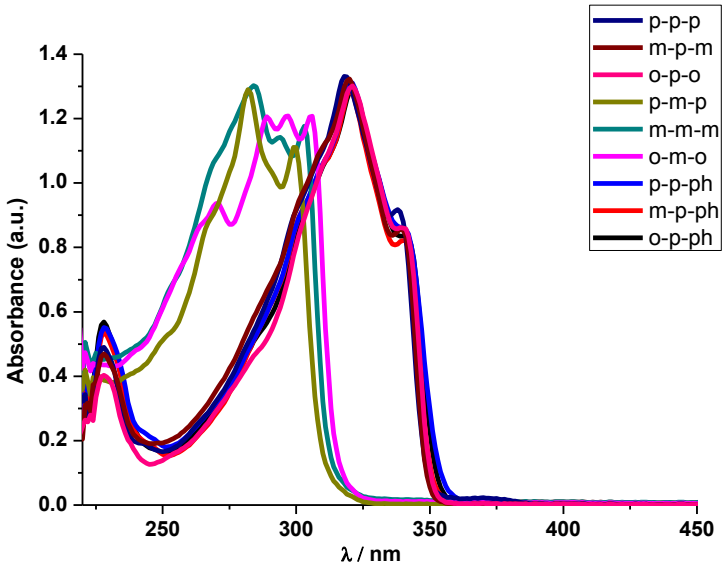

Fig. 3.6 UV-Vis absorption spectra for the molecules studied in this chapter.

The UV-Vis absorption measurements were conducted at 25 ^{o}C in DCM (2×10^{-5} M compound). Due to the broken conjugation caused by the *meta*-substituted core, the bent molecules show a significant (ca 30 nm) blue shift compared to their linear counterparts. The data shows that the presence and position of the nitrogen atoms have only a negligible effect on the absorption spectra.

3.4 Conductance Measurements

The pyridyl terminated oligo(aryleneethynylene) (OAE) derivatives shown in Scheme 3.1 were investigated to study the quantum interference (QI) effects in both central and anchor units. The central parts of these OAEs are typical phenyl rings with either *meta* or *para* di-substituted configurations. The anchor units are pyridyls with *ortho*, *meta* or *para* configurations of the nitrogen connected to the phenyl rings through triple bonds. The charge transport characteristics of these OAE derivatives in single molecular junctions have been studied using both the MCBJ and STM-BJ techniques at room temperature in Prof. Wandlowski's laboratory at the University of Bern. (For details see Chapter 7.)

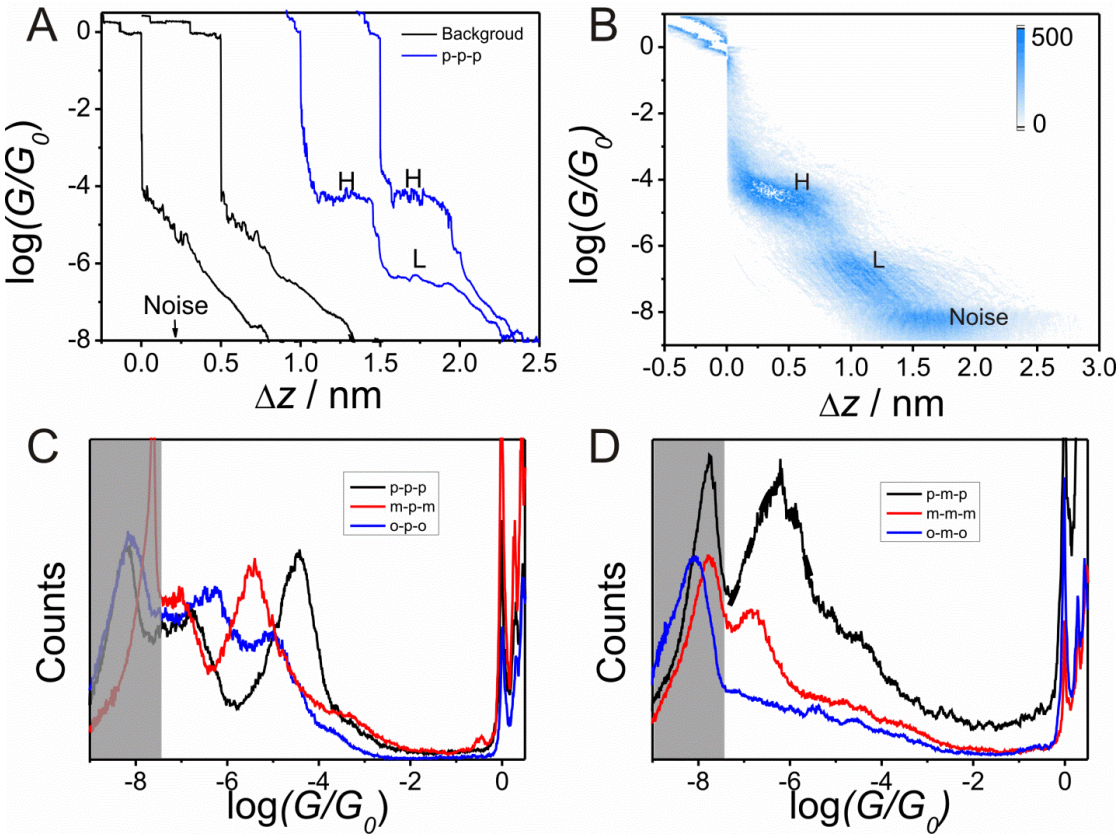

Fig. 3.7 MCBJ measurements data. (A) Typical individual conductance-distance traces of p-p-p (Blue) and pure tunneling traces (Black); (B) All-data point 2D conductance vs relative distance (Δ*z*) of p-p-p; C, D All-data point 1D conductance histograms constructed from 1000 traces of molecules in group1 (C) and group2 (D).

Fig. 3.7A displays the typical conductance versus relative displacement traces from measurement of molecule **p-p-p**. We observed a well-defined plateau at the range around -4.5 in the $\log(G/G_0)$ vs Δ*z* stretching traces, ascribed to the conductance feature of single-molecule junctions. Additionally, the plateau around < -6 was ascribed to the low conductance junction configuration. The overall shape of the stretching traces as recorded for each molecule is qualitatively similar, but varies in detail. Therefore, a careful statistical analysis of a large number of individual traces is required to extract representative results. During the conductance measurements, several thousands of individual conductance versus relative displacement traces (G vs Δ*z*) were recorded and analysed further by constructing all-data-points histograms without any data selection to extract statistically significant results from the different junction configurations. As demonstrated in our previous studies,[50] the stretching trace showed the changing of geometries in the molecular junction.

The 2D histograms of **p-p-p** in Fig. 3.7B show features of gold quantum contacts around $G \geq 1G_0$ and a second cloud-like pattern in $[10^{-5.0}\ G_0 < G < 10^{-3.6}\ G_0]$, centred at $G = 10^{-4.5}\ G_0$. We attribute the latter to the formation of single-molecule junctions (H). The corresponding characteristic conductance data are rather close to the positions of the conductance peak in the 1D histogram. The cloud-like pattern is observed in both MCBJ and STM-BJ measurements, in which the peak range shows a good agreement with each other. It was noted that all 2D conductance histograms reveal a small, but distinct, decrease of molecular conductance G with the increasing displacement *Δz*. Moreover, the ranges of the evolution step from the MCBJ measurement are invariably bigger than that from STM-BJ, in agreement with the peak width shown in the 1D histograms. These data are ascribed to the evolution of the junction configurations during the stretching measurement. Fig. 3.7C and D display the corresponding one-dimensional (1D) histograms of representative OAE molecules in group 1 and group 2 in a semilogarithmic scale, as constructed from 1000 experimental conductance versus distance traces for each compound.

Table 3.1 Conductance of pyridine terminated oligo(aryleneethynylene) (OPAE) derivatives from MCBJ and STM-BJ

Molecule	Conductance (Log(G/G₀))			Δz/ nm			JFP(%)*		Peak range (Log(G/G₀))		
	MCBJ		STM-BJ	MCBJ		STM-BJ	MCBJ	STM	MCBJ		STM-BJ
	High	Low		High	Low				High	Low	
p-p-p	-4.5	-7.0	-4.5	1.08	1.90	1.03	100	100	-3.6~-5.0	-6.2~-7.8	-3.5~-4.8
p-m-p	-6.3		-5.8	0.87		0.81	100	100	-5.0~-7.0		-5.4~-6.1
m-p-m	-5.5	-7.1	-5.5	1.0		0.95	100	89	-4.5~-6.2	-7.0~-7.8	-4.9~-5.9
m-m-m	-6.9		<-6	0.5		-	28		-6.2~-7.8		
o-p-o	-5.0	-6.3	-4.5	0.89	1.29	0.65	32	27	-3.8~-5.2	-5.5~-7	-3.9~-4.9
o-m-o				-		-					
p-p-p (2OMe)	-4.2	-7.1	-4.1	1.33	1.43	1.4	100	100	-3.8~-4.3	-6.0~-8	-3.6~-4.3
p-p-p (4OMe)	-4.2	-7.1	-4.1	0.88	1.26	0.85	100	100	-3.8~-4.5	-6.0~-7	-3.3~-4.9
p-p-p(4F)	-4.1	-7.1	-4.1	0.92	1.58	0.84	100	100	-3.5~-4.8	-6.0~-8.0	-3.3~-4.2

*JFP% = junction formation probability

The key parameters are summarised in Table 3.1. The sharp peaks around 1 G_0 represent the conductance of a single atom gold-gold contact. The prominent peaks between

10^{-7} G_0 < G < 10^{-4} G_0 represent molecular conductance features. The statistically most probable conductance of molecular junctions formed by the respective OAEs as trapped between two gold contacts were obtained by fitting Gaussians to the characteristic maxima in the conductance histograms.

Both STM-BJ and MCBJ measurements showed that the molecules bearing central phenyl rings in the *meta*-configuration (x-m-x, molecules group 2) presented lower conductance as compared to the isomers in the *para*-configuration (x-p-x, molecules group 1). It is established that electrons' transport through the single molecule generates the conductive properties of the molecule. Therefore, the idea of electron's wave nature during the flow of current was introduced into molecular electronics. As a common phenomenon, the quantum interference (QI) could be taken as an effective method to control the current flow through a single molecule. It has been reported that destructive interference existed in benzene derivatives with the *meta*-substitution and is responsible for the observed reduction of conductance.[105,112] In our case, it was demonstrated that the reduction of conductance in *meta*-substituted molecules was caused by the QI effect at the central phenyl ring, which leads to the phase shifts of transmission channels or interfering spatial pathways. However, we did not observe any electrical properties of **o-m-o** from either MCBJ or STM-BJ experiments. This is ascribed to the super-low molecular junction formation probability because of the combination of bent configuration and the hidden anchoring site in the **o-m-o** molecule.[53]

Additionally, we also considered possible QI effects in the anchor sites. For the linear derivatives, it is shown that the conductance of **m-p-m** ($10^{-5.5}$ G_0) is one order of magnitude lower than that of **p-p-p** ($10^{-4.5}G_0$). As for the bent derivatives, a similar phenomenon is shown for **m-m-m** ($10^{-6.9}$ G_0) and **p-m-p** ($10^{-6.1}$ G_0) with *meta*-configurations in the anchor sites. We have clearly established that the QI effect is more prominent in the central ring of this OAE series than in the terminal rings.

Moreover, the evolution of a molecular junction upon stretching provides important information about the stability and junction formation probability. We constructed relative displacement histograms (Δz) by calculating the displacement from the relative zero position at 0.7 G_0 to the end of the molecular conductance region, before the onset of the noise level. Referring to our previous work[101], we used Δz_{corr}= (0.5±0.1) nm to calibrate the relative displacement, $z^*=\Delta z+\Delta z_{corr}$, considered as the most probable characteristic plateau length of single-molecule junctions. No stretching traces shorter than 0.5 nm were observed, indicating that no significant contribution due to direct tunneling exists during the conductance

measurement. Therefore, it was demonstrated that the molecular junction formation probability of molecule **p-p-p** is 100%. Furthermore, the ratio of the contribution from the molecular junction to the whole density was calculated as the junction formation probability. As shown in table 3.1, the junction formation probability approaches 100% for molecules **p-p-p**, **p-m-p**, **m-p-m** and molecules in group 3. However, for molecules **m-m-m** and **o-p-o**, the junction formation probability deceased sharply to 28% (MCBJ) for **m-m-m**, and 32% (MCBJ)/27% (STM-BJ) for **o-p-o**, showing a trend of **p-p-p** > **m-p-m**, **o-p-o**, and **p-m-p** > **m-m-m**.

Accordingly, the plateau length of the junction also follows the similar trends **p-p-p** > **m-p-m** > **o-p-o**, and **p-m-p** > **m-m-m**. Therefore, it is clear that the anchor units (p, m, o) affect both the plateau length and the junction formation probability, as well as the conductance. For the molecules with *meta*-or *ortho*- configuration at the anchor sites, the nitrogen lone pair is more "hidden" in the phenyl ring framework. The hidden configuration will both change the binding geometry and limit the direct Au-N anchoring during the stretching measurements. These steric factors also explain the fact that no distinct electrical properties could be measured for molecule **o-m-o**.

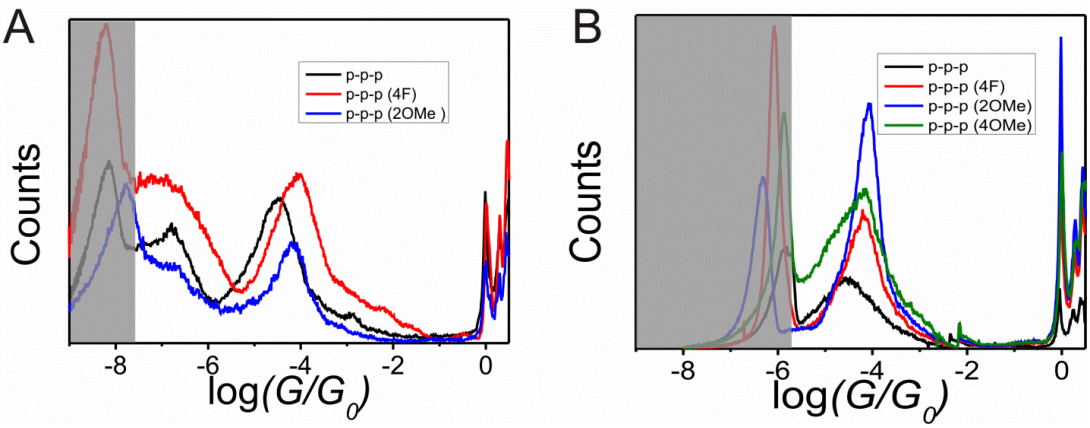

Fig. 3.8 All-data point 1D conductance histograms constructed from 1000 traces of molecules in group3 from MCBJ (A) and STM-BJ (B).

It is shown in Fig. 3.8 that molecules bearing fluorine or methoxy substituents in their central phenyl rings present similar conductances ($10^{-4.1}$-$10^{-4.2}$ G_0), which are higher than that of **p-p-p** ($10^{-4.5}$ G_0) without any substituents. This result illustrates that the fully π-conjugated rod-like OAE is resistive to the electronic effect of substituents on the central phenyl unit (as was also observed in more extensive studies of amine-terminated analogues: see Chapter 4). The higher conductance of molecules in group 3 compared to **p-p-p** was ascribed to the

different break point of obtaining the conductance features during the stretching process. At the breaking point of the molecules bearing central substituents, the π system of the anchor end may contribute to the connection between molecule and electrodes, enlarging the pathway through the electrode to the molecule.

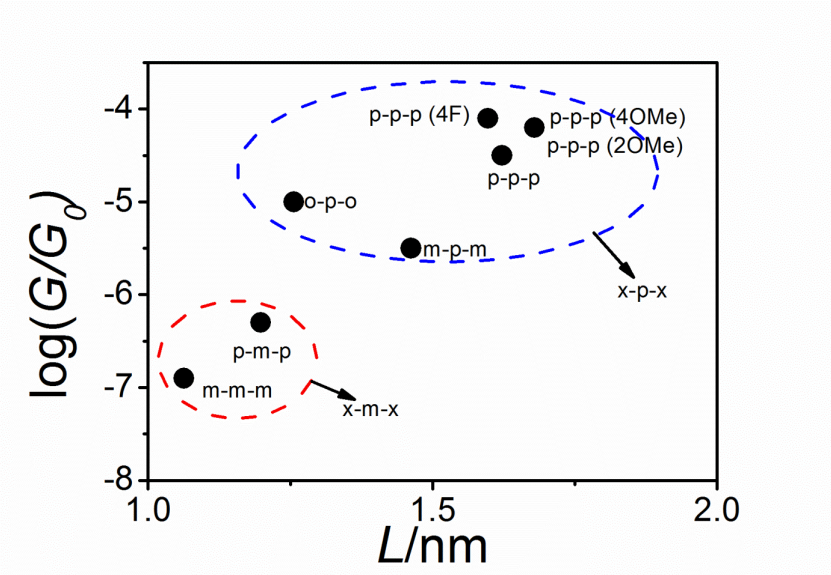

Fig. 3.9 Semilogarithmic plot of the most probable single-molecule junction conductance in units of log(G/G$_0$) versus length between centres of N---N atoms in the OAE derivatives.

Fig. 3.9 shows two distinct groups of molecules with obvious differences in conductance. Due to dramatic influence of the QI effect in the central phenyl ring, molecules bearing *meta*-substituted phenyl rings presented at least one order of magnitude lower conductance than those of *para*-substituted analogues.

To support our initial assignment of the lower conductance peaks (in table 3.1) to intermolecular π-π stacking and to understand the molecular junction formation process well, the molecules in group 4 with only one pyridyl anchor group were studied; their conductance histograms are shown in fig. 3.10 (left). The molecules **p-p-ph** and **m-p-ph** both showed three conductance peaks in the 1D histogram, labelled by numbers 1, 2, 3. According to the studies before, all of these three conductance peaks are attributed to π-π stacking in the junction. As shown in Fig. 3.10 (right), the π-π stacking region could involve sliding of the molecules during the stretching of the molecular junction, and the corresponding three bimolecular assemblies are formed, labelled 1-2-3. The conductance of the peak 3 is close to the low conductance value found in the OAEs (see table 3.1). As expected, no conductance peaks were observed for **o-p-ph**, due to the even lower junction formation probability than **o-p-o**.

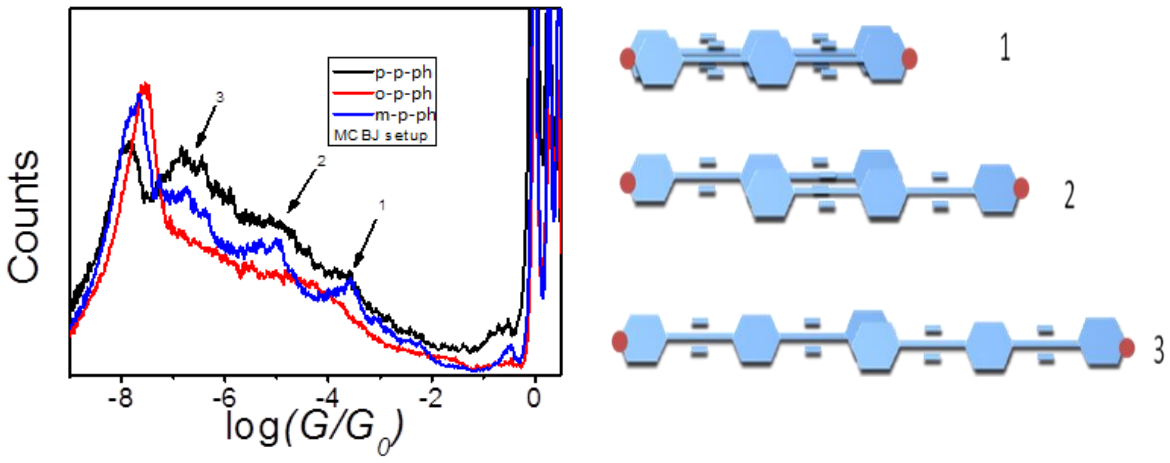

Fig. 3.10 All-data point 1D conductance histograms constructed from molecule group 4 (left). A schematic diagram of the intermolecular π-π stacking during the molecular junction stretching (right).

In the STM-BJ setup no clear peak related to π-π stacking was observed which indicates the conductance range sensitivity for STM setup is not wide enough to show these features. Noise peaks of the instrument interfere with π-π stacking peaks.

3.5 Conclusions

New families of OAE molecules bearing one or two pyridyl anchor groups were synthesised and characterised. It was proved that the configuration of the molecular structures defined the electronic properties of the molecules. It is proved that the *meta*-configuration in the central phenyl rings caused QI effects which dramatically reduced the conductance. Whereas, different substituents attached to the central phenyl rings did not affect the conductance. We found that *meta*- or *ortho*- configurations in the anchor sites also caused QI effects. The QI effect is more evident for structural changes at the central part of the molecule (linear versus bent) than varying the position of nitrogen in the terminal rings. These results suggest molecules of this type are candidates to build single molecular devices, such as tandem logical switches operated by a combination of constructive and destructive QI affected molecular structures.

Chapter 4. Conductance Invariance towards Functionalisation in Oligo(phenyleneethynylene) Molecular Junctions

4.1 Introduction

During the last decade, oligo(phenyleneethynylene) (OPE) derivatives have emerged as benchmark molecules for studying charge transport in molecular junctions. In particular, OPE3 systems have been widely studied in metal/single-molecule/metal junctions.[36,59,68,69,71]

One of the drawbacks of single-molecule junctions is their sensitivity to small changes, such as atomic rearrangements in the electrodes or variations in the molecule's terminal groups. For example, to achieve the assembly of metal/molecule/metal junctions, groups such as thiol, amine or pyridine are required at the termini of the molecules,[29,59,60] leading to a variety of measured conductances for the same parent compound. Such variability is a disadvantage, because it becomes difficult to tune a particular property of a given molecule, while keeping other features fixed. For this reason in this chapter, our aim is to demonstrate that certain substituents added to a parent compound lead to little or no change in transport properties. In particular, we study the resilience of OPE3-based single-molecule junctions to systematic variations of the electronic and steric properties of substituents on the central ring.

This resilience contrasts with the behaviour of a basic benzene unit, where the effect on the molecular-junction conductance of substituting one or more hydrogen atoms by different functional groups has been previously explored.[113-115] Modest conductance variations have been reported for benzene-diamine[113] and benzene-dithiaalkane[115] molecular junctions. However, as a consequence of the small size of benzene, a substituent at any site on the molecule can interact directly with the metallic electrodes and therefore it is difficult to disentangle such effects from the effect on the molecule alone. In this chapter we study the effect of functionalisation both on conductance and on stability for a longer prototype molecular wire, namely OPE3. The functionalised region of the molecule is kept further from the electrodes, avoiding possible direct interactions between the two. Additionally, we chose relatively weak amine binding groups, which play a less predominant role in the electron-transfer properties of the junctions than stronger groups.[28,114]

We compared six OPE3 diamino derivatives with functional groups varying from tetra-fluoro to tetra-methoxy groups, whose structures are shown in Fig 4.1. Our results show that the conductance values of the corresponding molecular junctions are almost identical, whereas the packing properties of the molecules in the junctions can be modified. These experimental results are consistent with theoretical calculations performed by David Manrique and Prof. Colin Lambert at Lancaster University which show that whenever the Fermi energy is close to the centre of the HOMO-LUMO gap, the effect of functional groups is practically negligible, even when the relative position of the HOMO and/or the LUMO is different.

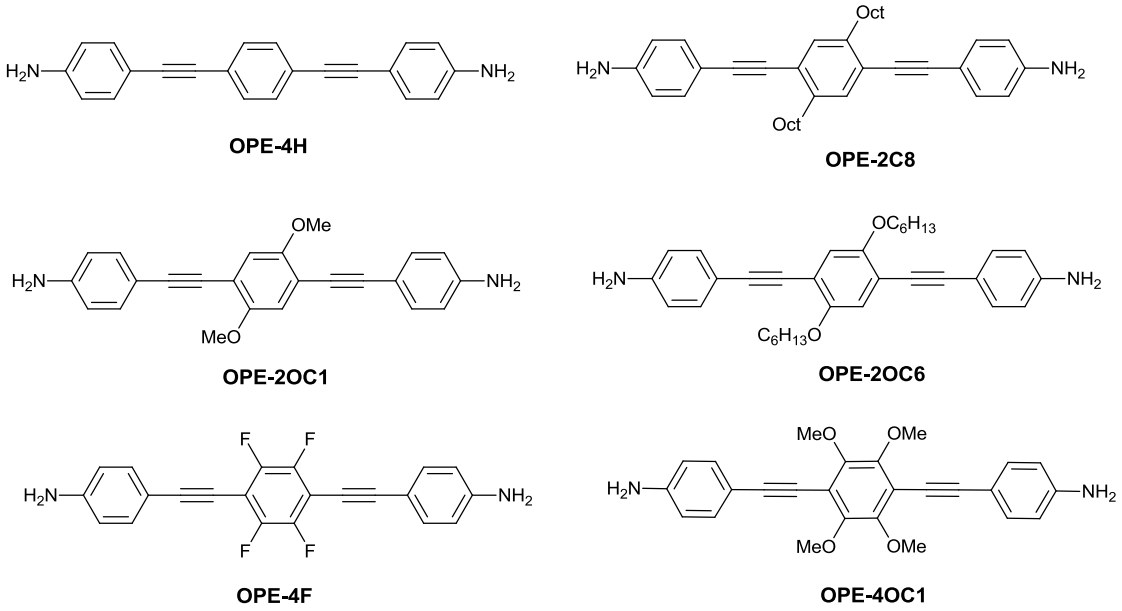

Fig. 4.1 Molecules studied in this chapter.

4.2 Synthesis

The OPE derivatives studied in this work are shown in Fig. 4.1 above. In all cases, the synthetic strategy uses a two-fold Pd-catalysed Sonogashira cross-coupling reaction of the corresponding diiodobenzene derivative with 4-ethynylaniline, following the literature precedent for the parent system **OPE-4H**.[78] The different substituents were chosen to provide systematic variation of the electronic and steric effects on the central ring: namely, strongly electron-donating methoxy and hexyloxy (**OPE-2OC1; OPE-4OC1 and OPE-2OC6**), weakly electron-donating octyl (**OPE-2C8**), and electron-withdrawing fluorine (**OPE-4F**). The hexyloxy and octyl substituents will have a similar steric effect, whereas the electron-donating effect of the former is greatly enhanced by the oxygen atoms attached to the benzene ring. Compound

OPE-4F and **OPE-2OC6** were synthesised by my former colleague Dr. Murat Gulcur. A sample of **OPE-4H** was obtained from Prof. Martin's group, University Complutense, Madrid. The synthetic procedures of the present author's work are described as follows.

Scheme 4.1 Synthesis of **OPE-2OC1**

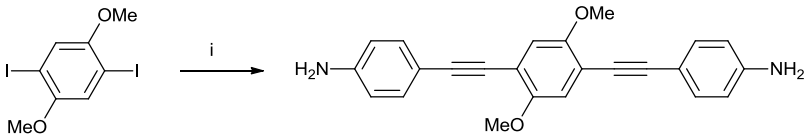

27 **OPE-2OC1**

Reagents and Conditions: (i) 4-ethynylaniline, $[Pd(PPh_3)_4]$, CuI, THF/Et_3N, 12 h, r.t., 40%.

A two-fold Pd-catalysed Sonogashira cross-coupling reaction with 4-ethynylaniline gave **OPE-2OC1** in 40% yield (Scheme 4.1).

Scheme 4.2 Synthesis of **OPE- 2C8**

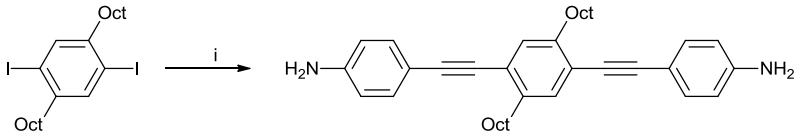

64 **OPE-2C8**

Reagents and Conditions: (i) 4-ethynylaniline, $[Pd(PPh_3)_4]$, CuI, THF/ Et_3N, 19 h, r.t., 61%.

A two-fold Pd-catalysed Sonogashira cross-coupling reaction of Compound **64** with 4-ethynylaniline gave **OPE- 2C8** in 61% yield (Scheme 4.2).

Scheme 4.3 Synthesis of **OPE-4OC1**

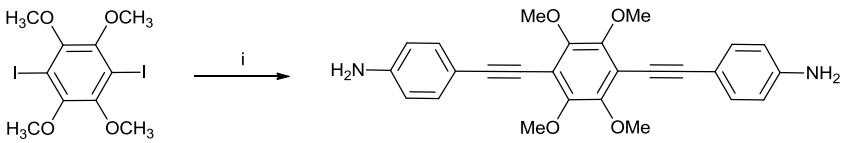

63 **OPE-4OC1**

Reagents and Conditions: (i) 4-ethynylaniline, $[Pd(PPh_3)_4]$, CuI, THF/ Et_3N, 24 h, reflux, 28%.

Compound **63** was reacted with 4-ethynylaniliane, as above, to give **OPE-4OC1** in 28% yield. All the OPE derivatives were isolated as pale yellow solids.

4.3 Optical Properties

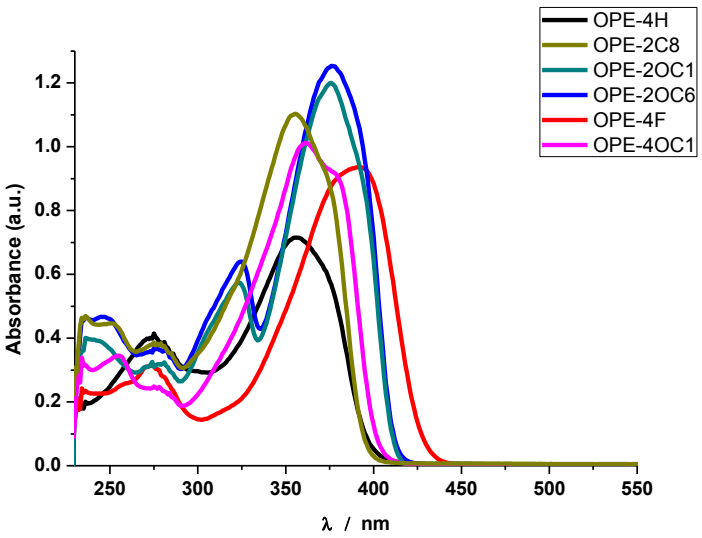

Fig. 4.2 UV-Vis absorption spectra in THF solution (1.25×10^{-5} M).

Figure 4.2 shows the UV-Vis absorption spectra of the six OPE derivatives in THF solution. The spectra of **OPE-2OC6** and **OPE-2OC1** are red shifted at λ_{max} compared to the parent **OPE-4H** as expected and reported in previous studies of analogues terminated with hydrogen atoms.[52,116] For **OPE-4F**, the spectrum is red shifted at λ_{max} compared to the parent molecule, possibly due to a charge-transfer interaction between electron-rich aminophenyl and electron deficient tetrafluorobenzene segments. Comparing the spectrum of **OPE-2C8** with the parent **OPE-4H** shows that the octyl chains do not significantly affect the position of the absorption bands.

4.4 Conductance Measurements

Single molecule conductance measurements reported below were conducted by Maria Teresa González in Prof. Nicolas Agrait's group at IMDEA-Nanociencia, Madrid. Molecular junctions were created using the break-junction technique (see detailed setup in Chapter 7). The experiments were conducted in two different environments, which produced slightly different results: with the tip and substrate immersed in a solution in trichlorobenzene (TCB); and in air, after immersing the substrates in a solution in dichloromethane (DCM) for several hours and then drying them. It was difficult to fully dry the substrates when using TCB as

solvent due to its high boiling point (214 °C, instead of 40 °C for DCM). For this reason, DCM was used for the measurements in air.

After exposing a gold substrate to a solution of the OPE molecules, the variation of conductance G was recorded while moving the tip out of contact with the substrate in the *z* direction, in successive break-junction cycles. Examples of these individual G vs *z* traces can be seen in Fig 4.3 (a), and are equivalent to those reported for **OPE-4H** for all the studied compounds.[117] Both in TCB and in air, several experimental runs were performed (changing to a new tip and substrate), with between 2000 and 5000 traces measured per run. Fig. 4.3 shows examples of the two-dimensional (2D) conductance histograms obtained from the G vs *z* traces of one experimental run. Plateaus produced in the last stages of the gold nanocontacts generate the features at 1 G_0 and above ($z < 0$), while plateaus due to the formation of molecular junctions generate the features between $\log(G/G_0) = -5$ and -4 ($z > 0$). The histograms of Fig. 4.3 were built after separating the traces with plateaus from those without plateaus. Comparing the histograms of Fig. 4.3, we observe that the shape of the prominence due to molecular junction plateaus is slightly different when working in TCB or in air from a DCM solution. The prominence extends to higher conductance and electrode-separation values in TCB, suggesting junctions with a larger number of molecules can be formed, which withstand slightly longer electrode separations before breaking.

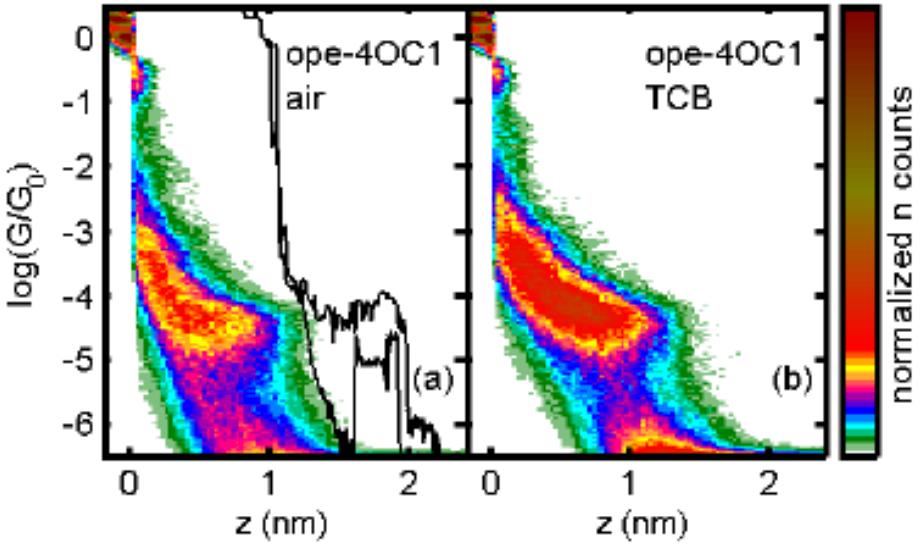

Fig. 4.3 Examples of the two-dimensional histograms built from the G vs *z* traces showing plateaus for OPE-4OC1 both in air from a DCM solution (a) and in TCB (b). Two examples of individual G vs *z* traces, shifted horizontally by 1 nm, are shown superimposed in part (a).

Two-dimensional histograms offer a complete overview of the molecular junction properties obtained in a break-junction experiment, but do not facilitate their quantitative comparison. Fig 4.4 (a) summarises the one-dimensional histograms for all the studied compounds, obtained in air from a DCM solution. Fig. 4.4 shows that the molecular-junction peaks centred near $\log(G/G_0)$ = -4.5 are very similar for all the compounds, with only **OPE-2OC6** and **OPE-2OC1** exhibiting a broader peak, which extends both to lower and higher conductance values than for the other analogs.

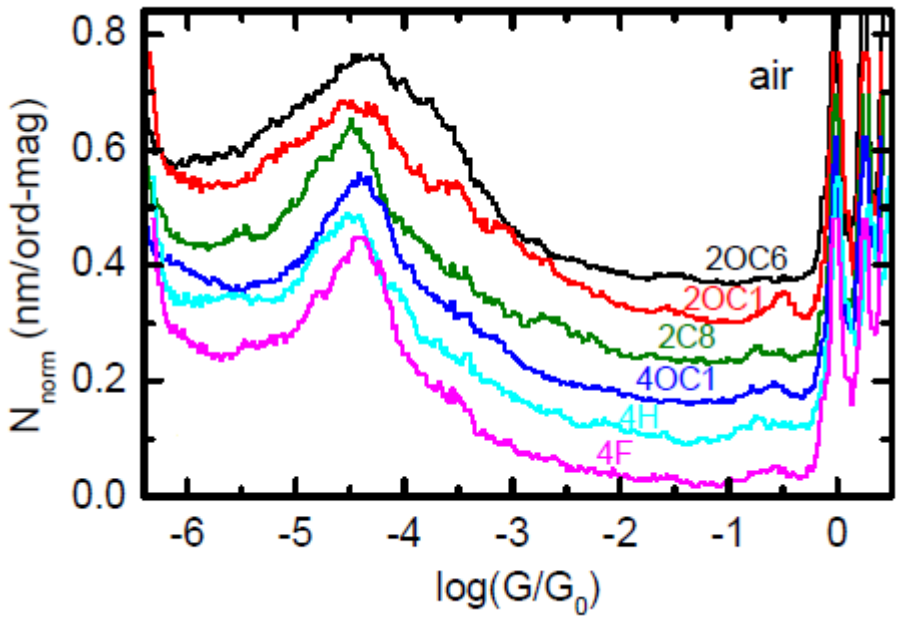

Fig. 4.4 One-dimensional logG-histograms for all the studied compounds deposited from a DCM solution and measured in air (shifted vertically for clarity).

Fig. 4.5 summarises the typical conductance values for all the analogs. These values were obtained by fitting a Gaussian to histogram peaks like those of Fig. 4.4, and averaging the maxima obtained from several equivalent experimental runs (at least three), for each analog and environment. Fig. 4.5 shows that the conductance maxima are rather constant for all the studied compounds, with a run-to-run dispersion that can be quite large (error bars in the figure). A correlation between the ionization potential (IP), and the molecular-junction conductance has been previously reported for diaminobenzene derivatives.[113]

In Fig. 4.5, the compounds are ordered according to their calculated IP, showing that there is no correlation between the conductance and the IP values in the present data for OPEs. This result establishes the resilience of the electrical conductance of OPE diamine junctions to

functionalisation. The UV-Vis absorption spectra obtained for all the analogs show that the molecular energy levels of OPE are modified by functionalisation as expected (Fig. 4.5).

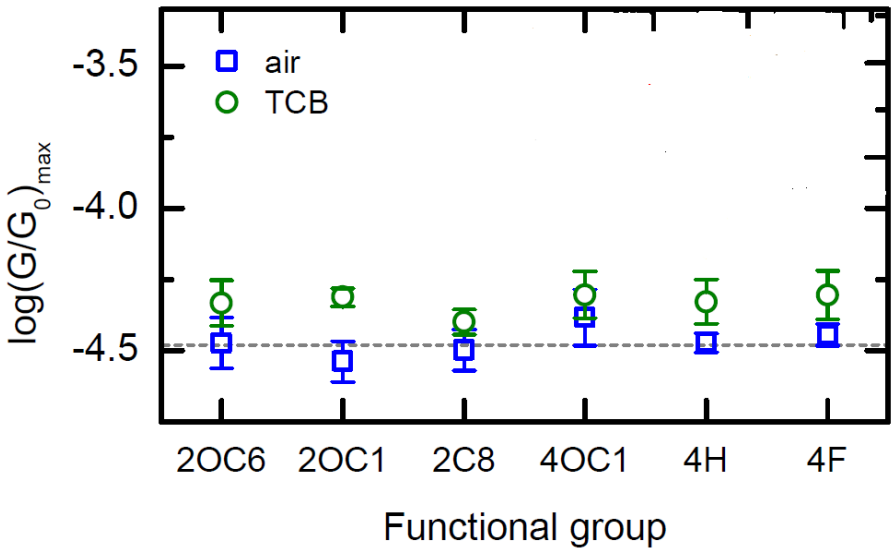

Fig. 4.5 Averaged maxima of the histograms peaks like those of Fig. 4.4 (average of at least three different experimental runs). The error bar is the standard deviation, which accounts for the run-to-run variation. The compounds have been ordered according to their ionization potential.

4.5 Conclusions

We have synthesised new OPE3 derivatives with a range of substituents on the central ring and in collaboration with IMDEA, Madrid we have compared the properties of molecular junctions formed by six OPE3 analogs with amino termini. By functionalising the central ring, we are able to modify the parent **OPE-4H** compound, without affecting the binding to the gold electrodes. In contrast with the known variability associated with changes to the terminal groups of such molecules or with atomic scale variations in the electrodes, our results show that the electrical properties of the OPE3 molecular junctions are very robust and remain essentially unaffected by the different functional groups. These results suggest that a specific function can be laterally added to an OPE diamino molecular wire without affecting its electrical transport properties, which is attractive for the design of more complex molecular architectures.

Chapter 5. The Synthesis of Functionalised Diaryltetraynes and their Transport Properties in Single-Molecule Junctions

5.1 Introduction

The study of carbon-rich compounds is a very active research topic in organic synthesis and materials chemistry.[118,119] For example, sp^2 hybridised systems (e.g. graphene, nanotubes, fullerenes) are widely investigated due to their fascinating reactivity and their outstanding electronic and optical properties.[120-122] However, the *sp* hybridised carbon allotrope $(–C{\equiv}C)_n–$ named carbyne is one of the least studied carbon allotropes due to its inaccessibility by standard synthetic routes and its insolubility.[123,124] Shorter chains of multiple conjugated alkyne units (i.e. diynes, oligoynes and polyynes) which possess terminal substituents to enhance their solubility and stability have been studied for many years.[125] They are fundamentally important molecules for experimental[126-129] and theoretical studies[130,131] of conjugation and charge-transport through carbon-rich backbones.

Oligoynes/polyyne chains $(–C{\equiv}C)_n$ have very attractive electron transport properties due to their almost cylindrical conjugation over the alternating single and triple bonds of the one-dimensional *sp*-backbone, leading to proposed applications as molecular wires, switches and non-linear optical components.[132,133] Theoretical studies suggest that polyynes could show metallic-like charge-transport characteristics when connected between two electrodes.[134,135]

The synthesis of oligoynes encounters problems as the stability decreases rapidly with the increasing number of the triple bonds in the backbone.[136] While a few C_8 derivatives [ie. $Ar–(C{\equiv}C)_4–Ar$, diaryltetraynes] and longer analogs with simple aryl end-groups are isolable at room temperature,[137,138] the established strategies for stabilising derivatives with $n \geq 4$ alkyne units are: (i) to covalently attach very bulky aryl or organometallic end-groups,[139,140] (ii) to shield the oligoyne backbone within a supramolecular rotaxane-like structure,[141,142] or (iii) to encapsulate the polyyne within a carbon nanotube.[143] The vast majority of synthetic studies on oligo/polyynes have concerned ways to stabilise longer derivatives.[144] In contrast, little attention has been given to the synthesis of derivatives which might be suitable for molecular electronics applications. This requires functionalisation with terminal substituents which will anchor the molecules to gold or other electrode materials.[43] The very bulky terminal groups which stabilise longer oligo/polyynes are not suitable for this purpose, and the traditional

anchoring groups (e.g, amine, thiol) are expected to make oligoynes unstable in ambient conditions due to inter- or intra-molecular reactions of the anchor group with the oligoyne backbone, thereby cross-linking or degrading the molecules.[145]

In this context, our group have recently reported that diaryltetrayne derivatives (**Ar4**) (Chart 5.1) with terminal pyridyl (**PY**)[75] 4-cyanophenyl (**CN**) and 2,3-dihydrobenzo[*b*]thien-5-yl (**BT**) end groups can be isolated, purified and fully characterised under standard laboratory conditions (20 ^{o}C, daylight and in air).[94] The transport properties of the **PY4**, **CN4** and **BT4** derivatives in Au/single-molecule/Au junctions were studied by scanning tunneling microscopy (STM) and mechanically controllable break junction (MCBJ) methods.[94] However, Dr. Gulcur observed that the **Ar4** analogues with 4-aminophenyl (**NH_2**) and 4-(thioacetyl)phenyl (**SAc**) end-groups rapidly decompose on attempted isolation and could not be purified.[94]

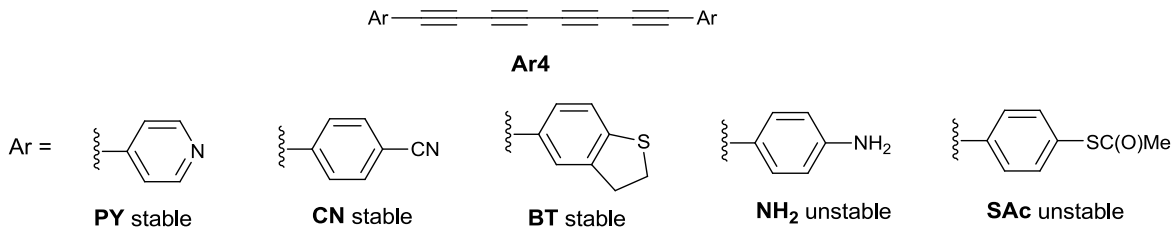

Chart 5.1 Structures of diaryltetraynes with functional end groups for definitions of 'stable' and 'unstable' see section 5.2.2.

We were interested in exploring new oligoynes to establish the scope of functionalised non-bulky end-groups which can be attached to the oligoyne chain and afford stable derivatives. We now present the synthesis of new diaryltetraynes with emphasis on derivatives which are stable under ambient conditions. New **Ar4** derivatives have been characterised by spectroscopic methods and X-ray crystallography; the ability of the stable derivatives to anchor in molecular junctions have been assessed and the electronic properties of Au/single-molecule/Au junctions are described. This new work, together with our previous reports[50,75,94] provides the most comprehensive study to date on the synthesis of functionalised oligoynes and their applications in molecular junctions.

5.2 Synthesis

Diaryltetrayne compounds **Ar4a-e** (Scheme 5.1) were synthesised by dimerisation of the trimethylsilyl protected precursor aryldiyne derivative **62a-e** under classical Eglington-

Galbraith coupling conditions.[146] Compounds **69a-d**,**f** were synthesised by reaction of the corresponding aryliodide with 1,3-butadiyne-1-trimethylsilane (BDTMS).[147] Due to the low reactivity of the starting material 5-bromo-benzo[*b*]thiophene (**65**), normal Sonogashira conditions at room temperature did not give the expected product. Unreacted starting materials were found. High temperature and a sealed vessel were used to conduct these particular reactions. Due to the instability of BDTMS (**68**) at high temperatures, compound **69f** was synthesised by a different route using 5-alkynylbenzo[*b*]thiophene (**66**) and trimethylsilyl acetylene. All steps proceeded in synthetically viable yields to afford the target diaryltetraynes **Ar4**. During the course of our work a similar synthesis of the nitrophenyl end-capped tetrayne **$NO_2$4** was reported by Szafert *et al.*[148] Compounds **Ar4a-d** were synthesised by former colleague Dr. Murat Gulcur.

Scheme 5.1 Synthesis of diaryltetraynes Ar4(a-f)

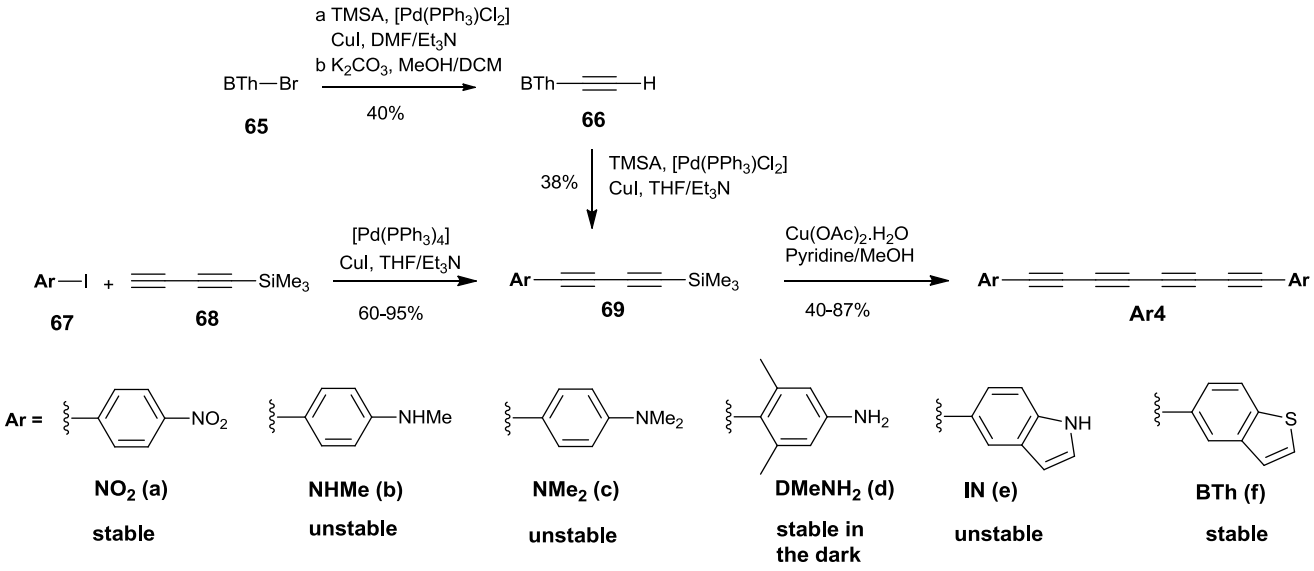

Moreover, to enable a comprehensive study to be undertaken of the length dependence of the single-molecule conductance for the BTh oligoyne series, the corresponding new butadiyne **BTh2** and tolane analogues **BTh1** were also synthesised (Scheme 5.2).

Scheme 5.2 Synthesis of compounds BTh1 and BTh2.

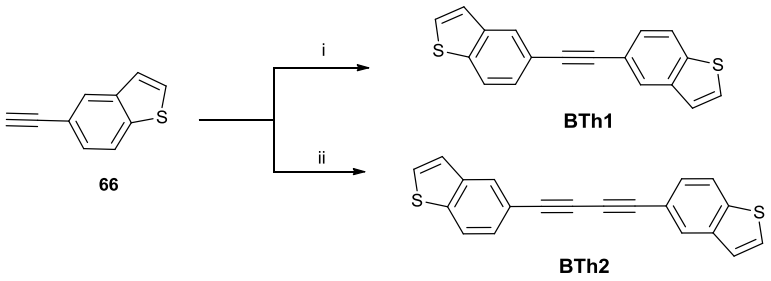

Reagents and Conditions: (i) **65**, [Pd(dppf)Cl_2], CuI, DMF/Et_3N, 16 h, 130 ^oC, 71%; (ii) [Pd(dppf)Cl_2], CuI, THF/Et_3N, 18 h, r.t., 50%.

5.3 Stability of the Diaryltetraynes

Having successfully synthesised the new derivatives **IN4** and **BTh4** we are now able to survey the stability of a wide range of functionalised diaryltetrayne derivatives. Dr. Gulcur had shown that **$NO_2$4** is stable under ambient laboratory conditions and a solid sample can be stored for several months on the shelf with no observable decomposition. The compound has very low solubility and could not be characterised by solution NMR techniques. However, a high resolution mass spectrum and the X-ray crystal structure confirmed the assigned structure.

In a previous study, the rapid decomposition under ambient conditions of 4-aminophenyl end-capped tetrayne **$NH_2$4** (Chart 5.1) was reported.[94] The probable decomposition process is an intermolecular reaction of the amino group with the *sp*-chain to form the observed dark-coloured insoluble product. In comparison to **$NH_2$4**, Dr. Gulcur observed increased stability for *N*-methylaniline end-capped tetrayne **NHMe4** which was characterised as soon as possible after isolation by ^1H, ^{13}C NMR, and mass spectroscopy. Crystals of **NHMe4** were grown in the dark and decomposition products were seen under ambient conditions. The dimethylamino analogue **$NMe_2$4** was found to be very light sensitive. Very recently, the synthesis and X-ray crystal structure of the pentayne analogue terminated with bulkier 4-(diisopropylamino)phenyl groups was reported by Diederich et al.[149]

Dr. Gulcur also found that partially shielding the oligoyne chain by *ortho*-methyl groups, compound **DMe$NH_2$4**, considerably increased the stability compared to the parent compound **$NH_2$4**. **DMe$NH_2$4** was unambiguously characterised by ^1H and ^{13}C NMR spectroscopy, mass spectrometry and X-ray crystallography, using single crystals which were grown in the dark. The NMR spectra of **DMe$NH_2$4** provided no evidence for decomposition upon storage in $CDCl_3$ in the NMR tube for 6 days in the dark after isolation. No precipitation

or colour change of the solution was observed during this time. This sample was then exposed to ambient laboratory light; after 2 h the formation of an insoluble brown-black precipitate was observed.

The new 5-indolyl end–capped tetrayne **IN4** was also light sensitive and thermally unstable. It was characterised by ^{1}H and ^{13}C NMR and mass spectrometry immediately after purification. The instability was observed as a colour change of the bright yellow crystals to dark green when exposed to ambient light at room temperature. Crystals of **IN4** for X-ray analysis were grown in the dark. In contrast, the new 5-benzothienyl analogue **BTh4** is stable for at least six months under ambient conditions, which is comparable long-term stability to the 2,3-dihydrobenzothienyl analogue **BT4** (Chart 5.1) .

5.4 X-Ray Crystal Structures of IN4 and BTh4.

The X-ray crystal structures of **IN4** and **BTh4** were solved by Dr. A. S. Batsanov. Both molecules have crystallographic C_i symmetry and therefore parallel arene rings. The tetrayne rod in **IN4** is practically linear, while in **BTh4** it is substantially bent. In **BTh4** the central bond C(12)–C(12′) forms 170.7° angles with C(7)–C(9) and C(7′)–C(9′) bonds. The molecular lengths are: **IN4** N...N′ 20.0 and **BTh4** S...S′ 20.7 Å. Similar bending was observed previously in some other diaryltetraynes synthesised by Dr. Gulcur.

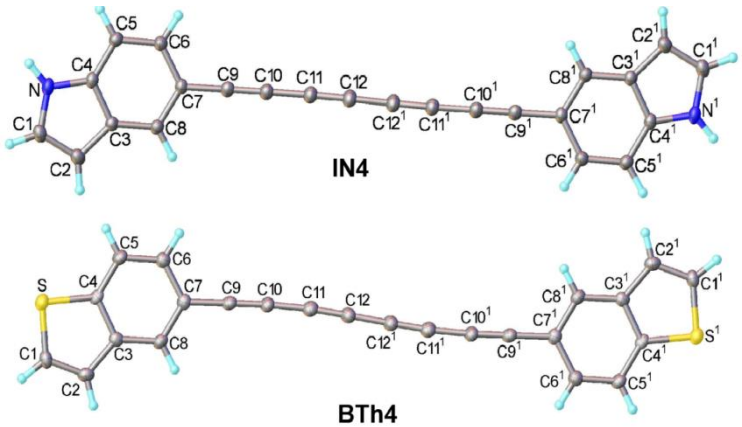

Fig. 5.1 X-ray molecular structures of IN4 and BTh4.

For **IN4** and **BTh4** the shortest C···C distances between tetrayne rods are close to the normal van der Waals contact (d = 3.5 Å) and the arene end-groups are stacked in a π–π

fashion. However, the slanting angle ϕ (50° for **IN4** and 70° for **BTh4**) is not favourable for topotactic 1,8-polymerisation, for which d = 3.5 Å and ϕ = 21° are optimal[148] (Fig. 5.2).

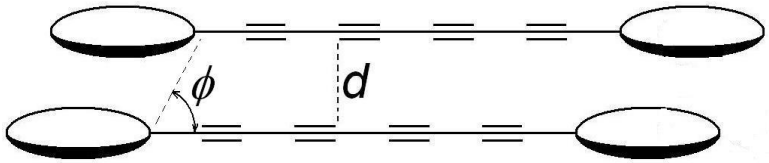

Fig. 5.2 Crystal packing simulation.

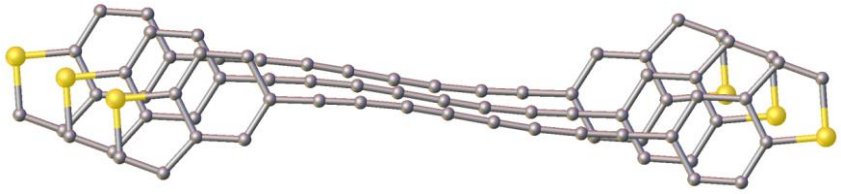

Fig. 5.3 Crystal packing of BTh4

5.5 Single-Molecule Conductance Measurements

The transport properties of single oligoyne wires were studied by STM-BJ[27,28] and complementary MCBJ[50,89] measurements in solution at room temperature and in the absence of oxygen in collaboration with Dr. Pavel Moreno-García in Prof. Wandlowski's group.

Figure 5.4A on the next page displays, as an example, typical conductance (G) versus relative distance (Δz) stretching traces, plotted in a semilogarithmic scale, as recorded for **BTh4** in TMB/THF. After formation of the contact between the gold tip and the Au(111) substrate, the tip was withdrawn with a rate of 58 nm s^{-1}. All curves show initially a step-like decrease of the conductance from 10 G_0 up to 1 G_0 with $G_0 = 2e^2/h$ = 77.5 µS being the quantum of conductance.[27] Subsequently, the conductance decreases abruptly by several orders in magnitude ("jump out of contact").[87] The very end of the gold contacts retracts by approximately (0.5 ± 0.1) nm, the so-called snap-back distance Δz_{corr}. Additional features, such as plateaus are observed at $G \leq 10^{-3} G_0$, which are attributed to the formation of (single) molecular junctions. The noise level is reached at $G < 10^{-6}$ G_0 in the STM-BJ experiments.

Several thousands of individual G versus Δz traces were recorded and subsequently analysed further by constructing all-data point histograms (without any data selection) to extract statistically significant results. Figure 5.4B displays the corresponding one-dimensional (1D) histogram of **BTh4** in a semilogarithmic scale. Peaks were observed for the breaking of Au-Au contacts as marked by integers of G_0, and one well-defined molecular-junction related

feature. A Gaussian fit led to G^* = 10^{-4} G_0 as the most probable single molecular junction conductance of **BTh4**. This value appears to be independent of the concentration of **BTh4** down to 1 μM.

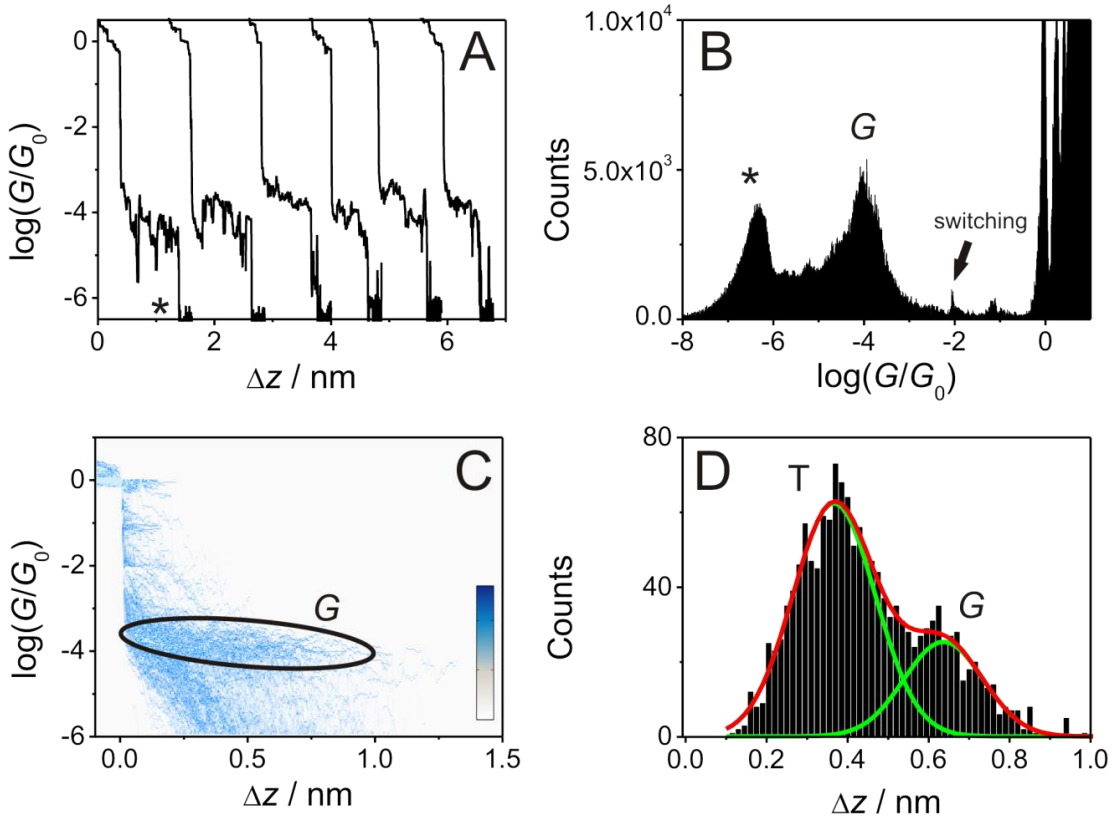

Figure 5.4 STM-BJ-based conductance measurements of BTh4 in TMB/THF (5 : 1, v/v) as recorded with V_{bias} = 0.065 V and a stretching rate of 58 nm s^{-1}. (A) Typical original conductance vs. distance traces. (B) 1D conductance histogram. The noise level is indicated by the asterix. The small spike at log (G/G_0) ≈ -2 represents an artefact related to the switching of the amplifier. (C) 2D conductance histogram generated from 1600 individual curves without any data selection. (D) Characteristic relative displacement length histogram.[50]

The above analysis was extended by constructing all-data point two-dimensional (2D) conductance vs. displacement histograms.[90,91] This representation provides direct access to the evolution of molecular junctions during the formation, stretching and break-down steps. Fig. 5.4C shows the corresponding data for **BTh4**. The individual G-Δz traces were aligned by setting the common origin to Δz = 0 at G = 0.7 G_0. The data also reveal quantized conductance features at $G \geq 1$ G_0. They correspond to the breaking of gold-gold contacts. An additional high-density data cloud is observed in $10^{-4.5}$ $G_0 \leq G \leq 10^{-3.5}$ G_0, centred on 10^{-4} G_0. This region represents the conductance range of a single **BTh4** molecule bridging the gold nanoelectrodes. The 2D histogram in Fig. 5.4C demonstrates further that the conductance decreases

monotonously with increasing relative displacement (or junction elongation) Δz. Similar results were obtained in complementary experiments employing the MCBJ-technique.

Analysing the evolution of a molecular junction upon stretching we constructed relative displacement (Δz) histograms by calculating the displacement from the relative zero position at 0.7 G_0 up to the end of the molecular conductance region of every individual trace.[50] The lower limit is defined as one order of magnitude beneath the most probable conductance G_H. Fig. 5.4D displays the characteristic displacement histograms of **BTh4**. The plot shows a uniform normal distribution (G) with a well-defined maximum Δz^* = (0.64 nm) as a measure of the most-probable plateau lengths of **BTh4** molecular junctions. Stretching traces shorter than 0.5 nm (T) were assigned to direct tunneling through solution without the formation of a molecular junction.[50] This consideration leads to a junction formation probability of 30% (Table 5.1).

Table 5.1 Single molecule conductance characteristics of molecular junctions formed by end-capped tetraynes attached to gold leads.

Molecule	L / nm[a]	Δz^*/ nm[b]	z^*/ nm[c]	G^*/G_0	JFP / %[d]	β/ nm^{-1}[e]	R_c/ kΩ[f]
BT4	2.08	1.40 ± 0.10	1.90 ± 0.10	2.0×10^{-4}	100	3.1 ± 0.2	115 ± 31
PY4	1.76	1.40 ± 0.10	1.90 ± 0.10	4.0×10^{-5}	100	2.9 ± 0.2	1900 ± 1100
CN4	2.28	0.70 ± 0.10	1.20 ± 0.10	4.0×10^{-6}	45	1.75 ± 0.1	58000 ± 20100
$NO_2$4[g]	2.14	0.60 ± 0.10	1.10 ± 0.10	1.0×10^{-7}	40	5.4 ± 0.3	980 ± 500
BTh4	2.08	0.64 ± 0.10	1.14 ± 0.10	1.0×10^{-4}	30	2.3 ± 0.2	1050 ± 650

[a] molecular length L, which is defined as the distance between the centres of the anchor atom at one end of a fully extended isolated molecule to the centre of the anchor atom at the other end. The lengths of the molecules were obtained from crystal structure data. [b] Δz^* is the most probable relative junction elongation (displacement); [c] $z^* = \Delta z^* + 0.5$ is the absolute junction elongation (displacement), [d] JFP is the junction formation probability, [e] β is the attenuation parameter as obtained from the length dependence (L) of families of oligoynes with 4, 2 and 1 triple bond(s) end-capped with the respective anchors (some of the original data are taken from ref. [94]. [f] Contact resistance as obtained from the semi-logarithmic correlation of conductance G versus molecular length L. [g] These data are based on the analysis of 600 out of 2000 traces.

Finally, the most probable absolute displacements z_H^* were obtained in a **BTh4** molecular junction formed between a gold STM-tip and an Au(111) surface by adding the snap-back distance Δz_{corr} = (0.5 ± 0.1) nm to the relative displacement Δz^*: $z_i^* = \Delta z^* + \Delta z_{corr}$,[50] which gives (1.14 ± 0.10) nm (Table 5.1). This value is smaller than the molecular length L, which is

defined as the distance between the centres of the sulfur anchor atom at one end of a fully extended isolated molecule to the centre of the anchor atom at the other end. In other words, the molecular junctions formed with **BTh4** break most often before the molecule is completely extended.

We compiled the data obtained for the entire family of stable diaryltetrayne molecular junctions following the methodology described above for **BTh4**. Table 5.1 summarises the characteristic data G^*, Δz^*, z^* and L for **BT4**, **PY4**, **CN4**, **$NO_2$4** and **BTh4**. We note that the low junction conductance value of **$NO_2$4** was obtained in the MCBJ setup, which allows more sensitive electrical measurements down to $10^{-8.5}$ G_0.[89] The following trend is seen in the most probable molecular junction conductances:

$$G^*(\mathbf{BT4}) > G^*(\mathbf{BTh4}) > G^*(\mathbf{PY4}) > G^*(\mathbf{CN}) > G^*(\mathbf{NO_2 4})$$

The junction formation probabilities decrease from 100% for **BT4** and **PY4** to values below 50% for the other three derivatives. In combination with the values of the most probable absolute displacements z^*, which are considerably smaller than the molecular length L, we conclude that tetrayne-type molecular junctions terminated with -**CN**, -**BTh** and -**NO_2** anchors are rather unstable and break at an inclined angle with respect to the surface normally before they are fully extended. The comparison with previous experimental observations[50,94] suggests that these termini are less favourable for the formation of stable molecular junctions. However, we note that the results of the current study deviate from recent observations of Zotti *et al*.[150] who concluded, based on MCBJ experiments in air under ambient conditions, that molecular junctions formed with **NO_2** capped tolanes are rather stable. This difference may arise from the nature of the different experimental conditions in both studies.

No reliable single molecule junction conductance measurements could be carried out for **NHMe4**, **DMeN$H_2$4**, **IN4**, **$NH_2$4** and **SH4** due to their limited chemical stability under current experimental conditions. In the case of **$NMe_2$4** the two methyl substituents of the nitrogen prevented the formation of stable molecular contacts, which led to bare tunneling traces.

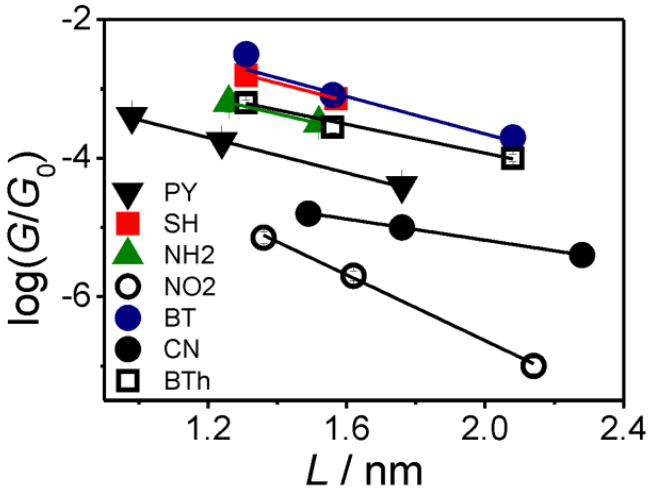

Figure 5.5 Most probable single junction conductance values *G of families of oligoynes as obtained from the analysis of the 1D and 2D conductance histograms in dependence on the length of the molecule.**

Fig. 5.5 compares the dependencies of the most probable single junction conductances on molecular length *L*, as constructed from the experimental data of the five tetraynes (**PY4**,[94] **$NO_2$4**,[94] **BT4**,[94] **CN4**[94] and **BTh4**) together with data for the shorter butadiyne and tolane analogues with seven different end-groups. Analysing these data with reference to a simple tunneling model, which is represented by $G^* = G^*_c \cdot \exp(-\beta \cdot L)$, leads to the attenuation constant β and to the contact conductance G_c^*. $G_c^* = 1/R_c$ represents an effective contact conductance reflecting the electronic coupling at the molecule-electrode interface. R_c is the corresponding contact resistance. β is the attenuation constant, which characterises the electronic coupling in a specific molecular backbone as a function of its length. The experimentally determined β values range between (1.75 ± 0.1) nm^{-1} (**CN**) to (5.4 ± 0.3) nm^{-1} (**NO_2**). The distinctly different values of β demonstrate that the nature of the anchor group controls the strength of the electronic coupling to the metal leads, the position of the energy levels involved in the electron transport across the single molecule junction as well as their coupling into the wire backbone. For comparison, data are added for the **NH_2** and **SH** end-capped oligoynes despite the limited data set due to the instability of the tetraynes.[94] The resulting values of the attenuation constant β are comparable with those of other π-conjugated molecular wires, such as oligo(phenyleneethynylene)s,[69,101,151] oligophenyleneimine[64] and oligo(phenylenevinylene)s.[152] We conclude that stable molecular wires bearing an oligoyne backbone in combination with proper anchor groups may act as promising building blocks in more complex molecular assemblies combining functional units.

5.6 Conclusions

We have synthesised new oligoyne derivatives with emphasis on obtaining stable diaryltetraynes with anchor groups which are suitable for attaching the molecules to gold electrodes. The tetraynes **Ar4a-f** have been synthesised by dimerisation of the trimethylsilyl-protected precursor aryldiyne derivative under classical Eglington-Galbraith coupling conditions. Under ambient laboratory conditions (20 ^{o}C, daylight and in air) the tetraynes **$NO_2$4** and **BTh4** are stable for at least six months without observable decomposition, whereas **NHMe4**, **$NMe_2$4**, **$DMeNH_2$4** and **IN4** decompose within a few hours or days. These results, in combination with previous studies,[94] provide a comprehensive assessment of the range of functional groups which can be tolerated at the terminal positions of diaryloligoynes. The X-ray molecular structures are reported for **IN4** and **BTh4**. STM-BJ and MCBJ techniques have been employed to probe the single-molecule conductance characteristics of the series of oligoynes with terminal 4-nitrophenyl and 5-benzothienyl groups and four, two and one triple bond(s) in the backbone. We conclude that with careful choice of the anchor group oligoynes are a viable family of stable molecular wires for molecular electronics applications. It remains a challenge to synthesise longer oligoynes (i.e. with > four triple bonds) that are stable and contain functional groups that enable the molecules to anchor to gold electrodes.

Chapter 6. Anthraquinone Functionalised Molecular Switch

6.1 Introduction

Among all the interesting properties of molecular electronics, the ability to tune and control the conductance of the device is under the most intense studies.[153] As discussed in Chapter 1, molecules that can be switched between two distinct "on" and "off" states have been reported. The inducement can be either light,[154,155] bias voltage,[37] or electrochemical conditions.[30] In 2006, van Dijk *et al.* studied a molecular wire bearing an anthraquinone core and thioacetyl end groups. By a two-electron reduction process, the core can be switched from cross conjugated (low conductance "off") to linear conjugated (high conductance "on"). As discussed in Chapter 3, cross conjugated systems suffer from a destructive quantum interference which dramatically reduces the conductance.[156]

Due to the possibilities to be electrochemically switched between "on" and "off" states, anthraquinone centred molecular wires have received intense studies both theoretically[157] and experimentally.[158,159]

By measuring single molecule conductance of three oligo(phenyleneethynylene) (OPE)-type dithiolated molecules, namely an anthracence-based linearly conjugated wire (**70**), an 9,10-anthraquinone-based cross-conjugated wire (**71**), and a 9,10-dihydroanthracene-based wire (**72**) (Fig. 6.1), Hong *et al.*[89] reported that the conductance of the cross-conjugated molecule **71** is five times lower than that of the broken π-conjugated molecule **72** and the conductance of **72** is several hundred times lower than that of linearly conjugated molecule **70**. They pointed out that the lower conductance of **71** is due to destructive quantum interference present in the molecular bridge.[157]

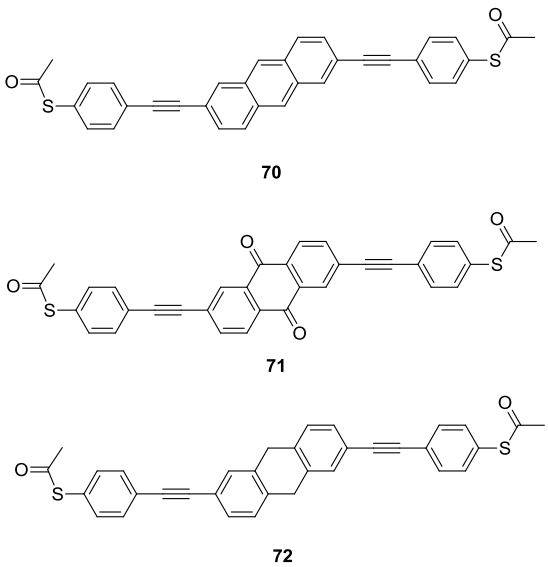

Fig. 6.1 Molecule structures studied in Hong's work. (Reproduced from reference[89])

Fracasso *et al.*[158] also reported a similar sequence when these molecules formed self-assembled monolayers (SAMs). More recent studies have reported the destructive quantum interference present in the anthranquinone core.[159,160]

However, among all these studies, few of them reported the switching between linear conjugation and cross conjugation at the stage that a single molecule is assembled between two electrodes. To further explore the influence of quantum interference on the single molecule conductance and to enable successful switching during single molecule measurements, we designed the following molecules which are shown in Scheme 6.1 and 6.2.

6.2 Synthesis

Scheme 6.1 synthesis of 2,6-AQ and 1,5-AQ

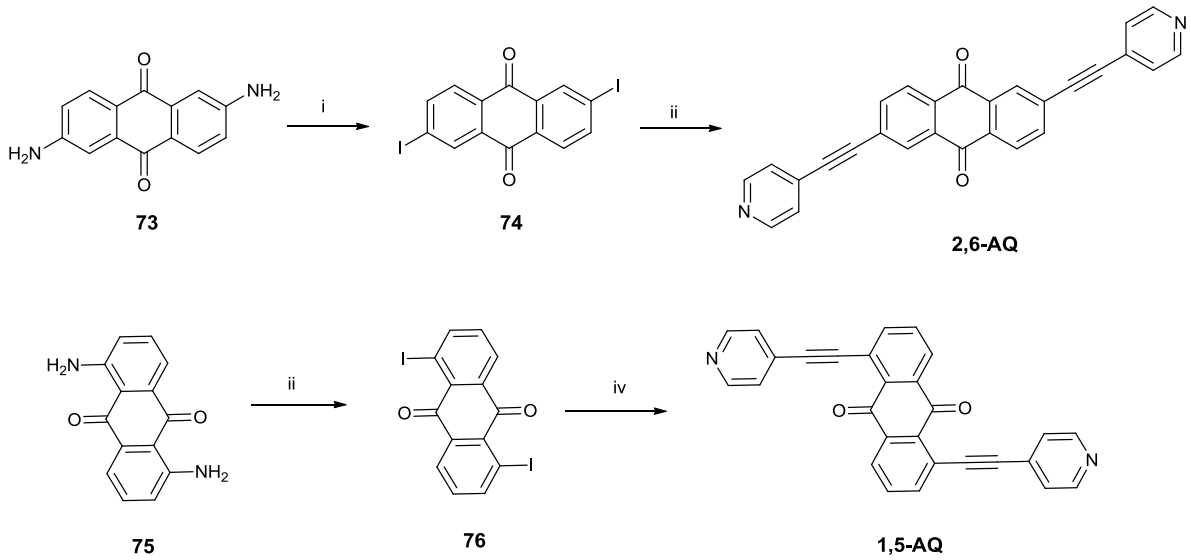

Reagents and conditions: (i) $NaNO_2$, KI, H_2SO_4/H_2O, 5 h, 80 ^oC, 71%; (ii) 4-iodopyridine, $[Pd(PPh_3)_4]$, CuI, THF/Et_3N, 22 h, 50 ^oC, 62%. (iii) $NaNO_2$, KI, H_2SO_4/H_2O, 5 h, 80 ^oC, 33%; (iv) 4-iodopyridine, $[Pd(PPh_3)_4]$, CuI, THF/Et_3N, 19 h, 50 ^oC, 50%.

Iodoarenes were chosen as the intermediates, instead of bromoarenes, due to the enhanced reactivity of iodo derivatives with 4-ethynylpyridine. 2,6-Diiodoanthraquinone (**74**) and 1,5-diiodoanthraquinone (**76**) were successfully obtained from standard iodination processes. The final products **2,6-AQ** and **1,5-AQ** were synthesised under Sonogashira conditions with moderate yields (62% and 50%, respectively).

However, after conducting the same iodination process which yielded the previous iodoarenes on 1,4-diaminoanthraquinone (**77**), the product was not the expected 1,4-diiodoanthraquinone (**78**). Instead it was 1-amino-4-iodoanthraquinone (**79**) in 50% yield. The same product was produced when this reaction was repeated. As it is known that the iodination process goes through a diazonium salt intermediate, it is unfavourable for a benzene ring to bear two positive charges at the same time, which could explain the failure to obtain **78** directly. Accordingly, the mono-iodinated compound **79** was iodinated again in a second step to yield the expected diiodo intermediate (**78**). The final product **1,4-AQ** was then produced under Sonogashira conditions in 90% yield (Scheme 6.2).

Scheme 6.2 synthesis of 1,4-AQ

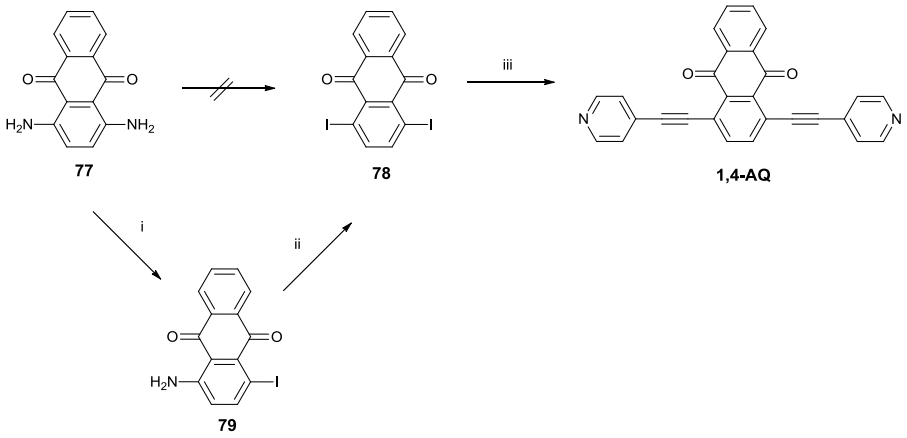

Reagents and conditions: (i) $NaNO_2$, KI, H_2SO_4/H_2O, 5 h, 80 ^oC, 50%; (ii) $NaNO_2$, KI, H_2SO_4/H_2O, 5 h, 80 ^oC, 51%; (iii) 4-iodopyridine, $[Pd(PPh_3)_4]$, CuI, THF/Et_3N, 20 h, 50 ^oC, 90%.

6.3 Conclusions

Three new isomeric molecules (**2,6-AQ, 1,5-AQ** and **1,4-AQ)** bearing an anthraquinone core were synthesised and fully characterised. With the variation of positions of the anchor groups linking onto the anthraquinone core, the influence of QI effects can be studied. New techniques which combine electrochemistry and break junction techniques will enable the switching properties of these molecules to be studied. These molecules are currently being tested in Prof. Wandlowski's group in Bern.

Chapter 7. Experimental Procedures

7.1 Experimental Setups for the Techniques Used to Measure Single Molecular Conductance

MCBJ Techniques Used in Bern

The MCBJ experiments are based on the formation and breaking of a nanogap between a notched, freely suspended gold wire (0.1 mm diameter, 99.999%, Goodfellow), fixed on spring steel sheets (10 mm × 30 mm, thickness 0.25 mm) with a two-component epoxy glue (Stycast 2850 FT with catalyst 9). The sample sheets were fixed between two holders. A Kel-F liquid cell with a Kalrez O-ring was mounted onto the sheet. During the measurements, the steel sheet could be bent with a pushing rod, which was controlled by a combination of a stepper motor and a piezo stack. The bending was initialized by the stepper motor. Once the measured current decreased to a value, corresponding to 15 G_0, the stepper motor is stopped, and the piezo stack was activated. This strategy reduced significantly noise contributions from the operation of the stepper motor. The movement of the piezo stack controlled the breaking and the reformation of nanoscale contacts, typically in the range between the noise threshold ($G < 10^{-8}\ G_0$) and a high conductance limit, which was set to 10 G_0. Molecular junctions could form upon breaking the gold-gold nanocontacts. The entire cycle was repeated at least 1000 times to obtain statistically relevant data. In the MCBJ setup, the current could be recorded as a feedback signal at a given bias voltage (typically between 0.020 and 0.200 V). The two ends of the "broken wire" were taken as working electrodes WE1 and WE2.

The MCBJ unit is controlled by a lab-built bipotentiostat with two bipolar tuneable logarithmic *I–V* converters as current measuring units, which are operated by a custom-designed micro-controller. The system provides three analog signals: the potential of WE1, the voltage difference between the two working electrodes WE1 and WE2 (bias voltage V_{bias}), driving the current through the two gold electrodes for the conductance measurements, and the voltage output of the piezo stack in the range of 0 to 50 V, allowing the displacement of the piezo stack up to 8 µm with rates ranging from 3 to 3000 nm s^{-1}. The latter translates into lateral pulling (pushing) rates between the two gold leads of 0.1 to 100 nm s^{-1}. The distance between the two gold electrodes in the MCBJ setup was calibrated with complementary STM-BJ experiments assuming that the tunneling decay is identical under the same experimental conditions.

STM-BJ Techniques Used in Bern

The STM-BJ experiments were carried out with a modified Molecular Imaging Pico SPM equipped with a dual-channel preamplifier and housed in an all-glass argon-filled chamber. The current (i_T)-distance (Δz) measurements were performed with a separate, lab-built analog ramp unit. The sample electrodes were Au(111) disks, 2 mm height and 10 mm in diameter, or gold single crystal bead electrodes. The Au(111) substrates were flame-annealed before each experiment. The STM tips were uncoated, electrochemically etched gold wires (Goodfellow, 99.999%, 0.25 mm diameter). The solutions were prepared from 1,3,5-trimethylbenzene (TMB, Aldrich, p.a.) and tetrahydrofuran (THF, Aldrich, p.a.), volume ratio 4 : 1, containing typically 0.1 mM of the target molecules. The substrate surface was inspected by STM-imaging before the start of each set of i_T-Δz measurements. Typically, we recorded 2000 to 3000 individual traces with a pulling rate of 58 nm s^{-1}.

STM-BJ Techniques Used in IMDEA-Nanociencia

The equipment is a lab-built scanning tunneling microscope (STM), designed for high stability measurements, at room temperature, in air or liquid environments. Commercial gold substrates on quartz (Arrandee) were cleaned in boiling ethanol, and flame-annealed with a butane flame. As STM tips, a 0.25 mm gold wire (99.99%), freshly cut before use, was used. A liquid cell made of PEEK was fixed over the gold substrate with the help of a Kalrez O-ring, which assured the tightness of the cell. During the break-junction experiment, the tip moved vertically (with a 0.8 pm resolution) in and out of contact with the substrate to form and break gold contacts, during which time the conductance G = I/V of the circuit was measured. A bias voltage V of 200 mV was maintained between the tip and the substrate, and a linear current-to-voltage converter with two amplification stages was used to measure the current I in the circuit. A 200 kΩ resistor, in-series with the substrate-tip circuit, prevented the current to increase out of the measurement range when a gold contact a few atoms thick is formed. This allowed us to verify that a gold contact was reformed in each break-junction cycle. The gains in this work were 10^7 V/A after the first amplification stage, and 2×10^9 V/A after the second. These conditions allowed a range of conductance down to 5×10^{-7} G_0 to be explored Experiments were performed in two different environments, which produced slightly different results: with the tip and substrate immersed in a solution in trichlorobenzene (TCB); and in air, after immersing the substrates in a solution in dichloromethane (DCM) for several hours and then drying it. It was found to be difficult to fully dry the substrates when using TCB as solvent

due to its high boiling point (214 °C, instead of 40 °C for DCM). For this reason, DCM was used for the measurements in air.

7.2 General Experimental Procedures

All reactions were conducted under a blanket of argon which was dried by passage through a column of phosphorus pentoxide unless otherwise stated. All commercial chemicals were used without further purification. Anhydrous toluene, tetrahydrofuran (THF), dichloromethane (DCM) and diethyl ether (Et_2O) were dried through an HPLC column on an Innovative Technology Inc. solvent purification system. Petroleum ether (PE) used for column chromatography is bp. 40-60 °C fractions and was used as received. Column chromatography was carried out using 40-60 µm mesh silica (Fluorochem). Analytical thin layer chromatography (TLC) was performed on 20 mm pre-coated plates of silica gel (Merck, silica gel 60F254); visualization was made using ultraviolet light (254 and 365 nm). NMR spectra were recorded on: Bruker Avance-400, Varian VNMRS 700 and Varian Inova 500 spectrometers. Chemical shifts are reported in ppm relative to $CDCl_3$ (7.26 ppm), CD_2Cl_2 (5.32 ppm), DMSO-d_6 (2.50 ppm), acetone-d_6 (2.09 ppm) or tetramethylsilane (0.00 ppm). Melting points were determined in open-ended capillaries using a Stuart Scientific SMP40 melting point apparatus at a ramping rate of 2 °C/min. Mass spectra were measured on a Waters Xevo OTofMS with an ASAP probe. Electron ionisation (EI) mass spectra were recorded on a Thermoquest Trace or a Thermo-Finnigan DSQ. Ion analyses were performed on a Dionex 120 Ion Chromatography detector. Elemental analyses were performed on a CE-400 Elemental Analyzer. UV-Vis absorption spectra were obtained on a Unicam UV2 UV/Vis spectrometer.

7.3 General Synthetic Procedures

General Procedure for Sonogashira Cross-Coupling Reactions (I): To a solution of the iodoarene (1.0 eq), $[Pd(PPh_3)_4]$, or $[PdCl_2(PPh_3)_2]$, (3-5% mole) and CuI (3-5% mole) in THF/Et_3N (3:1 v/v) or THF/(*i*-Pr)$_2$NH (3:1 v/v) mixture (7 mL per 1 mmol of iodoarene), the alkyne was added and the mixture was stirred at 20 °C under argon for 6-36 h. The solvent was removed by vacuum evaporation and the product was purified by column chromatography using the eluent stated.

General Procedure for Deprotection of TMS-protected Species (II): The protected species was dissolved in THF/MeOH mixture or THF, and excess K_2CO_3 or tetrabutylammonium fluoride

(TBAF) (1 M in THF) was added. The reaction was monitored by TLC. When complete, NH_4Cl (10% aq) or water was added and the mixture was extracted into DCM. The organic layer was dried with $MgSO_4$ and the solvent was removed by vacuum evaporation. Purification was achieved by column chromatography using the eluent as stated.

General Procedure for Deprotection Reactions of an Isopropanol Protected Species (III): (a) To achieve mono-deprotection of a di-protected derivative. To a stirred solution of the 3-hydroxy-3- methylbutynyl compound in toluene was added excess NaOH, and the mixture was heated to 70 °C. TLC analysis was used to monitor the reaction. When the desired mono-deprotected derivative was observed to be the major product, the reaction was quenched with water and saturated NH_4Cl solution was added. The product mixture was extracted with dichloromethane and the organic layer was separated and dried with $MgSO_4$. The solvent was removed by vacuum evaporation and the product was purified by column chromatography using the eluent stated.

(b) To achieve bis-deprotection of a di-protected derivative. The same procedure as described in (**a**) was followed, except the reaction temperature was 100 °C.

General Procedure for Oxidative Homo-Couplings of TMS-Alkynes (IV): TMS-alkyne was dissolved in MeOH/pyridine (1:1 v/v) mixture (10 ml per mmol) and $Cu(OAc)_2.H_2O$ (2 equiv., 0.400 g per mmol) was added to the mixture in one portion and stirred until the reaction is complete (judged by TLC). The reaction was quenched by adding saturated NH_4Cl solution (5 ml per mmol) and diluted with DCM (25 ml per mmol), dried over $MgSO_4$ and the solvents were removed under reduced pressure. The crude product was purified either by column chromatography or recrystallization.

7.3.1 Experimental for Chapter 2

1,4-diiodo-2,5-dimethoxybenzene; 27

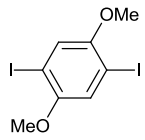

To a solution of **26** (3.138 g, 22.7 mmol), in acetic acid (150 ml), water (15 ml) and concentrated sulphuric acid (1.5 ml), potassium iodate (4.24 g, 19.8 mmol) and iodine (5.79g, 22.9 mmol) were added and the reaction mixture was stirred at 100 °C for 18 h. Water was added to quench the reaction and DCM was used to extract the product. The organic layer was then washed with 10% $Na_2S_2O_3$ (aq) and water, and dried with $MgSO_4$. White crystals **27** (5.88

g, 63% yield) were gained from recrystallization using ethanol. m.p.: 173.0-174.5 °C. ^{1}H NMR (400 MHz, $CDCl_3$): δ 7.19 (s, 2H), 3.83 (s, 6H); ^{13}C NMR ($CDCl_3$, 100 MHz): δ 153.5, 121.8, 85.6, 57.4. MS (ASAP+) *m/z* : 390.1 (M^+, 100%). The NMR spectroscopic data are in agreement with those in the literature.[79]

1,4-bis(4-ethynylpyridine)-2,5-dimethoxylbenzene; OPE3b/p-p-p (2OMe)

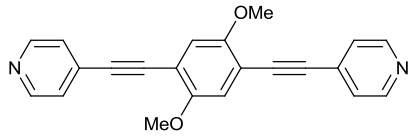

OAE3b. General Procedure (I): **27** (100 mg, 0.27 mmol), CuI (2.5 mg), [$Pd(PPh_3)_4$], (15.6 mg), 4-ethynylpyridine[161] (58 mg, 0.56 mmol), THF/Et_3N (12 ml), 18 h, r.t.. Solvent was removed by vacuum evaporation. Purification by column chromatography using diethyl ether/ethyl acetate (1:1 v/v) as eluent gave **OAE3b** (26 mg, 30% yield). m.p.: 189.1-190.2 °C. ^{1}H NMR (400 MHz, $CDCl_3$) δ 8.63 (dd, *J* = 4.5, 1.6 Hz, 4H), 7.44 (dd, *J* = 4.5, 1.6 Hz, 4H), 7.07 (s, 2H), 3.94 (s, 6H). ^{13}C NMR ($CDCl_3$, 101 MHz): δ 154.57, 150.04, 131.49, 125.72, 116.19, 113.63, 92.71, 90.21, 56.78; HR-MS (ASAP+) m/z Calcd for $C_{22}H_{16}N_2O_2$ $[M]^+$ 340.1212, found m/z: $[M]^+$ 340.1229. Calcd for $C_{22}H_{16}N_2O_2$: C, 77.63; H, 4.74; N, 8.23. Found: C, 77.79; H, 4.89; N, 8.10.

1,4-diiodo-2,5-hexyloxybenzene; 29

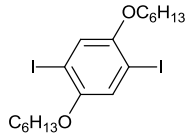

To a solution of **28** (1.7 g, 6.1 mmol), in acetic acid (45 mL), water (4.5 mL) and concentrated sulphuric acid (0.45 mL), potassium iodate (0.8 g, 3.8 mmol) and iodine (1.7 g, 6.8 mmol) were added and the reaction mixture was stirred at 100 °C for 24 h. Water was added to quench the reaction and DCM was used to extract the product. The organic layer was then washed with 10% $Na_2S_2O_3$ (aq) and water, and dried with $MgSO_4$. White crystals **29** (2.4 g, 74% yield) were obtained from recrystallization using ethanol. m.p.: 62.0-63.3 °C. ^{1}H NMR (400 MHz, $CDCl_3$) δ 7.19 (s, 2H), 3.95 (t, *J* = 6.6 Hz, 4H), 1.82 (m, 4H), 1.54 (m, 4H), 1.37 (m, 8H), 0.94 (m, *J* = 6.6 Hz, 6H). ^{13}C NMR (101 MHz, $CDCl_3$) δ 151.86, 121.77, 85.33, 69.36, 30.49, 28.14, 24.74, 21.62, 13.08. The NMR spectroscopic data are in agreement with those in the literature.[162]

1,4-Bis(2-methyl-3-butyn-2-ol)-2,5-bis(hexyloxy)benzene; 30

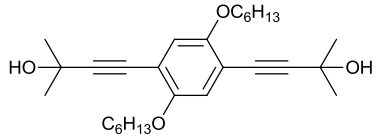

General Procedure (I): **29** (3.00 g, 5.7 mmol), [$PdCl_2(PPh_3)_2$] (400 mg), CuI (108 mg), 2-methyl-3-butyn-2-ol (2.34 g, 28.5 mmol), THF/Et_3N (37 ml), 20 h, r.t.. Solvent was removed by vacuum evaporation and purification by column chromatography using DCM/ethyl acetate (95:5 v/v) as eluent gave **30** as a white solid (2.40 g, 95% yield). m.p.: 107.0-108.0 °C. ^{1}H NMR (400 MHz, $CDCl_3$) δ 6.78 (s, 2H), 3.86 (t, *J* = 6.6 Hz, 4H), 2.05 (s, 2H), 1.70 (m, 4H), 1.57 (s, 12H), 1.41 (m, 4H), 1.26 (m, 8H), 0.84 (t, *J* = 6.6 Hz, 6H). ^{13}C NMR (101 MHz, $CDCl_3$) δ 153.54, 117.02, 113.33, 99.03, 78.44, 69.45, 65.75, 31.58, 31.43, 29.30, 25.69, 22.62, 14.03. HR-MS (ASAP+) *m/z* calcd for $C_{28}H_{42}O_4$ $[M]^+$ 442.3083, found *m/z* : $[M]^+$ 442.3066.

2,5-Dihexyloxy-4-(2-methyl-3-butyn-2-ol)iodobenzene; 31

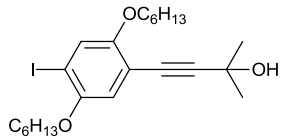

General Procedure (I): **29** (1.00 g, 1.9 mmol), CuI (24.7 mg), [$Pd(PPh_3)_4$] (150 mg), 2-methyl-3-butyn-2-ol (174 mg, 2.1 mmol), THF/Et_3N (25ml), 8 h, r.t.. Solvent was removed by vacuum evaporation. Purification by column chromatography using DCM as eluent gave **31** as a pale brown oil. (0.57 g, 45% yield). ^{1}H NMR (400 MHz, $CDCl_3$) δ 7.18 (s, 1H), 6.73 (s, 1H), 3.86 (m, 4H), 1.72 (m, 4H), 1.55 (s, 6H), 1.43 (m, 4H), 1.28 (m, 8H), 0.84 (m, 6H). ^{13}C NMR (101 MHz, $CDCl_3$) δ 154.56, 151.94, 123.89, 116.36, 113.17, 98.78, 87.67, 78.41, 70.31, 69.91, 65.98, 31.80, 31.72, 31.64, 29.50, 29.36, 25.96, 25.92, 25.90, 22.87, 22.82, 14.29. The NMR spectroscopic data are in agreement with those in the literature.[163]

1-(Ethynyl)-4-(2-methyl-3-butyn-2-ol)-2,5-bis(hexyloxy)benzene; 32

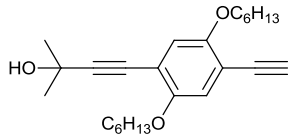

General Procedure (III) (a): **30** (2.00 g, 4.5 mmol), NaOH (10 g), toluene (100 ml), 6 h, 70 °C. Purification by column chromatography using DCM as eluent gave **32** as a yellow solid (1.10 g, 65% yield). m.p.: 48.2-49.0 °C. ^{1}H NMR (400 MHz, $CDCl_3$) δ 6.77 (s, 2H), 6.72 (s, 2H), 3.79 (m, 4H), 3.16 (s, 1H), 1.88 (s, 1H) 1.63 (m, 4H), 1.46 (s, 6H), 1.32 (m, 4H), 1.18 (m, 8H), 0.75(m, 6H).

^{13}C NMR (101 MHz, $CDCl_3$) δ 154.1, 153.4, 117.7, 117.1, 114.0, 112.6, 99.2, 82.1, 79.9, 78.3, 69.6, 69.4, 65.7, 31.5, 31.5, 31.5, 31.4, 29.2, 29.1, 25.6, 25.5, 22.6, 14.0, 13.9. The NMR spectroscopic data are in agreement with those in the literature.[163]

Compound 33

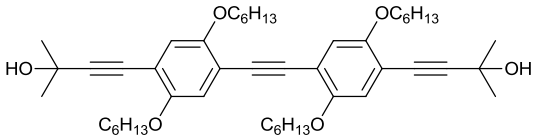

General Procedure (I): **31** (1.6 g, 3.3 mmol), CuI (31 mg), $[Pd(PPh_3)_4]$ (191 mg), THF/Et_3N (26 ml), **32** (1.0 g, 2.6 mmol), 18 h, 50 °C. Solvent was removed by vacuum evaporation. Purification by column chromatography using DCM/ethyl acetate (9:1 v/v) as eluent gave **33** as a yellow solid (2.0 g, 95% yield). m.p.: 107.3-107.8 °C. ^{1}H NMR (400 MHz, $CDCl_3$) δ 6.88 (s, 2H), 6.83 (s, 2H), 3.90 (m, 8H), 1.96 (s, 2H), 1.74 (m, 8H), 1.56 (s, 12H), 1.43 (m, 8H), 1.28 (m, 16H), 0.83 (m, 12H). ^{13}C NMR (101 MHz, $CDCl_3$) δ 153.64, 153.40, 117.30, 117.00, 114.28, 113.34, 99.16, 91.17, 78.58, 69.72, 69.41, 65.79, 31.60, 31.45, 29.34, 29.26, 25.72, 25.64, 22.62, 14.04, 14.02. HR-MS (ASAP+) m/z calcd for $C_{48}H_{70}O_6$ $[M+H]^+$ 743.5251, found m/z : $[M+H]^+$ 743.5236.

1,2-bis(4-ethynyl-2,5-bis(hexyloxy)phenyl)ethyne; 34

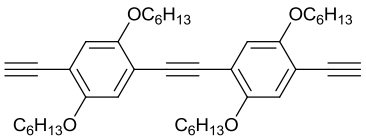

General Procedure (III) (b): 33 (1.0 g, 1.3 mmol), NaOH (10 g), toluene (100 ml), 22 h. Purified by column chromatography using DCM/hexane (1:3 *v*/*v*) as eluent to give a yellow solid **34** (300 mg, 36% yield). m.p.: 83.2-83.8 °C. ^{1}H NMR (400 MHz, $CDCl_3$) δ 6.91 (s, 2H), 6.90 (s, 2H), 3.92 (m, 8H), 3.27 (s, 2H), 1.75 (m, 8H), 1.42 (m, 8H), 1.27 (m, 16H), 0.83 (m, 12H). ^{13}C NMR (101 MHz, $CDCl_3$) δ 154.16, 153.36, 118.00, 117.11, 114.87, 112.70, 91.21, 82.28, 80.02, 69.75, 69.65, 31.59, 31.53, 29.24, 29.15, 25.63, 25.60, 22.61, 22.57, 14.00. HR-MS (ASAP+) *m/z* calcd for $C_{42}H_{58}O_4$ $[M]^+$ 626.4335, found *m/z* : $[M]^+$ 626.4325.

OAE4

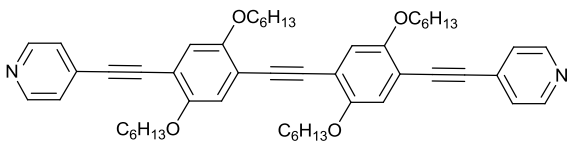

General Procedure (I): 4-iodopyridine (82 mg, 0.4 mmol), [$Pd(PPh_3)_4$] (18 mg), CuI (3 mg), **34** (100 mg, 0.16 mmol), THF/Et_3N (6 ml), 23 h, r.t.. Solvent was removed by vacuum evaporation and purification by column chromatography using DCM/ethyl acetate (4:1 v/v) gave **OAE4** as a bright yellow solid (110 mg, 88% yield). Crystals for X-ray analysis were grown from dichloromethane/ethanol solution. m.p. 107.0-107.5 °C. ^{1}H NMR (700 MHz, $CDCl_3$) δ 8.60 (d, *J* = 5.6 Hz, 4H), 7.37 (d, *J* = 5.6 Hz, 4H), 7.02 (s, 2H), 7.01 (s, 2H), 4.03 (m, 8H), 1.84 (m, 8H), 1.52 (m, 8H), 1.34 (m, 16H), 0.89 (m, 12H); ^{13}C NMR (151 MHz, $CDCl_3$) δ 153.98, 153.45, 149.61, 131.69, 125.41, 117.14, 116.96, 115.33, 112.66, 91.94, 91.75, 90.80, 69.74, 69.51, 31.58, 31.54, 29.25, 29.23, 25.71, 25.64, 22.62, 14.01, 13.99; HR-MS (ASAP+) *m/z* Calcd for $C_{52}H_{65}N_2O_4$ $[M+H]^+$ 781.4944, found *m/z* : $[M+H]^+$ 781.4937.

1,4-Bis(ethynyl)-2,5-bis(hexyloxy)benzene; 35

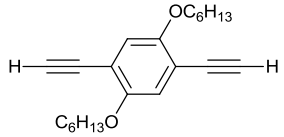

General Procedure (III) (b): **30** (2.00 g, 4.5 mmol), NaOH (10 g), toluene (100 ml), 12 h at 100 ^{o}C. Purification by column chromatography using DCM as eluent gave **35** as a yellow solid (1.20 g, 82% yield). m.p.: 72.2-73.5 °C. ^{1}H NMR (400 MHz, $CDCl_3$) δ 6.90 (s, 2H), 3.92 (t, *J*=6.8 Hz, 4H), 3.27 (s, 2H), 1.74 (m, 4H), 1.42 (m, 4H), 1.26 (m, 8H), 0.82 (m, 6H). ^{13}C NMR (101 MHz, $CDCl_3$) δ 154.16, 117.78, 113.28, 82.36, 79.77, 69.69, 31.49, 29.09, 25.57, 22.57, 13.99. The NMR spectroscopic data are in agreement with those in the literature.[164]

Compound 36

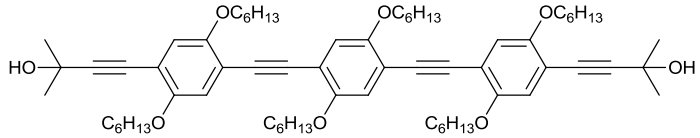

General Procedure (I): **35** (800 mg, 2.45 mmol), [$Pd(PPh_3)_4$] (283 mg), CuI (46 mg), **31** (2.6 g, 5.36 mmol), THF/Et_3N (40 ml), 18 h, r.t.. Solvent was removed by vacuum evaporation and purification by column chromatography using DCM/ethyl acetate (100:5 v/v) gave **36** as a bright yellow solid (1.20 g, 47% yield). m.p.: 125.3-126.8 °C. ^{1}H NMR (400 MHz, $CDCl_3$) δ 6.93 (s, 2H), 6.90 (s, 2H), 6.84 (s, 2H), 3.92 (m, 12H), 2.01 (s, 2H), 1.76 (m, 12H), 1.57 (s, 12H), 1.44 (m, 12H), 1.27 (m, 24H), 0.83 (m, 18H). ^{13}C NMR (101 MHz, $CDCl_3$) δ 151.65, 151.51, 151.43, 115.34, 115.31, 115.02, 112.35, 112.32, 111.35, 97.18, 89.37, 89.36, 76.60, 67.75, 67.71, 67.43, 63.80,

29.62, 29.61, 29.46, 27.35, 27.31, 27.28, 23.73, 23.68, 23.66, 20.64, 20.63, 12.04, 12.02. HR-MS (ASAP+) *m/z* calcd for $C_{68}H_{98}O_8$ $[M]^+$ 1042.7262, found *m/z*: $[M]^+$ 1042.7274.

Compound 37

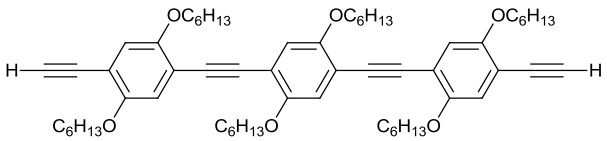

General Procedure (III) (b): **36** (400 mg, 0.38 mmol), NaOH (2 g), toluene (40 ml), 23 h 100 °C. Purification by column chromatography using DCM/hexane (2:3 v/v) as eluent gave **37** as a yellow solid (250 mg, 70% yield). m.p.: 95.3-95.9 °C. ^{1}H NMR (400 MHz, $CDCl_3$) δ 7.00 (s, 2H), 6.99(s, 2H), 6.97 (s, 2H), 4.01 (m, 12H), 3.34 (s, 2H), 1.83 (m, 12H), 1.50 (m, 12H), 1.34 (m, 24H), 0.89 (m, 18H). ^{13}C NMR (101 MHz, $CDCl_3$) δ 154.35, 153.72, 153.52, 118.12, 117.43, 117.22, 115.14, 114.45, 112.76, 91.77, 91.46, 82.53, 80.26, 69.93, 69.86, 69.81, 31.84, 31.77, 29.51, 29.47, 29.37, 25.90, 25.84, 22.87, 22.82, 14.27. The NMR spectroscopic data are in agreement with those in the literature.[165]

OAE5

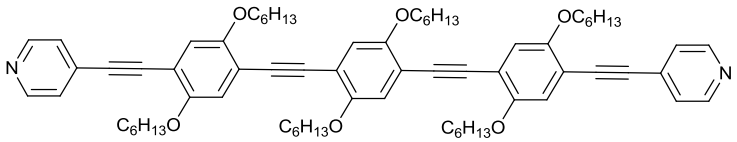

General Procedure (I): 4-iodopyridine (62 mg, 0.3 mmol), $[Pd(PPh_3)_4]$ (14 mg), CuI (3 mg), **37** (100 mg, 0.12 mmol), THF/Et_3N (3 ml), 20 h, r.t.. Solvent was removed by vacuum evaporation and purification by column chromatography using hexane/ethyl acetate (1:4 v/v) gave **OAE5** as a bright yellow solid (80 mg, 68% yield). Crystals for X-ray analysis were grown from dichloromethane/ethanol solution. m.p. 127.2-128.2 °C. ^{1}H NMR (700 MHz, $CDCl_3$) δ 8.59 (d, *J* = 5.7 Hz, 4H), 7.36 (d, *J* = 5.7 Hz, 4H), 7.01 (m, 6H), 4.02 (m, 12H), 1.84 (m, 12H), 1.51 (m, 12H), 1.33 (m, 24H), 0.88 (m, 18H); ^{13}C NMR (176 MHz, $CDCl_3$) δ 153.99, 153.53, 153.41, 149.63, 131.67, 125.40, 117.24, 117.18, 116.95, 115.54, 114.27, 112.49, 92.05, 91.87, 91.31, 90.81, 69.76, 69.66, 69.50, 31.59, 31.58, 31.54, 29.27, 29.24, 29.23, 25.70, 25.66, 25.64, 22.61, 14.00, 13.98; HR-MS (ASAP+) *m/z* Calcd for $C_{72}H_{93}N_2O_6$ $[M+H]^+$ 1081.7034, found *m/z* : $[M+H]^+$ 1081.7070.

4-(2-methyl-3-butyn-2-ol)-iodophenyl; 39

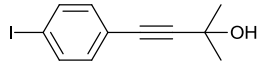

General Procedure (I): **38** (5.0 g, 15.19 mmol), [$Pd(PPh_3)_4$] (526 mg), CuI (144 mg), 2-methyl-3-butyn-2-ol (1.02 g, 12.15 mmol), THF/Et_3N (140 ml), 5 h, r.t.. Solvent was removed by vacuum evaporation and purification by column chromatography using DCM/hexane (2:3 v/v) gave **39** as a bright yellow solid (2.0 g, 46% yield). m.p.: 87.3-88.1 °C. ^{1}H NMR (400 MHz, $CDCl_3$) δ 7.66 (d, *J* = 4.8 Hz, 2H), 7.16 (d, *J* = 4.8 Hz, 2H), 2.03 (s, 1H), 1.63 (s, 6H). ^{13}C NMR (101 MHz, $CDCl_3$) δ 137.42, 133.15, 122.27, 95.15, 94.08, 81.26, 65.65, 31.40. The NMR spectroscopic data are in agreement with those in the literature.[166]

Compound 40

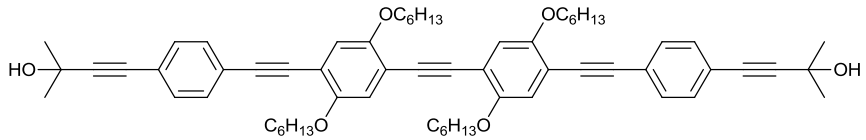

General Procedure (I): **34** (350 mg, 0.56 mmol), $Pd[PPh_3]_4$ (64 mg), CuI (10 mg), **39** (400 mg, 1.4 mmol), THF/Et_3N (14 ml), 20 h, r.t.. Solvent was removed by vacuum evaporation and purification by column chromatography using DCM/ethyl acetate (100:3 v/v) gave **40** as a bright yellow solid (460 mg, 87% yield). m.p.: 155.4-156.7 °C. ^{1}H NMR (400 MHz, $CDCl_3$) δ 7.46 (d, *J* =8.3 Hz, 4H), 7.39 (d, *J* =8.3 Hz, 4H), 7.01 (s, 2H), 7.00 (s, 2H), 4.02 (m, 8H), 2.02 (s, 2H), 1.84 (m, 8H), 1.62 (s, 12H), 1.52 (m, 8), 1.34 (m, 16H), 0.90 (m, 12H). ^{13}C NMR (101 MHz, $CDCl_3$) δ 153.87, 153.69, 131.79, 131.60, 123.55, 122.76, 117.23, 117.20, 114.72, 113.89, 95.91, 94.75, 91.87, 88.11, 82.08, 69.91, 69.76, 65.85, 31.86, 31.85, 31.66, 29.55, 29.50, 26.00, 25.91, 22.89, 14.30. HR-MS (ASAP+) *m/z* calcd for $C_{64}H_{78}O_6$ $[M]^+$ 942.5798, found *m/z*: $[M]^+$ 942.5781.

Compound 41

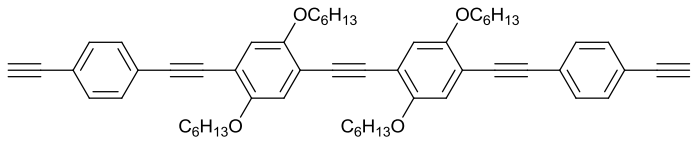

General Procedure (III) (b): **40** (400 mg, 0.4 mmol), NaOH (2 g), toluene (40 ml), 25 h. Purification by column chromatography using DCM/hexane (2:3 v/v) as eluent gave **41** as a yellow solid (210 mg, 60% yield). m.p.: 126.3-127.5 °C. ^{1}H NMR (400 MHz, $CDCl_3$) δ 7.47 (m, 8H), 7.01 (s, 2H), 7.00 (s, 2H), 4.03 (m, 8H), 3.18 (s, 2H), 1.85 (m, 8H), 1.54 (m, 8H), 1.34 (m, 16H), 0.89 (m, 12H). ^{13}C NMR (101 MHz, $CDCl_3$) δ 153.90, 153.70, 132.27, 131.63, 124.19, 122.02,

117.21, 117.20, 114.77, 113.80, 94.54, 91.83, 88.32, 83.55, 79.14, 69.92, 69.77, 31.85, 31.84, 29.94, 29.55, 29.50, 25.99, 25.91, 22.88, 14.29. HR-MS (ASAP+) *m/z* calcd for $C_{58}H_{66}O_4$ $[M]^+$ 826.4961, found *m/z* : $[M]^+$ 826.4932.

OAE6

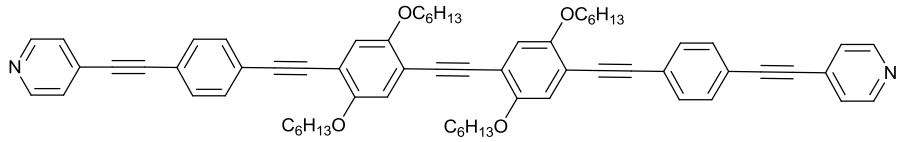

General Procedure (I): 4-iodopyridine (62 mg, 0.3 mmol), $[Pd(PPh_3)_4]$ (14 mg), CuI (3 mg), **41** (100 mg, 0.12 mmol), THF/Et_3N (3 ml), 15 h, r.t.. Solvent was removed by vacuum evaporation and purification by column chromatography using hexane/ethyl acetate (1:4 v/v) gave **OAE6** as a bright yellow solid (80 mg, 68% yield). m.p.: 214.2-215.2 °C. ^{1}H NMR (600 MHz, $CDCl_3$) δ 8.62 (bs, 4H), 7.52 (bs, 8H), 7.39 (d, *J* = 4.2 Hz, 4H), 7.01 (s, 2H), 7.00 (s, 2H), 4.03 (m, 8H), 1.85 (m, 8H), 1.53 (m, 8H), 1.34 (m, 16H), 0.89 (m, 12H); ^{13}C NMR (151 MHz, $CDCl_3$) δ 153.72, 153.49, 149.53, 131.78, 131.54, 131.43, 125.58, 124.44, 121.64, 117.02 (2 overlapping peaks), 114.68, 113.51, 94.30, 93.85, 91.64, 88.61, 88.30, 69.72, 69.55, 31.60, 31.59, 29.30, 29.26, 25.74, 25.65, 22.62, 14.02; HR-MS (ASAP+) *m/z* Calcd for $C_{68}H_{73}N_2O_4$ $[M+H]^+$ 981.5570, found *m/z* : $[M+H]^+$ 981.5566.

4-((4-iodophenyl)ethynyl)pyridine; 42

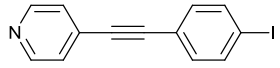

General Procedure (I): **38** (2.4 g, 7.29 mmol), $[Pd(PPh_3)_4]$ (339 mg), CuI (55 mg), 4-ethynylpyridine (600 mg, 5.88 mmol), THF/Et_3N (50 ml), 8 h, r.t.. Solvent was removed by vacuum evaporation and purification by column chromatography using DCM/ethyl acetate (100:3 v/v) gave **42** as a yellow oil (600 mg, 33% yield) which on storage became a yellow solid, m.p.: 199.6-201.5 °C. ^{1}H NMR (400 MHz, $CDCl_3$) δ 8.60 (d, *J* = 8.4 Hz 2H), 7.71 (d, *J* = 8.4 Hz, 2H), 7.33 (d, *J* = 8.4 Hz, 2H), 7.20 (d, *J* = 8.4 Hz, 2H). ^{13}C NMR (101 MHz, $CDCl_3$): δ 150.03, 137.94, 133.48, 131.30, 125.69, 121.78, 95.69, 93.15, 88.17. The NMR spectroscopic data are in agreement with those in the literature.[167]

OAE7

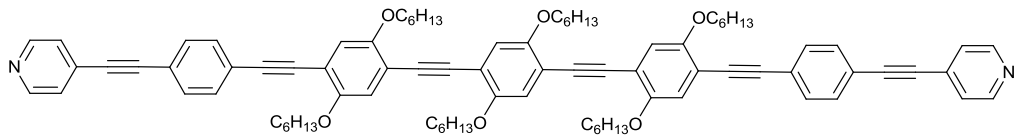

General Procedure (I): **42** (57 mg, 0.17 mmol), [$Pd(PPh_3)_4$] (9 mg), CuI (2 mg), **37** (70 mg, 0.07 mmol), THF/Et_3N (3 ml), 20 h, r.t.. Solvent was removed by vacuum evaporation and purification by column chromatography using DCM/ Ethyl Acetate (10:1 v/v) gave **OPE7** as a yellow solid (60 mg, 67% yield). Crystals for X-ray analysis were grown from dichloromethane/ethanol solution. m.p.: 203.5-204.2 °C. ^{1}H NMR (600 MHz, $CDCl_3$) δ 8.61 (d, *J* = 6.0 Hz, 4H), 7.52 (s, 8H), 7.39 (d, *J* = 6.0 Hz, 4H), 7.01 (m, 3H), 4.03 (m, 12H), 1.84 (m, 12H), 1.52 (m, 12H), 1.34 (m, 24H), 0.89 (m, 18H). ^{13}C NMR (151 MHz, $CDCl_3$) δ 153.73, 153.50, 153.47, 149.49, 131.79, 131.54, 131.50, 125.55, 124.47, 121.61, 117.23, 117.04, 117.01, 114.78, 114.28, 113.42, 94.26, 93.92, 91.78, 91.45, 88.64, 88.27, 69.73, 69.67, 69.54, 31.61, 31.59, 29.30, 29.29, 29.26, 25.75, 25.67, 25.65, 22.62, 14.02; HR-MS (ASAP+) *m/z* Calcd for $C_{88}H_{101}N_2O_6$ $[M+H]^+$ 1281.7700, found *m/z* : $[M+H]^+$ 1281.7615.

OAE8a

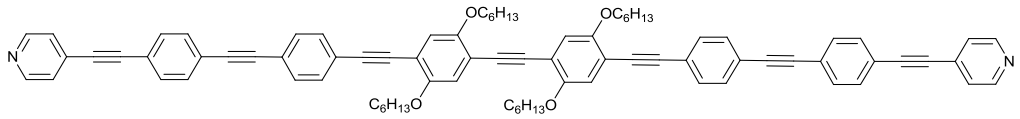

General Procedure (I): **41** (110 mg, 0.09 mmol), [$Pd(PPh_3)_4$] (14 mg), CuI (3 mg), **42** (100 mg, 0.12 mmol), THF/Et_3N (5 ml), 16 h, r.t.. The yellow product could not be purified and NMR spectra could not be obtained due to insolubility. **OPE8a** was characterised only by mass spectrometry and a single crystal X-ray structure. MS (MALDI) *m/z*: 1181.5 ($[M+H]^+$, 100%), 1216.5 (55%). Crystals for X-ray analysis were grown from dichloromethane/ethanol solution.

Compound 43

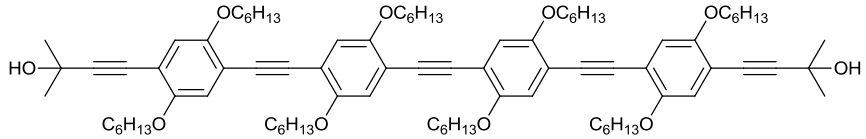

General Procedure (I): **34** (150 mg, 0.24 mmol), [$Pd(PPh_3)_4$] (27 mg), CuI (6 mg), **31** (256 mg, 0.6 mmol), THF/Et_3N (12 ml), 24 h, 50 °C. Solvent was removed by vacuum evaporation and purification by column chromatography using DCM/ethyl acetate (99:1 v/v) gave **43** as a bright yellow solid (250 mg, 78% yield). m.p.: 154.5-155.3 °C. ^{1}H NMR (400 MHz, $CDCl_3$) δ 7.01 (bs,

4H), 6.97 (s, 2H), 6.91 (s, 2H), 4.00 (m, 16H), 2.14 (s, 2H), 1.84 (m, 16H), 1.64 (s, 12H), 1.51 (m, 16H), 1.34 (m, 32H), 0.90 (m, 24H). ^{13}C NMR (151 MHz, $CDCl_3$) δ 153.61, 153.48 (2 overlapping peaks), 153.39, 117.26 (2 overlapping peaks), 117.24, 116.96, 114.31, 114.29, 114.25, 113.30, 99.18, 91.54, 91.37 (2 overlapping peaks), 78.56, 69.70, 69.66, 69.39, 65.76, 31.61, 31.43, 29.29, 29.25, 25.71, 25.66, 22.62, 14.02. HR-MS (ASAP+) *m/z* calcd for $C_{88}H_{127}O_{10}$ $[M+H]^+$ 1343.9429, found *m/z* : $[M+H]^+$ 1343.9384.

Compound 44

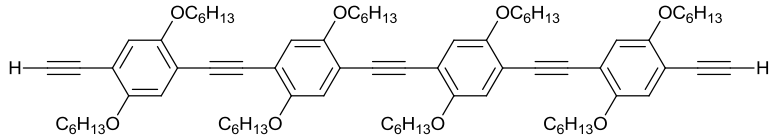

General Procedure (III) (b): **43** (150 mg, 0.11 mmol), NaOH (2 g), toluene (20 ml), 18 h, 100 °C. Purification by column chromatography using DCM/petroleum ether (2:3 v/v) as eluent gave **44** as a yellow solid (110 mg, 80% yield). m.p.: 104.0-105.0 °C. ^{1}H NMR (400 MHz, $CDCl_3$) δ 7.02 (s, 2H), 7.01 (s, 2H), 7.00 (s, 2H), 6.98 (s, 2H), 4.02 (m, 16H), 3.35 (s, 2H), 1.85 (m, 16H), 1.51 (m, 16H), 1.34 (m, 32H), 0.89 (m, 24H). ^{13}C NMR (101 MHz, $CDCl_3$) δ 154.35, 153.73, 153.70, 153.52, 118.12, 117.44, 117.42, 117.22, 115.16, 114.58, 114.37, 112.75, 91.81, 91.46, 82.55, 80.28, 69.93, 69.88, 69.86, 69.81, 31.86, 31.85, 31.78, 29.53, 29.48, 29.37, 25.92, 25.89, 25.85, 22.88, 22.83, 14.28. HR-MS (ASAP+) *m/z* calcd for $C_{82}H_{114}O_8$ $[M]^+$ 1226.8513, found *m/z* : $[M]^+$ 1226.8513.

OAE8b

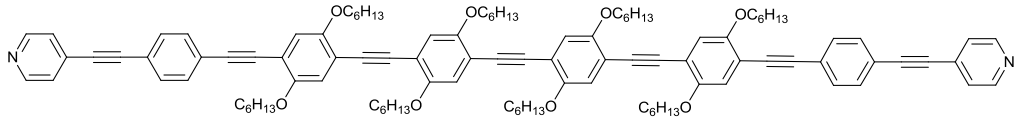

General Procedure (I): **44** (110 mg, 0.09 mmol), $[Pd(PPh_3)_4]$ (10 mg), CuI (2 mg), **42** (82 mg, 0.27 mmol), THF/Et_3N (4 ml), 21 h, r.t.. Solvent was removed by vacuum evaporation and purification by column chromatography using petroleum ether / ethyl acetate (1:1 v/v) to give **OAE8b** as a yellow solid (50 mg, 35% yield). m.p.: 199.5 -200.6 °C. ^{1}H NMR (600 MHz, $CDCl_3$) δ 8.61 (d, *J* = 5.2 Hz, 4H), 7.53 (s, 8H), 7.38 (d, *J* = 5.2 Hz, 4H), 7.02 (m, 8H), 4.04 (m, 16H), 1.86 (m, 16H), 1.53 (m, 16H), 1.35 (m, 32H), 0.89 (m, 24H). ^{13}C NMR (151 MHz, $CDCl_3$) δ 153.74, 153.52, 153.50, 153.48, 149.72, 131.78, 131.54, 131.26, 125.48, 124.44, 121.67, 117.26, 117.24, 117.06, 117.02, 114.81, 114.40, 114.21, 113.42, 94.28, 93.68, 91.83, 91.61, 91.44, 88.65, 88.34, 69.74, 69.68, 69.66, 69.54, 31.62, 31.61, 31.60, 29.32, 29.30, 29.27, 25.76, 25.68, 25.57,

22.64,14.03. HR-MS (ASAP+) *m/z* calcd for $C_{108}H_{128}N_2O_8$ $[M]^+$ 1580.9671, found m/z : $[M]^+$ 1580.9725.

Compound 45

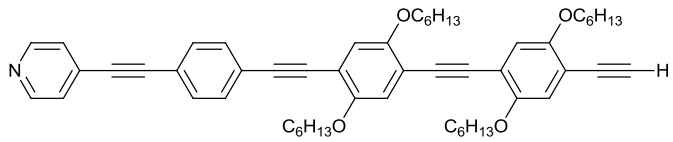

General Procedure (I): **34** (78 mg, 0.25 mmol), $[Pd(PPh_3)_4]$ (15 mg), CuI (2 mg), **42** (200 mg, 0.32 mmol), THF/Et_3N (4 ml), 18 h, r.t.. Solvent was removed by vacuum evaporation and purification by column chromatography using DCM gave **45** as a yellow oil (120 mg, 60% yield) which solidified on standing. m.p.: 155 °C (decomp.). ^{1}H NMR (400 MHz, $CDCl_3$) δ 8.62 (d, *J* = 6.4 Hz, 2H), 7.53 (s, 4H), 7.39 (d, *J* = 6.4 Hz, 2H), 7.00 (m, 4H), 4.01 (m, 8H), 3.35 (s, 1H), 1.83 (m, 8H), 1.51 (m, 8H), 1.33 (m, 16H), 0.89 (m, 12H). ^{13}C NMR (101 MHz, $CDCl_3$) δ 154.34, 153.93, 153.71, 153.53, 149.86, 132.03, 131.79, 131.62, 125.79, 125.78, 124.66, 121.89, 118.09, 117.21, 115.03, 114.84, 113.70, 112.84, 112.83, 94.53, 94.03, 91.68, 91.65, 88.83, 88.55, 82.59, 80.24, 69.91, 69.81, 69.75, 31.84, 31.77, 29.54, 29.46, 29.36, 25.99, 25.88, 25.84, 22.87, 22.82, 14.28. HR-MS (ASAP+) *m/z* calcd for $C_{55}H_{65}NO_4$ $[M+H]^+$ 804.4992, found *m/z* : $[M+H]^+$ 804.4982.

OAE9

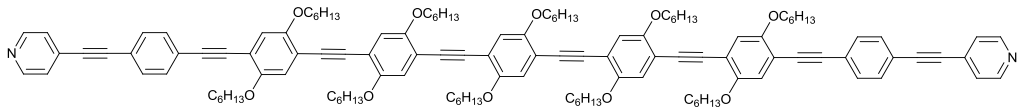

General Procedure (I): **29** (26 mg, 0.05 mmol), $[Pd(PPh_3)_4]$ (6 mg), CuI (1 mg), **45** (100 mg, 0.13 mmol), THF/Et_3N (4 ml), overnight, r.t.. Solvent was removed by vacuum evaporation and purification by column chromatography using DCM / ethyl acetate (7:3 v/v) gave **OAE9** as a yellow solid (20 mg, 21% yield). m.p.: 202.1-203.5 °C. ^{1}H NMR (400 MHz, $CDCl_3$) δ 8.62 (d, *J* = 6.0 Hz, 4H), 7.54 (bs, 8H), 7.40 (d, *J* = 6.0 Hz, 4H), 7.02 (m, 10H), 4.03 (m, 20H), 1.86 (m, 20H), 1.53 (m, 20H), 1.34 (m, 40H), 0.89 (m, 30H); ^{13}C NMR (101 MHz, $CDCl_3$) δ 153.95, 153.74, 153.71(two overlapping peak), 153.69, 149.91, 132.04, 131.80, 131.59, 125.77, 124.68, 121.89, 117.98, 117.44, 117.22, 115.01, 114.79, 114.61, 114.50, 114.38, 113.61, 112.82, 94.52, 94.01, 92.07, 91.87, 91.80, 91.66, 88.88, 88.56, 69.95, 69.88, 69.75, 31.87, 31.85, 31.78, 29.53, 29.50, 26.00, 25.92, 25.86, 22.89, 14.29. MS (ASAP+) *m/z* : 1883.1 ($[M+H]^+$, 100%).

7.3.2 Experimental for Chapter 3

1,4-bis(4-pyridinylethynyl)benzene; p-p-p

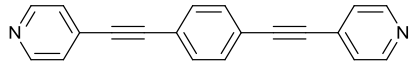

General Procedure (I): **38** (200 mg, 0.61 mmol), CuI (12 mg), [$Pd(PPh_3)_4$] (71 mg), 4-ethynylpyridine (187 mg, 1.83 mmol), THF/Et_3N (12 ml), 18 h, 50 ^oC. Solvent was removed by vacuum evaporation. Purification by column chromatography using dichloromethane/ethyl acetate (3:2 v/v) as eluent gave **p-p-p** as a pale solid (110 mg, 64% yield). m.p.: 194.8-196.2 °C. ^1H NMR (400 MHz, $CDCl_3$) δ 8.62 (d, *J* = 5.9 Hz, 4H), 7.54 (s, 4H), 7.36 (d, *J* = 5.9 Hz, 4H). ^{13}C NMR (101 MHz, $CDCl_3$) δ 150.12, 132.15, 131.20, 125.74, 123.10, 93.35, 89.08. HR-MS (ASAP+) *m/z* calcd for $C_{20}H_{13}N_2$ $[M+H]^+$ 281.1000, found *m/z* : $[M+H]^+$ 281.1034. UV/Vis (CH_2Cl_2) λ_{max} (ε) 228 (24510), 318 (66541), 338 (45872 M^{-1} cm^{-1}) nm. The NMR spectroscopic data are in agreement with those in the literature.[77]

1,4-bis(3-pyridinylethynyl)benzene; m-p-m

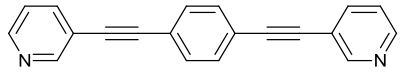

General Procedure (I): **38** (200 mg, 0.61 mmol), CuI (12 mg), [$Pd(PPh_3)_4$] (71 mg), 3-ethynylpyridine (187 mg, 1.83 mmol), THF/Et_3N (12 ml), 17 h, r.t.. Solvent was removed by vacuum evaporation. Purification by column chromatography using dichloromethane/ethyl acetate (1:9 v/v) as eluent gave **m-p-m** (130 mg, 76% yield). m.p.: 190.1-193.0 ^oC. ^1H NMR (400 MHz, $CDCl_3$) δ 8.77 (bs, 2H), 8.56 (m, 2H), 7.81 (m, 2H), 7.54 (s, 4H), 7.30 (m, 2H). ^{13}C NMR (101 MHz, $CDCl_3$) δ 152.50, 149.05, 138.67, 131.92, 123.31, 123.10, 120.36, 92.34, 88.25. Calcd for $C_{20}H_{12}N_2$: C, 85.69; H, 4.31; N, 9.99. Found: C, 85.51; H, 4.25; N, 9.97. HR-MS (ASAP+) *m/z* calcd for $C_{20}H_{12}N_2$ $[M]^+$ 280.1000, found *m/z* : $[M]^+$ 280.1008. UV/Vis (CH_2Cl_2) λ_{max} (ε) 228 (23483), 320 (66161), 339 (42852 M^{-1} cm^{-1}) nm.

1,4-bis(2-pyridinylethynyl)benzene; o-p-o

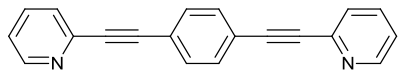

General Procedure (I): **38** (200 mg, 0.61 mmol), CuI (12 mg), [$Pd(PPh_3)_4$] (71 mg), 2-ethynylpyridine (187 mg, 1.83 mmol), THF/Et_3N (12 ml), 18 h, 50 ^oC. Solvent was removed by vacuum evaporation. Purification by column chromatography using dichloromethane/ethyl acetate (3:2 v/v) as eluent gave **o-p-o** (120 mg, 71% yield). m.p.: 190.8-192.3 ^oC. ^1H NMR (400

MHz, $CDCl_3$) δ 8.63 (m, 2H), 7.69 (m, 2H), 7.58 (s, 4H), 7.53 (m, 2H), 7.25 (m, 2H). ^{13}C NMR (101 MHz, $CDCl_3$) δ 150.39, 143.40, 136.44, 132.22, 127.51, 123.20, 123.04, 90.81, 88.83. Calcd for $C_{20}H_{12}N_2$: C, 85.69; H, 4.31; N, 9.99. Found: C, 85.53; H, 4.28; N, 9.97. HR-MS (ASAP+) *m/z* calcd for $C_{20}H_{12}N_2$ $[M]^+$ 280.1000, found *m/z* : $[M]^+$ 280.0982. UV/Vis (CH_2Cl_2) λ_{max} (ε) 228 (20170), 321 (65073), 339 (43069 $M^{-1}\,cm^{-1}$) nm.

1,3-bis(4-pyridinylethynyl)benzene; p-m-p

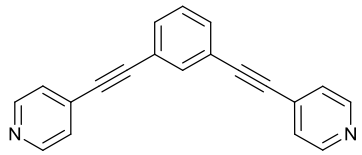

General Procedure (I): **60** (120 mg, 0.36 mmol), CuI (7 mg), $[Pd(PPh_3)_4]$ (41 mg), 4-ethynylpyridine (112 mg, 1.02 mmol), THF/Et_3N (12 ml), 24 h, r.t.. Solvent was removed by vacuum evaporation. Purification by column chromatography using dichloromethane/ethyl acetate (1:1 v/v) as eluent gave **p-m-p** (90 mg, 88% yield). m.p.: 132.8-134.2 ^{o}C. ^{1}H NMR (400 MHz, $CDCl_3$) δ 8.58 (d, *J* = 4.8 Hz, 4H), 7.72 (t, *J* = 1.6 Hz, 1H), 7.52 (dd, *J* = 7.8, 1.6 Hz, 2H), 7.37 (s, 1H), 7.34 (d, *J* = 4.8 Hz, 4H). ^{13}C NMR (101 MHz, $CDCl_3$) δ 150.04, 135.25, 132.57, 131.19, 129.01, 125.74, 122.90, 92.83, 87.69. Calcd for $C_{20}H_{12}N_2$: C, 85.69; H, 4.31; N, 9.99. Found: C, 85.48; H, 4.27; N, 9.93. HR-MS (ASAP+) *m/z* calcd for $C_{20}H_{12}N_2$ $[M]^+$ 280.1000, found *m/z* : $[M]^+$ 280.0985. UV/Vis (CH_2Cl_2) λ_{max} (ε) 282 (64504), 299 (55539 $M^{-1}\,cm^{-1}$) nm.

1,3-bis(3-pyridinylethynyl)benzene; m-m-m

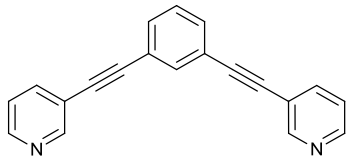

General Procedure (I): **60** (200 mg, 0.61 mmol), CuI (12 mg), $[Pd(PPh_3)_4]$ (71 mg), 3-ethynylpyridine (85.8 mg, 1.32 mmol), THF/Et_3N (12 ml), 17 h, r.t.. Solvent was removed by vacuum evaporation. Purification by column chromatography using dichloromethane/ethyl acetate (1:9 v/v) as eluent gave **m-m-m** (100 mg, 58% yield). m.p.: 84.0-85.7 ^{o}C. ^{1}H NMR (400 MHz, $CDCl_3$) δ 8.74 (d, *J* = 1.5 Hz, 2H), 8.52 (dd, *J* = 4.9, 1.7 Hz, 2H), 7.76 (m, 2H), 7.70 (m, 1H), 7.49 (m, 2H), 7.33 (m, 1H), 7.25 (m, 2H). ^{13}C NMR (101 MHz, $CDCl_3$) δ 152.48, 149.00, 134.92, 132.03, 128.90, 123.29, 123.23, 120.31, 91.78, 86.96. Calcd for $C_{20}H_{12}N_2$: C, 85.69; H, 4.31; N, 9.99. Found: C, 85.57; H, 4.29; N, 9.92. HR-MS (ASAP+) *m/z* calcd for $C_{20}H_{12}N_2$ $[M]^+$ 280.1000,

found *m/z* : $[M]^+$ 280.1011. UV/Vis (CH_2Cl_2) λ_{max} (ε) 284 (65117), 294 (57107), 303 (58830 M^{-1} cm^{-1}) nm.

1,3-bis(2-pyridinylethynyl)benzene; o-m-o

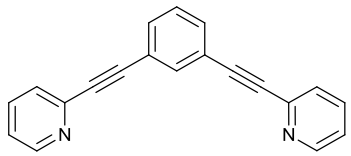

General Procedure (I): **60** (250 mg, 0.76 mmol), CuI (14 mg), $[Pd(PPh_3)_4]$ (88 mg), 2-ethynylpyridine (234 mg, 2.28 mmol), THF/Et_3N (12 ml), 20 h, 50 °C. Solvent was removed by vacuum evaporation. Purification by column chromatography using dichloromethane/ethyl acetate (1:9 v/v) as eluent gave light yellow solid **o-m-o** (110 mg, 52% yield). m.p.: 72.3-73.8 °C. ^1H NMR (400 MHz, $CDCl_3$) δ 8.66 (m, 2H), 7.85 (m, 1H), 7.72 (td, *J* = 7.7, 1.8 Hz, 2H), 7.62 (dd, *J* = 7.8, 1.6 Hz, 2H), 7.56 (dt, *J* = 7.8, 1.1 Hz, 2H), 7.39 (t, *J* = 8.1Hz, 1H), 7.28 (m, 2H). ^{13}C NMR (101 MHz, $CDCl_3$) δ 150.29, 143.29, 136.41, 135.42, 132.58, 128.84, 127.50, 123.19, 122.92, 89.51, 88.20. Calcd for $C_{20}H_{12}N_2$: C, 85.69; H, 4.31; N, 9.99. Found: C, 85.57; H, 4.29; N, 9.92. HR-MS (ASAP+) *m/z* calcd for $C_{20}H_{13}N_2$ $[M+H]^+$ 281.1079, found *m/z* : $[M+H]^+$ 281.1059. UV/Vis (CH_2Cl_2) λ_{max} (ε) 271 (46874) 289 (60295), 297 (60414), 306 (60373 M^{-1} cm^{-1}) nm.

1,2,4,5-tetrafluoro-3,6-bis(4-ethynylpyridine)benzene; p-p-p (4F)

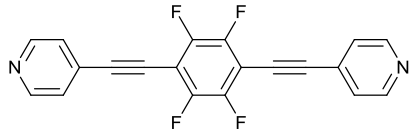

General Procedure (I): **61** (250 mg, 0.625 mmol), CuI (3 mg), $[Pd(PPh_3)_4]$ (9 mg), 4-ethynylpyridine (150 mg, 1.5 mmol), Et_3N (10 ml), 10 h, 84 °C. Solvent was removed by vacuum evaporation. Purification by column chromatography using dichloromethane/ethyl acetate (9:1 v/v) as eluent gave a yellow solid **p-p-p (4F)** (110 mg, 50% yield). m.p.: 269.3-270.3 °C. ^1H NMR (400 MHz, $CDCl_3$) δ 8.69 (dd, *J* = 5.9, 2.8 Hz, 2H), 7.46 (dd, *J* = 5.9, 2.8 Hz, 2H). ^{13}C NMR (126 MHz, $CDCl_3$) δ 150.29, 147.84, 145.99, 129.62, 125.75, 100.29, 78.51. Calcd for $C_{20}H_8F_4N_2$: C, 68.19; H, 2.29; N, 7.95. Found: C, 68.04; H, 2.30; N, 7.84. HR-MS (ASAP+) m/z calcd for $C_{20}H_9F_4N_2$ $[M+H]^+$ 353.0702, found m/z : $[M]^+$ 353.0707.

2,3,5,6-Tetramethoxy-1,4-diiodobenzene; 63

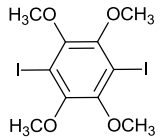

To a solution of **62** (300 mg, 1.52 mmol) in THF (18 ml), n-BuLi (1.8 ml, 2.5 M in hexanes) was added dropwise in a duration of 30 min at -78 °C. The solution was then stirred at -78 °C for 30 min and then at room temperature for 1 h before I_2 (1.9 g) was added slowly at -78 °C. The solution was then stirred at room temperature for 12 h. Dichloromethane was added to dilute the mixture, then the mixture was washed with 10% KOH solution, followed by saturated $Na_2S_2O_3$ solution and water. Solvent was removed by vacuum evaporation to give a solid crud. Recrystallization from EtOH gave a white solid **63** (600 mg, 88% yield). m.p.: 136.5-138.3 °C. ^{1}H NMR (400 MHz, $CDCl_3$) δ 3.87 (s, 12H). ^{13}C NMR (101 MHz, $CDCl_3$) δ 149.61, 91.64, 60.68. HR-MS (ASAP+) *m/z* calcd for $C_{10}H_{12}O_4I_2$ $[M]^+$ 449.8825, found *m/z* : $[M]^+$ 449.8825.

1,4-bis(4-ethynylpyridine)-2,3,5,6-tetramethoxylbenzene; p-p-p (4OMe)

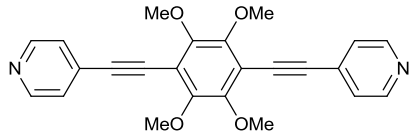

General Procedure (I): 63 (150 mg, 0.33 mmol), CuI (6.6 mg), $[Pd(PPh_3)_4]$ (38 mg), 4-ethynylpyridine (85.8 mg, 1.32 mmol), THF/Et_3N (12 ml), 18 h, reflux. Solvent was removed by vacuum evaporation. Purification by column chromatography using dichloromethane/ethyl acetate (3:2 v/v) as eluent gave a white solid **p-p-p (4Ome)** (87 mg, 65% yield). m.p.: 218.2-219.2 °C. ^{1}H NMR (400 MHz, $CDCl_3$) δ 8.63 (d, *J* = 6.0 Hz, 4H), 7.42 (d, *J* = 6.0 Hz, 4H), 3.99 (s, 12H). ^{13}C NMR (101 MHz, $CDCl_3$) δ 150.7, 150.0, 131.3, 125.6, 114.2, 96.6, 85.8, 61.7. Calcd for $C_{24}H_{20}N_2O_4$: C, 71.99; H, 5.03; N, 7.00. Found: C, 71.88; H, 5.00; N, 6.77. HR-MS (ASAP+) *m/z* calcd for $C_{24}H_{20}N_2O_4$ $[M]^+$ 400.1423, found *m/z* : $[M]^+$ 400.1417.

1-phynylethynyl-4-pyridinylethynylbenzene ; p-p-ph

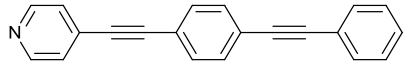

General Procedure (I): **42** (200 mg, 0.66 mmol), CuI (38 mg), $[Pd(PPh_3)_4]$ (81 mg), 4-ethynylpyridine (81 mg, 0.79mmol), THF/Et_3N (12 ml), 24 h, 50 °C. Solvent was removed by vacuum evaporation. Purification by column chromatography using dichloromethane/ethyl acetate (99:1 v/v) as eluent gave a yellow solid **p-p-ph** (105 mg, 57% yield). m.p.: 212.5-

214.9°C. ^{1}H NMR (400 MHz, CD_2Cl_2) δ 8.60 (dt, *J* = 4.4, 1.8 Hz, 2H), 7.57 (m, 6H), 7.40 (m, 5H). ^{13}C NMR (101 MHz, CD_2Cl_2) δ 150.08, 132.05, 131.80, 131.10, 128.89, 128.68, 125.58, 124.29, 122.99, 122.09, 93.29, 91.82, 88.89, 88.51. Calcd for $C_{21}H_{13}N$: C, 89.89; H, 4.65; N, 4.86. Found: C, 90.12; H, 4.67; N, 4.94. HR-MS (ASAP+) *m/z* calcd for $C_{21}H_{14}N_1$ $[M+H]^+$ 280.1126, found *m/z* : $[M+H]^+$ 280.1117. UV/Vis (CH_2Cl_2) λ_{max} (ε) 321 (65518), 340 (41093 $M^{-1}cm^{-1}$) nm.

1-phynylethynyl-3-pyridinylethynylbenzene; m-p-ph

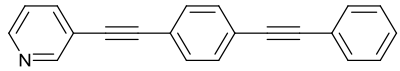

General Procedure (I): **42** (200 mg, 0.66 mmol), CuI (38 mg), $[Pd(PPh_3)_4]$ (81 mg), 3-ethynylpyridine (81 mg, 0.79mmol), THF/Et_3N (12 ml), 28 h, 50 °C. Solvent was removed by vacuum evaporation. Purification by column chromatography using dichloromethane as eluent gave a pale solid **m-p-ph** (120 mg, 65% yield). m.p.: 183.1-185.3°C. ^{1}H NMR (400 MHz, Acetone-d_6) δ 8.76 (m, 1H), 8.59 (dd, *J* = 4.9, 1.7 Hz, 1H), 7.95 (dt, *J* = 8.0, 1.9 Hz, 1H), 7.60 (m, 6H), 7.44 (m, 4H). ^{13}C NMR (126 MHz, Acetone-d_6) δ 152.16, 149.34, 138.50, 131.97, 131.88, 131.73, 129.05, 128.87, 123.89, 123.60, 123.01, 122.71, 120.07, 91.84, 91.55, 88.79, 87.99. Calcd for $C_{21}H_{13}N$: C, 90.29; H, 4.69; N, 5.01. Found: C, 90.12; H, 4.67; N, 4.94. HR-MS (ASAP+) *m/z* calcd for $C_{21}H_{13}N_1$ $[M]^+$ 279.1048, found *m/z* : $[M]^+$ 279.1032. UV/Vis (CH_2Cl_2) λ_{max} (ε) 228 (26794), 320 (64353), 340 (41093 $M^{-1}cm^{-1}$) nm.

1-phynylethynyl-2-pyridinylethynylbenzene; o-p-ph

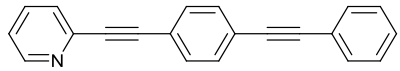

General Procedure (I): **42** (200 mg, 0.66 mmol), CuI (38 mg), $[Pd(PPh_3)_4]$ (81 mg), 2-ethynylpyridine (81 mg, 0.79mmol), THF/Et_3N (12 ml), 28 h, 50 °C. Solvent was removed by vacuum evaporation. Purification by column chromatography using dichloromethane/hexane (4:1 v/v) as eluent gave a pale solid **o-p-ph** (110 mg, 52% yield). m.p.: 172.1-172.9°C. ^{1}H NMR (700 MHz, Acetone-d_6) δ 8.62 (d, *J* = 4.1 Hz, 1H), 7.84 (td, *J* = 7.7, 1.8 Hz, 1H), 7.63 (m, 5H), 7.58 (m, 2H), 7.43 (m, 3H), 7.39 (ddd, *J* = 7.7, 4.8, 1.2 Hz, 1H). ^{13}C NMR (176 MHz, Acetone-d_6) δ 150.19, 143.01, 136.33, 131.91, 131.64, 131.49, 128.80, 128.61, 127.30, 123.80, 123.25, 122.75, 122.26, 91.36, 90.71, 88.53, 87.50. Calcd for $C_{21}H_{13}N$: C, 90.29; H, 4.69; N, 5.01. Found: C, 89.57; H, 4.66; N, 4.85. HR-MS (ASAP+) *m/z* calcd for $C_{21}H_{13}N_1$ $[M]^+$ 279.1048, found *m/z* : $[M]^+$ 279.1032. UV/Vis (CH_2Cl_2) λ_{max} (ε) 228 (28424), 321 (64699), 341 (41895 $M^{-1}cm^{-1}$) nm.

7.3.3 Experimental for Chapter 4

1,4-bis(4-ethynylaniline)-2,5-dimethoxylbenzene; OPE-2OC1

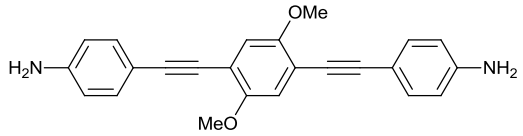

General Procedure (I): **27** (200 mg, 0.54 mmol), CuI (5 mg), [$Pd(PPh_3)_4$] (30 mg), 4-ethynylaniline (132 mg, 1.12 mmol), THF/Et_3N (24 ml), 12 h, r.t.. Solvent was removed by vacuum evaporation. Purification by column chromatography using dichloromethane as eluent gave **OPE-2OC1** as a light yellow solid (75 mg, 40% yield). m.p.: 231.0-232.0 ^{o}C. ^{1}H NMR (400 MHz, $CDCl_3$) δ 7.31 (d, *J* = 8.5 Hz, 4H), 6.92 (s, 2H), 6.57 (d, *J* = 8.5 Hz, 4H), 3.82 (s, 6H), 3.76 (s, 4H). ^{13}C NMR ($CDCl_3$, 101 MHz): 154.04,146.93, 133.30, 115.96, 114.92, 113.83, 113.07, 95.89, 84.01, 56.79. HR-MS (ASAP+) *m/z* calcd for $C_{24}H_{21}N_2O_2$ $[M+H]^+$ 369.1603, found *m/z* : $[M+H]^+$ 369.1595. Anal. Calcd for $C_{24}H_{20}N_2O_2$: C, 78.24; H, 5.47; N, 7.60. Found: C, 78.24; H, 5.49; N, 7.64. UV/Vis (CH_2Cl_2) λ_{max} (ε) 274 (26043), 324 (45855), 376 (96043 $M^{-1}cm^{-1}$) nm.

1,4-bis(4-ethynylaniline)-2,5-dioctylbenzene; OPE-2OC8

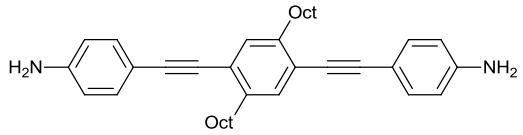

General Procedure (I): **64** (150 mg, 0.27 mmol), CuI (10 mg), [$Pd(PPh_3)_4$](62 mg), 4-ethynylaniline (80 mg, 0.68 mmol), THF/Et_3N (4 ml), 19 h, r.t.. Solvent was removed by vacuum evaporation. Purification by column chromatography using dichloromethane/hexane (3:2 v/v) as eluent gave a yellow solid **OPE-2C8** (87 mg, 61% yield). m.p.: 89.4-90.7 °C. ^{1}H NMR (400 MHz, $CDCl_3$) δ 7.33 (dd, *J* = 6.8, 4.8 Hz, 4H), 7.31 (s, 2H), 6.65 (dd, *J* = 6.8, 4.8 Hz, 4H), 3.82 (s, 4H), 2.78 (t, 4H), 1.67 (m, 4H), 1.31 (m, 20H), 0.87 (t, 6H). ^{13}C NMR (101 MHz, $CDCl_3$) δ 146.79, 141.98, 133.04, 132.12, 122.72, 114.99, 113.25, 94.66, 86.78, 34.41, 32.16, 30.87, 29.85, 29.78, 29.55, 22.92, 14.39. HR-MS (ASAP+) *m/z* calcd for $C_{38}H_{48}N_2$ $[M]^+$ 532.3817, found *m/z* : $[M]^+$ 532.3824. Anal. Calcd. for $C_{38}H_{48}N_2$: C, 85.66; H, 9.08; N, 5.26. Found: C, 85.75; H, 9.14; N, 5.34. UV/Vis (CH_2Cl_2) λ_{max} (ε) 251 (35710), 275 (30940), 355 (88228 $M^{-1}cm^{-1}$) nm.

1,4-bis(4-ethynylaniline)-2,3,5,6-tetramethoxylbenzene; OPE-4OC1

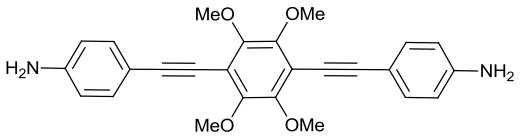

General Procedure (I): **63** (150 mg, 0.33 mmol), CuI (12 mg), [$Pd(PPh_3)_4$] (76 mg), 4-ethynylaniline (77 mg, 0.66 mmol), THF/Et_3N (6 ml), 24 h, reflux. Solvent was removed by vacuum evaporation. Purification by column chromatography using dichloromethane/ethyl acetate (9:1 v/v) as eluent gave a pale solid OPE-4OC1 (40 mg, 28% yield). m.p.: 222 °C (decomp.). ^{1}H NMR (400 MHz, CD_2Cl_2) δ 7.36 (d, *J* = 8.5 Hz, 4H), 6.68 (d, *J* = 8.5 Hz, 4H), 3.96 (s, 12H) 3.95 (s, 4H). ^{13}C NMR (176 MHz, CD_2Cl_2) δ 148.31, 145.79, 131.16, 112.87, 112.17, 110.55, 98.25, 77.78, 59.51. HR-MS (ASAP+) *m/z* calcd for $C_{26}H_{24}N_2O_4$ $[M]^+$ 428.1736, found *m/z* : $[M]^+$ 428.1727. Anal. Calcd. for $C_{26}H_{24}N_2O_4$: C, 72.88; H, 5.65; N, 6.54. Found: C, 72.69; H, 5.56; N, 6.61. UV/Vis (CH_2Cl_2) λ_{max} (ε) 255 (27642), 275 (19892), 361 (80946 $M^{-1}cm^{-1}$) nm.

7.3.4 Experimental for Chapter 5

1,8-Bis(indol-5-yl)octa-1,3,5,7-tetrayne; IN4

General Procedure (I): 5-iodoindole **(67e)** (300 mg, 1.23 mmol), CuI (12 mg), [$Pd(PPh_3)_4$] (70 mg), BDTMS (**68**) (226 mg, 1.85 mmol), THF/Et_3N (10 ml), 24 h, 50 °C. The solvent was removed by vacuum evaporation to yield a product presumed to be [(indole-5-yl)buta-1,3-diyn-1-yl]trimethylsilane (**69e**) which could not be purified by column chromatography. **General Procedure (IV)** was conducted directly on the brown crude material: $Cu(OAc)_2.H_2O$ (320 mg), MeOH/pyridine (4 ml/4 ml) 23 h, r.t.. Purification by column chromatography using DCM/hexane (3:7 v/v) as eluent gave a yellow solid **IN4** (70 mg, 35% overall yield from 5-iodoindole). mp: 130 °C (decomp.) which turned green in ambient conditions within a week. ^{1}H NMR (400 MHz, (DMSO-d_6) δ 11.51 (s, 2H), 7.94 (s, 2H), 7.47 (m, 2H), 7.43 (d, *J* = 8.4 Hz, 2H), 7.32 (dd, *J* = 8.4, 1.6 Hz, 2H), 6.49 (m, 2H). ^{13}C NMR (101 MHz, DMSO-d_6) δ 137.46, 128.33, 128.25, 127.57, 126.39, 113.10, 109.12, 102.51, 82.29, 72.35, 66.93, 65.04. HR-MS ($ASAP^+$) *m/z* Calcd for $C_{24}H_{12}N_2$ $[M]^+$ 328.1000, found m/z : $[M]^+$ 328.1014.

5-alkynylbenzo[*b*]thiophene; 66

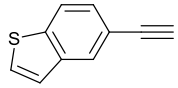

General Procedure (I): **65** (500 mg, 2.35 mmol), CuI (22 mg), [Pd(dppf)Cl_2] (96 mg), TMSA (1.15 g, 1.17 mmol), DMF/Et_3N (16 ml), 21 h, 130 °C. Solvent was removed by vacuum evaporation. The resulting solids were immediately added into a mixture of DCM/MeOH (10/20 ml) and K_2CO_3 (600 mg, 4.35 mmol) was added successively. The reaction process was checked by TLC. Purification by column chromatography using pentane as eluent gave a light yellow solid **66** (130 mg, 40% yield). m.p.: 79.3-81.2 °C. ^{1}H NMR (400 MHz, $CDCl_3$) δ 8.02 (s, 1H), 7.84 (d, *J* = 8.3 Hz, 1H), 7.48 (m, 2H), 7.31 (d, *J* = 5.5 Hz, 1H), 3.17 (s, 1H). ^{13}C NMR (101 MHz, $CDCl_3$) δ 140.42, 139.71, 127.89, 127.88, 127.81, 123.93, 122.76, 118.25, 84.33, 77.16. The NMR spectroscopic data are in agreement with those in the literature.[168]

[(Benzothiophen-5-yl)buta-1,3-diyn-1-yl]trimethylsilane; 69f

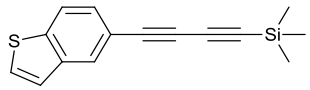

Trimethylsilylacetylene (TMSA) (930 mg, 9.4 mmol), [Pd(PPh_3)Cl_2] (33 mg) and CuI (9 mg) was added to a solution of **66** (150 mg, 0.94 mmol) in THF/Et_3N (12 ml). Air was bubbled constantly through the solution until the reaction was complete after 12 hours at r.t.. Purification by column chromatography using PE as eluent gave **69f** as a yellow solid (90 mg, 38% yield). m.p.: 91.3-92.4 °C. ^{1}H NMR (400 MHz, $CDCl_3$) δ 7.97 (s, 1H), 7.81 (d, *J* = 8.3 Hz, 1H), 7.48 (d, *J* = 5.5 Hz, 1H), 7.44 (d, *J* = 8.3 Hz, 1H), 7.30 (d, *J* = 5.5 Hz, 1H), 0.26 (s, 9H). ^{13}C NMR (101 MHz, $CDCl_3$) δ 140.93, 139.66, 128.47, 128.06, 127.96, 123.87, 122.84, 117.36, 90.67, 88.24, 77.46, 73.98, 0.00. HR-MS (ASAP$^+$) *m/z* Calcd for $C_{15}H_{15}SiS$ $[M+H]^+$ 255.0664, found *m/z* : $[M+H]^+$ 255.0662.

1,8-Bis(benzothiophen-5-yl)octa-1,3,5,7-tetrayne; BTh4

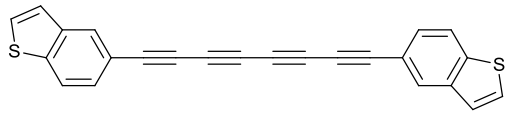

General Procedure (IV): **69f** (80 mg, 0.31 mmol), $Cu(OAc)_2.H_2O$ (130 mg), MeOH/pyridine (3 ml/3 ml), 22 h, r.t.. Purification by column chromatography using DCM/PE (5:95 v/v) as eluent gave **BTh4** as a bright yellow solid (50 mg, 87% yield). m.p.: 160 °C (decomp.). ^{1}H NMR (600 MHz, CD_2Cl_2) δ 8.08 (s, 2H), 7.89 (d, *J* = 8.3 Hz, 2H), 7.57 (d, *J* = 5.5 Hz, 2H), 7.51 (d, *J* = 8.3 Hz, 2H), 7.38 (d, *J* = 5.5 Hz, 2H). ^{13}C NMR (151 MHz, CD_2Cl_2) δ 141.54, 139.53, 128.92, 128.18,

127.97, 123.59, 122.82, 115.95, 78.38, 73.60, 66.73, 63.63. HR-MS (ASAP+) *m/z* Calcd for $C_{24}H_{10}S_2$ $[M]^+$ 362.0224, found *m/z* : $[M]^+$ 362.0224. UV/Vis (CH_2Cl_2) λ_{max} (ε) 309 (130301), 328 (136920), 350 (69825), 377 (69282), 409 (43824 $M^{-1}cm^{-1}$) nm.

1,2-Bis(benzothiophen-5-yl)ethyne; BTh1

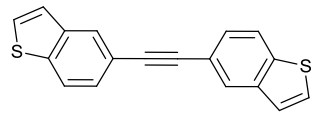

General Procedure (I): **66** (100 mg, 0.63 mmol), CuI (6 mg), [Pd(dppf)Cl_2] (23 mg), **65** (162 mg, 0.76 mmol), DMF/Et_3N (6 ml), 16 h, 130 °C. Solvent was removed by vacuum evaporation. Purification by column chromatography using dichloromethane/hexane (1:9 v/v) as eluent gave **BTh1** as a yellow solid (130 mg, 71% yield). m.p.: 218.1-220.8 °C. ^{1}H NMR (400 MHz, $CDCl_3$) δ 8.04 (dd, *J* = 1.6, 0.7 Hz, 2H), 7.86 (dt, *J* = 8.4, 0.7 Hz, 2H), 7.52 (ddd, *J* = 8.3, 1.6, 2H), 7.49 (dd, *J* = 5.5, 0.5 Hz, 2H), 7.34 (dd, *J* = 5.5, 0.8 Hz, 2H). ^{13}C NMR (101 MHz, $CDCl_3$) δ 139.81, 139.79, 127.58, 127.53, 127.09, 123.93, 122.69, 119.48, 89.43. HR-MS (ASAP+) *m/z* Calcd for $C_{18}H_{11}S_2$ $[M+H]^+$ 291.0302, found *m/z* : $[M+H]^+$ 291.0298. UV/Vis (CH_2Cl_2) λ_{max} (ε) 301 (36987), 320 (31305 $M^{-1}cm^{-1}$) nm.

1,4-Bis(benzothiophen-5-yl)1,3-butadiyne; BTh2

66 (80 mg, 0.51 mmol), [Pd(PPh_3)Cl_2] (18 mg) and CuI (5 mg) was added to a mixture of THF/Et_3N (3 ml / 1 ml). Air was bubbled constantly through the solution for 18 h at r.t. Purification by column chromatography using dichloromethane/hexane (1:9 *v*/*v*) as eluent gave **BTh2** as a yellow solid (40 mg, 50% yield). m.p.: 213.5-214.5 °C. ^{1}H NMR (400 MHz, CD_2Cl_2) δ 8.06 (dd, *J* = 1.6, 0.7 Hz, 2H), 7.90 (dt, *J* = 8.4, 0.8 Hz, 2H), 7.57 (dd, *J* = 5.5, 0.8 Hz, 2H), 7.50 (m, 2H), 7.38 (dd, *J* = 5.5, 0.8 Hz, 2H). ^{13}C NMR (101 MHz, CD_2Cl_2) δ 140.90, 139.79, 128.18, 128.16, 127.86, 123.85, 122.90, 117.65, 81.91, 73.54. HR-MS (ASAP+) *m/z* Calcd for $C_{20}H_{10}S_2$ $[M]^+$ 314.0224, found *m/z* : $[M]^+$ 314.0221. UV/Vis (CH_2Cl_2) λ_{max} (ε) 302 (39770), 322 (52067), 346 (44558 $M^{-1}cm^{-1}$) nm.

7.3.5 Experimental for Chapter 6

2,6-diiodoanthraquinone; 74

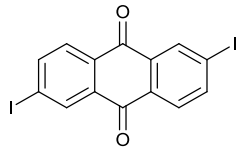

To a suspension of **73** (4.77 g, 20 mmol) in 2.4 M H_2SO_4 (110 ml) solution, $NaNO_2$ (8.28 g) solution was added dropwise. The mixture was left at -15 ^oC for 30 mins before KI (36.5 g) solution was added dropwise. The reaction was left to rise to r.t. and heated to 80 ^oC for 5 h. The mixture was filtered and the residue was washed subsequently with NH_4Cl solution, $NaHCO_3$ solution, $Na_2S_2O_3$ solution and water before leaving it in the oven to dry. Purification by column chromatography using dichloromethane/hexane (1:9 v/v) as eluent gave a light yellow solid **74** (6.5 g, 71% yield). m.p.:281.1-283.7 ^oC. ^1H NMR (400 MHz, $CDCl_3$) δ 8.64 (d, *J* = 1.7 Hz, 2H), 8.17 (dd, *J* = 8.3, 2.0, 2H), 7.98 (d, *J* = 8.2 Hz, 2H). ^{13}C NMR (101 MHz, $CDCl_3$) δ 183.87, 143.59, 137.60, 136.56, 132.29, 128.97, 102.95. The NMR spectroscopic data are in agreement with those in the literature.[169]

2,6-bis(4-ethynylpyridine)-9,10-anthraquinone; 2,6-AQ

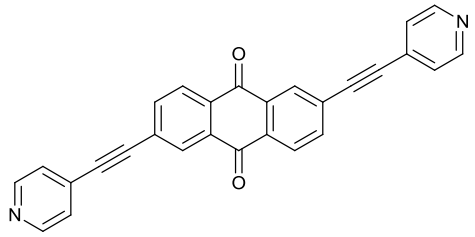

General Procedure (I): 74 (200 mg, 0.43 mmol), [$Pd(PPh_3)_4$] (50 mg), CuI (8 mg), 4-ethynylpyridine (112 mg, 1.1 mmol), THF/Et_3N (20 ml), 22 h, 50 ^oC. Purification by column chromatography using dichloromethane/ethyl acetate (1:99 v/v) as eluent gave a light yellow solid **2,6-AQ** (110 mg, 62% yield). m.p.: 307 ^oC (decomp.). ^1H NMR (400 MHz, $CDCl_3$) δ 8.66 (dd, *J* = 6.4, 3.2 Hz, 4H), 8.46 (d, *J* = 1.6 Hz, 2H), 8.33 (d, *J* = 8.0 Hz, 2H), 7.94 (dd, *J* = 8.1, 1.7 Hz, 2H), 7.43 (dd, *J* = 6.4, 3.2 Hz, 4H). ^{13}C NMR (101 MHz, $CDCl_3$) δ 181.82, 150.21, 137.09, 133.68, 132.98, 130.94, 130.51, 128.79, 127.87, 125.81, 92.01, 91.40. HR-MS (ASAP+) *m/z* Calcd for $C_{28}H_{15}N_2O_2$ $[M+H]^+$ 411.1134, found *m/z* : $[M]^+$ 411.1128. Anal. Calcd for $C_{28}H_{14}N_2O_2$: C, 81.94; H, 3.44; N, 6.83. Found: C, 81.84; H, 3.28; N, 7.01.

1,5-diiodo-9,10-anthraquinone; 76

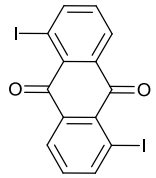

To a suspension of **75** (4.77 g, 20 mmol) in 2.4 M H_2SO_4 (110 ml) solution, $NaNO_2$ (8.28 g) solution was added dropwise. The mixture was left at -15 °C for 30 mins before KI (36.5 g) solution was added dropwise. The reaction was left to rise to r.t. and heated to 80 °C for 5 h. The mixture was filtered and the residue was washed subsequently with NH_4Cl solution, $NaHCO_3$ solution, $Na_2S_2O_3$ solution and water before leaving it in the oven to dry. Purification by column chromatography using dichloromethane/hexane (3:2 v/v) as eluent gave an orange solid **76** (3.00 g, 33% yield). m.p.: 303 °C (decomp.). ^{1}H NMR (700 MHz, CD_2Cl_2) δ 8.42 (dd, *J* = 7.8, 1.2 Hz, 2H), 8.37 (dd, *J* = 7.8, 1.3 Hz, 2H), 7.43 (t, *J* = 7.8 Hz, 2H). ^{13}C NMR (176 MHz, CD_2Cl_2) δ 180.43, 148.12, 136.24, 134.09, 131.94, 128.48, 92.35.

1,5-bis(4-ethynylpyridine)-9,10-anthraquinone; 1,5-AQ

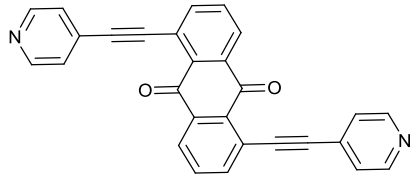

General Procedure (I): 76 (250 mg, 0.54 mmol), [$Pd(PPh_3)_4$] (62 mg), CuI (10 mg), 4-ethynylpyridine (168 mg, 1.62 mmol), THF/Et_3N (20 ml), 19 h, 50 °C. Purification by column chromatography using dichloromethane/ethyl acetate (2:98 v/v) as eluent gave a yellow solid. (110 mg, 50% yield). m.p.: 253 °C (decomp.). ^{1}H NMR (700 MHz, $CDCl_3$) δ 8.67 (dd, *J* = 5.6, 2.8 Hz, 4H), 8.42 (dd, *J* = 7.7, 1.3 Hz, 2H), 7.99 (dd, *J* = 7.6, 1.3 Hz, 2H), 7.81 (t, J = 7.7 Hz, 2H), 7.56 (dd, *J* = 5.6, 2.8 Hz, 4H). ^{13}C NMR (176 MHz, $CDCl_3$) δ 181.28, 149.88, 140.01, 135.05, 133.35, 132.89, 131.19, 128.48, 125.77, 122.16, 92.83, 92.43. HR-MS (ASAP+) *m/z* Calcd for $C_{28}H_{15}N_2O_2$ $[M+H]^+$ 411.1134, found *m/z* : $[M]^+$ 411.1127. Anal. Calcd for $C_{28}H_{14}N_2O_2$: C, 81.94; H, 3.44; N, 6.83. Found: C, 81.96; H, 3.29; N, 6.96.

1-amino-4-iodo-9,10-anthraquinone; 79

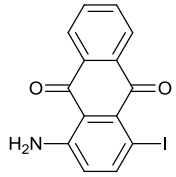

To a suspension of **77** (4.77 g, 20 mmol) in 2.4 M H_2SO_4 (110 ml) solution, $NaNO_2$ (8.28 g) solution was added dropwise. The mixture was left at -15 ^oC for 30 mins before KI (36.5 g) solution was added dropwise. The reaction was left to rise to r.t. and heated to 80 ^oC for 5 h. The mixture was filtered and the solid residue was washed sequentially with NH_4Cl solution, $NaHCO_3$ solution, $Na_2S_2O_3$ solution and water before leaving it in the oven to dry. Purification by column chromatography using dichloromethane/hexane (3:2 v/v) as eluent gave an orange solid **79** (3.5 g, 50% yield). m.p.: 210 ^oC (decomp.). ^1H NMR (400 MHz, $CDCl_3$) δ 8.28 (m, 2H), 8.03 (d, *J* = 8.9 Hz, 1H), 7.77 (m, 2H), 6.66 (d, *J* = 8.9 Hz, 1H). ^{13}C NMR (101 MHz, $CDCl_3$) δ 184.30, 182.15, 151.70, 148.55, 133.84, 133.74, 133.49, 133.16, 133.08, 127.23, 126.34, 123.64, 115.60, 78.78. MS (ASAP+) m/z : 350.0 ($[M+H]^+$, 100%).

1,4-diiodo-9,10-anthraquinone; 78

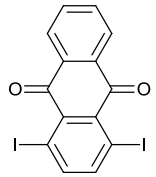

To a suspension of **79** (3.0 g, 8.6 mmol) in 2.4 M H_2SO_4 (30 ml) solution, $NaNO_2$ (3.56 g) solution was added dropwise. The mixture was left at -15 ^oC for 30 mins before KI (15.7 g) solution was added dropwise. The reaction was left to rise to r.t. and heated to 80 ^oC for 5 h. The mixture was filtered and the residue was washed sequentially with NH_4Cl solution, $NaHCO_3$ solution, $Na_2S_2O_3$ solution and water before leaving it in the oven to dry. Purification by column chromatography using dichloromethane/hexane (2:3 v/v) as eluent gave a yellow solid **78** (2.0 g, 51% yield). m.p.: 216.3-218.5 ^oC. ^1H NMR (400 MHz, $CDCl_3$) δ 8.23 (dd, *J* = 5.8, 3.3Hz, 2H), 7.97 (s, 2H), 7.78 (m, 2H). ^{13}C NMR (101 MHz, $CDCl_3$) δ 181.20, 148.17, 134.79, 134.56, 133.32, 127.32, 94.28. MS (ASAP+) m/z: 460.9 ($[M+H]^+$, 100%).

1,4-bis(4-ethynylpyridine)-9,10-anthraquinone; 1,4-AQ

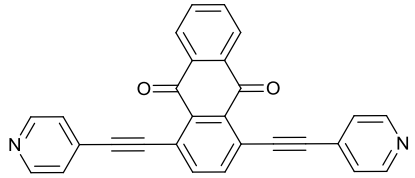

General Procedure (I): 78 (250 mg, 0.54 mmol), $[Pd(PPh_3)_4]$ (62 mg), CuI (10 mg), 4-ethynylpyridine (168 mg, 1.62 mmol), THF/Et_3N (20 ml), 20 h, 50 °C. Purification by column chromatography using dichloromethane/ethyl acetate (2:98 v/v) as eluent gave a yellow solid **1,4-AQ** (200 mg, 90% yield). m.p.: 270 °C (decomp.). ^{1}H NMR (400 MHz, $CDCl_3$) δ 8.68 (m, 4H), 8.32 (dd, *J* = 5.8, 3.3 Hz, 2H), 7.95 (s, 2H), 7.83 (dd, *J* = 5.8, 3.3 Hz, 2H), 7.56 (m, 4H). ^{13}C NMR (101 MHz, $CDCl_3$) δ 181.81, 150.15, 139.08, 135.20, 134.58, 133.35, 131.29, 127.48, 126.00, 123.18, 94.58, 93.30. HR-MS (ASAP+) *m/z* Calcd for $C_{28}H_{15}N_2O_2$ $[M+H]^+$ 411.1134, found *m/z* : $[M]^+$ 411.1154. Anal. Calcd for $C_{28}H_{14}N_2O_2$: C, 81.94; H, 3.44; N, 6.83. Found: C, 80.93; H, 3.57; N, 6.97.

Appendix I. List of seminars attended

- 10/11/10: Martyn Twigg, Johnson Matthey, “Controlling emissions from cars – Chemistry, success and challenges”
- 12/11/10: Michael Bendikov, Weizmann Institute of Science, Israel, “Novel organic electronic materials”
- 23/02/11: Laura Herz, University of Oxford, “Ultraphotoexcitation dynamics in organic/inorganic hybrid materials”
- 09/03/11: N. Champness, Nottingham, UK, “*Molecular Organisation: Working with Molecules on the Nanoscale*”
- 03/05/11: Michael Willis, University of Oxford, “New reactivity and selectivity in rhodium and palladium catalysts”
- 11/05/11: Peter Skabara, University of Strathclyde, “Complex conjugated architectures – from synthesis through to device applications”
- 11/05/11: Carmen Nicasio, University of Seville, “Carbon-heteroatom bond forming reactions catalysed by copper and nickel complexes”
- 13/05/11: Henri Doucet, University of Rennes, “Palladium catalysed arylations or alkenylations of heteroaromatics *via* C-H bond activation”
- 18/05/11: Randy Thummel, University of Houston, “Designing heterocyclic ligands to help capture the sun”
- 21/06/11: Jacob Israelachvilli, University of California, Santa Barbara, “The search for the hydrophobic interaction potential”
- 12/09/11: Chihaya Adachi, Kyushu University, “A new concept for light emitting materials and devices”
- 09/11/11: Leone Spiccia, Monash University, “Harvesting solar energy in photoelectrochemical solar cells”
- 14/11/11: Jonathan Sessler, University of Texas, “Recent advances in calixpyrrole chemistry”
- 07/12/11: Jianliang Xiao, University of Liverpool, “Metal-organo cooperative catalysis: Asymmetric hydrogenation with achiral metal catalysts”
- 17/01/12: Xile Hu, EPFL, “Catalysts made of earth-abundant elements for making C-C and H-H bonds”

- 31/01/12: Niek Buurma, Cardiff University, “Physical organic chemistry in water”
- 28/02/12: Peter Scott, University of Warwick, “Chiral metal compounds in catalysis and medicine”
- 13/03/12: Paul Quigley, Shasun, “Aromatic bond formation: An overview”
- 03/04/12: Jean-François Halet, University of Rennes, “An example of conjugated systems containing boron moieties”
- 03/04/12: Todd Marder, University of Durham, “Diethynyrhodacyclopentadienes: A new class of luminescent organometallics”
- 04/04/12: Paul Low, University of Durham, “Twists and turns: The surprising redox chemistry of ruthenium complexes”
- 03-04 April 2012: Durham-Rennes Mini Symposium.
- 04/04/12: Véronique Guerchais, University of Rennes, “Synthetic strategies to functionalised luminescent cyclometallated Ir(III) complexes”
- 01/05/12: David Parker, Durham University, “Lanthanide coordination chemistry: Probe, excite, measure, relax”
- 09/05/12: Etienne Baranoff, University of Birmingham, “Cyclometallated iridium(III) complexes: to OLED materials… and beyond”
- 31/10/12: Dr. Gordon Florence, University of St. Andrews, “Metal catalysts for the activation of renewable resources to make polymers”
- 27/02/13: Prof. Herbert Mayr, LMU Munich, “Reactivity scales for designing organic syntheses”
- 01/05/13: Prof. Michael Ward, University of Sheffield, “Self-assembly and host-guest chemistry of polyhedral coordination cages”
- 23/10/13: Prof. Bernard Golding, Newcastle University, “Trifluoroethanol, the magic solvent in the search for new cancer therapies”
- 22/01/14: Prof. Ronald Raines, University of Wisconsin-Madison, “RSC Jeremy Knowles Award Lecture”

Appendix II. Proton NMRs for OAEs

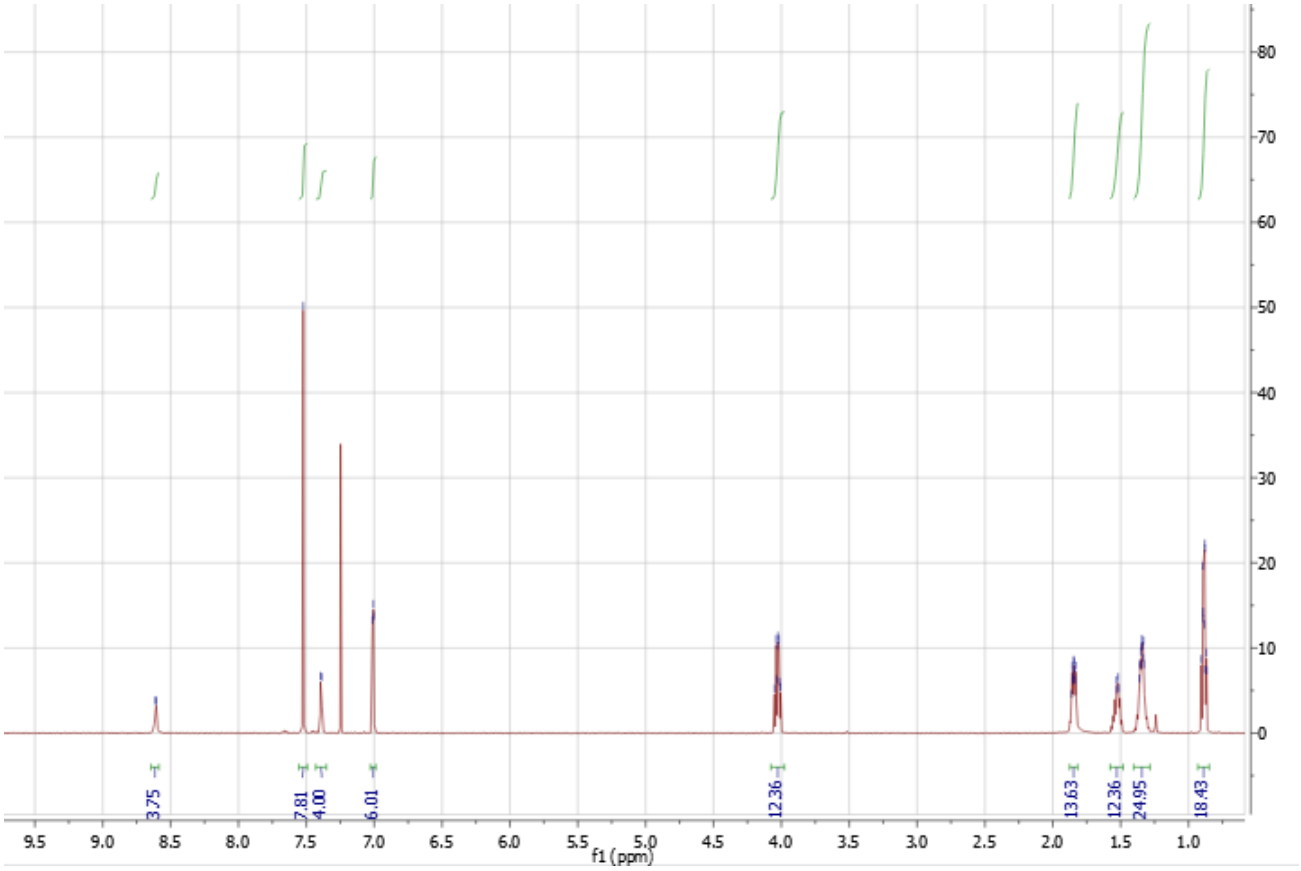

^{1}H NMR spectrum of OAE7 in $CDCl_3$.

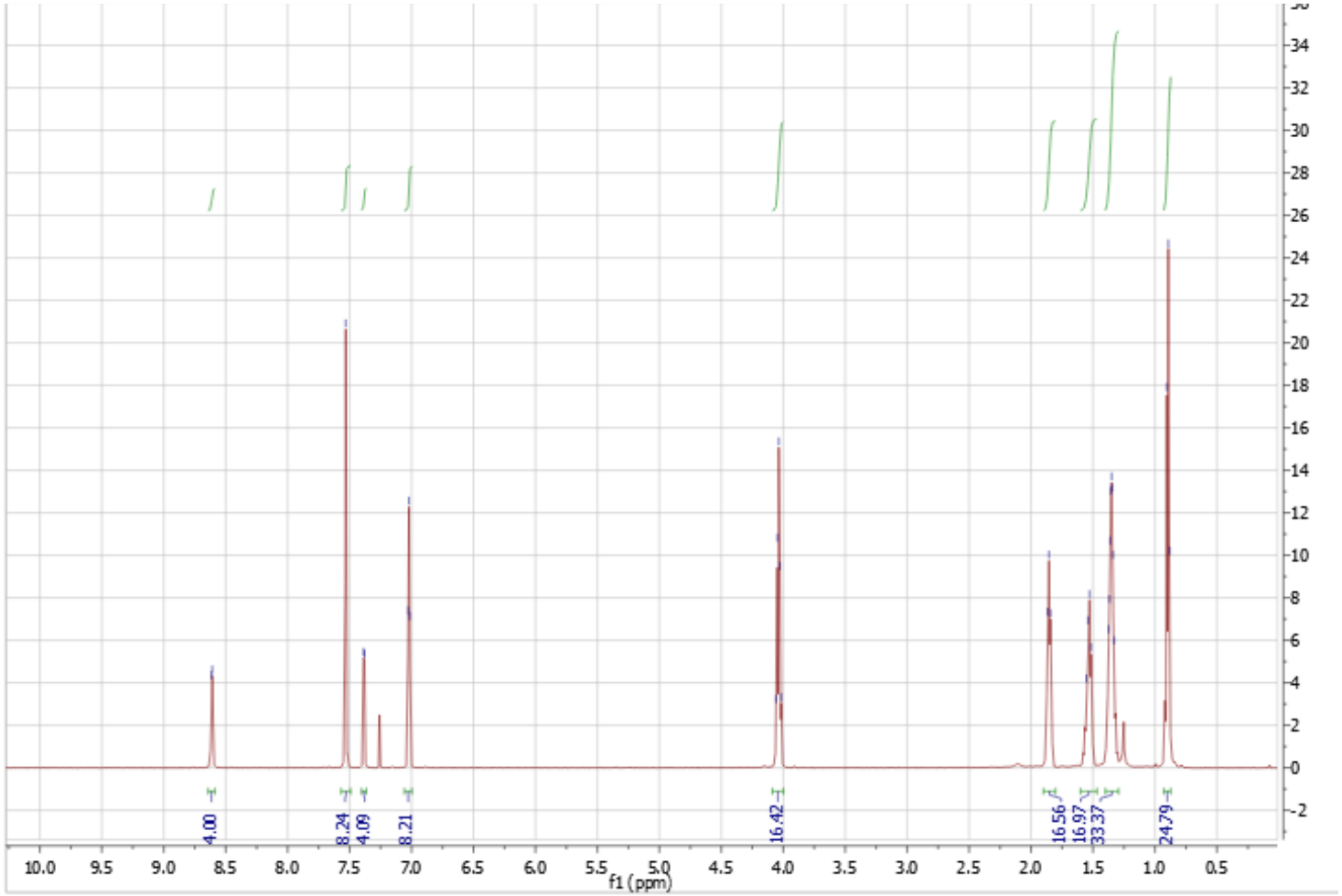

^{1}H NMR spectrum of OAE8b in $CDCl_3$.

^{1}H NMR spectrum of OAE9 in $CDCl_3$.

Bibliography

(1) Reed, M. A.; Zhou, C.; Muller, C. J.; Burgin, T. P.; Tour, J. M. *Science* **1997**, *278*, 252.
(2) Moore, G. E. *Electronics* **1965**, *38*, 114.
(3) Moore, G. E. *IEDM Tech. Dig.* **1975**, 11.
(4) Myhrvold, N. Moore's law Corollary: Pixel Power. [Online Early Access]. Published Online: 2006. http://www.nytimes.com/2006/06/07/technology/circuits/07essay.html?_r=0 (accessed 06/02/2014).
(5) Keyes, R. W. *SSCC, Newsletter, IEEE* **2006**, *11*, 25.
(6) Michael, K. Moore's law to roll on for another decade. [Online Early Access]. Published Online: 2003. http://news.cnet.com/2100-1001-984051.html.
(7) Mack, C. A. *IEEE TRANSACTIONS ON SEMICONDUCTOR MANUFACTURING* **2011**, *24*, 202.
(8) Michael, K. New life for Moore's law. [Online Early Access]. Published Online: 2005. http://news.cnet.com/New-life-for-Moores-Law/2009-1006_3-5672485.html.
(9) *International techonology Roadmap for Semiconductors* [Online Early Access]. Published Online: 2010. http://www.itrs.net/Links/2010ITRS/Home2010.htm.
(10) Ghosh, A. W.; Damle, P. S.; Datta, S.; Nitzan, A. *MRS Bulletin* **2004**, *29*, 391.
(11) González, M. T.; Wu, S.; Huber, R.; van der Molen, S. J.; Schönenberger, C.; Calame, M. *Nano Lett.* **2006**, *6*, 2238.
(12) Low, P. J. *Dalton Trans.* **2005**, 2821.
(13) Aviram, A.; Ratner, M. A. *Chem. Phys. Lett.* **1974**, *29*, 277.
(14) McCreery, R. L.; Bergren, A. J. *Adv. Mater.* **2009**, *21*, 4303.
(15) Puigmarti-Luis, J.; Minoia, A.; Lei, S.; Geskin, V.; Li, B.; Lazzaroni, R.; De Feyter, S.; Amabilino, D. B. *Chem. Sci.* **2011**, *2*, 1945.
(16) Adaligil, E.; Slowinski, K. *J. Electroanal. Chem.* **2010**, *649*, 142.
(17) Chen, J.; Reed, M. A.; Rawlett, A. M.; Tour, J. M. *Science* **1999**, *286*, 1550.
(18) Morgenstern, K.; Lorente, N.; Rieder, K.-H. *Phys. Status Solidi B* **2013**, *250*, 1671.
(19) Li, X. L.; Hua, S. Z.; Chopra, H. D.; Tao, N. J. *Micro & Nano Letters* **2006**, *1*, 83.
(20) Thuo, M. M.; Reus, W. F.; Nijhuis, C. A.; Barber, J. R.; Kim, C.; Schulz, M. D.; Whitesides, G. M. *J. Am. Chem. Soc.* **2011**, *133*, 2962.
(21) Lopinski, G. P.; Moffatt, D. J.; Wayner, D. D. M.; Zgierski, M. Z.; Wolkow, R. A. *J. Am. Chem. Soc.* **1999**, *121*, 4532.
(22) Pitters, J. L.; Dogel, I.; DiLabio, G. A.; Wolkow, R. A. *J. Phys. Chem. B* **2006**, *110*, 2159.
(23) Nazin, G. V.; Qiu, X. H.; Ho, W. *Science* **2003**, *302*, 77.
(24) Donhauser, Z. J.; Mantooth, B. A.; Kelly, K. F.; Bumm, L. A.; Monnell, J. D.; Stapleton, J. J.; Price, D. W.; Rawlett, A. M.; Allara, D. L.; Tour, J. M.; Weiss, P. S. *Science* **2001**, *292*, 2303.
(25) Kelley, T. W.; Granstrom, E.; Frisbie, C. D. *Adv. Mater.* **1999**, *11*, 261.
(26) Cui, X. D.; Primak, A.; Zarate, X.; Tomfohr, J.; Sankey, O. F.; Moore, A. L.; Moore, T. A.; Gust, D.; Harris, G.; Lindsay, S. M. *Science* **2001**, *294*, 571.
(27) Xu, B.; Tao, N. J. *Science* **2003**, *301*, 1221.
(28) Li, C.; Pobelov, I.; Wandlowski, T.; Bagrets, A.; Arnold, A.; Evers, F. *J. Am. Chem. Soc.* **2007**, *130*, 318.
(29) Chen, F.; Hihath, J.; Huang, Z.; Li, X.; Tao, N. J. *Annu. Rev. Phys. Chem.* **2007**, *58*, 535.
(30) Haiss, W.; van Zalinge, H.; Higgins, S. J.; Bethell, D.; Höbenreich, H.; Schiffrin, D. J.; Nichols, R. J. *J. Am. Chem. Soc.* **2003**, *125*, 15294.
(31) Haiss, W.; Nichols, R. J.; van Zalinge, H.; Higgins, S. J.; Bethell, D.; Schiffrin, D. J. *PCCP* **2004**, *6*, 4330.
(32) Agraït, N.; Yeyati, A. L.; van Ruitenbeek, J. M. *Phys. Rep.* **2003**, *377*, 81.
(33) J, M.; JW, E. *J. Appl. Phys.* **1985**, *58*, 3888.

(34) Muller, C. J.; van Ruitenbeek, J. M.; de Jongh, L. J. *Phys. Rev. Lett.* **1992**, *69*, 140.
(35) Grüter, L.; González, M. T.; Huber, R.; Calame, M.; Schönenberger, C. *Small* **2005**, *1*, 1067.
(36) Huber, R.; González, M. T.; Wu, S.; Langer, M.; Grunder, S.; Horhoiu, V.; Mayor, M.; Bryce, M. R.; Wang, C.; Jitchati, R.; Schönenberger, C.; Calame, M. *J. Am. Chem. Soc.* **2008**, *130*, 1080.
(37) Lörtscher, E.; Ciszek, J. W.; Tour, J.; Riel, H. *Small* **2006**, *2*, 973.
(38) Dulić, D.; van der Molen, S. J.; Kudernac, T.; Jonkman, H. T.; de Jong, J. J. D.; Bowden, T. N.; van Esch, J.; Feringa, B. L.; van Wees, B. J. *Phys. Rev. Lett.* **2003**, *91*, 207402.
(39) Kronemeijer, A. J.; Akkerman, H. B.; Kudernac, T.; van Wees, B. J.; Feringa, B. L.; Blom, P. W. M.; de Boer, B. *Adv. Mater.* **2008**, *20*, 1467.
(40) Kim, Y.; Hellmuth, T. J.; Sysoiev, D.; Pauly, F.; Pietsch, T.; Wolf, J.; Erbe, A.; Huhn, T.; Groth, U.; Steiner, U. E.; Scheer, E. *Nano Lett.* **2012**, *12*, 3736.
(41) Xiang, D.; Jeong, H.; Lee, T.; Mayer, D. *Adv. Mater.* **2013**, *25*, 4845.
(42) Gittins, D. I.; Bethell, D.; Schiffrin, D. J.; Nichols, R. J. *Nature* **2000**, *408*, 67.
(43) Weibel, N.; Grunder, S.; Mayor, M. *Org. Biomol. Chem.* **2007**, *5*, 2343.
(44) Li, Z.; Han, B.; Meszaros, G.; Pobelov, I.; Wandlowski, T.; Blaszczyk, A.; Mayor, M. *Faraday Discuss.* **2006**, *131*, 121.
(45) van Dijk, E. H.; Myles, D. J. T.; van der Veen, M. H.; Hummelen, J. C. *Org. Lett.* **2006**, *8*, 2333.
(46) Sørensen, J. K.; Vestergaard, M.; Kadziola, A.; Kilså, K.; Nielsen, M. B. *Org. Lett.* **2006**, *8*, 1173.
(47) Metzger, R. M. *Acc. Chem. Res.* **1999**, *32*, 950.
(48) Elbing, M.; Ochs, R.; Koentopp, M.; Fischer, M.; von Hänisch, C.; Weigend, F.; Evers, F.; Weber, H. B.; Mayor, M. *PNAS* **2005**, *102*, 8815.
(49) Robertson, N.; McGowan, C. A. *Chem. Soc. Rev.* **2003**, *32*, 96.
(50) Hong, W.; Manrique, D. Z.; Moreno-García, P.; Gulcur, M.; Mishchenko, A.; Lambert, C. J.; Bryce, M. R.; Wandlowski, T. *J. Am. Chem. Soc.* **2012**, *134*, 2292.
(51) Tour, J. M. *Acc. Chem. Res.* **2000**, *33*, 791.
(52) James, P. V.; Sudeep, P. K.; Suresh, C. H.; Thomas, K. G. *J. Phys. Chem. A* **2006**, *110*, 4329.
(53) Wu, S. M.; Gonzalez, M. T.; Huber, R.; Grunder, S.; Mayor, M.; Schonenberger, C.; Calame, M. *Nat. Nanotechnol.* **2008**, *3*, 569.
(54) Martín, S.; Grace, I.; Bryce, M. R.; Wang, C.; Jitchati, R.; Batsanov, A. S.; Higgins, S. J.; Lambert, C. J.; Nichols, R. J. *J. Am. Chem. Soc.* **2010**, *132*, 9157.
(55) Chen, F.; Li, X.; Hihath, J.; Huang, Z.; Tao, N. *J. Am. Chem. Soc.* **2006**, *128*, 15874.
(56) Kiguchi, M.; Takahashi, T.; Kanehara, M.; Teranishi, T.; Murakoshi, K. *J. Phys. Chem. C* **2009**, *113*, 9014.
(57) Venkataraman, L.; Klare, J. E.; Tam, I. W.; Nuckolls, C.; Hybertsen, M. S.; Steigerwald, M. L. *Nano Lett.* **2006**, *6*, 458.
(58) Mayor, M.; Weber, H. B.; Reichert, J.; Elbing, M.; von Hänisch, C.; Beckmann, D.; Fischer, M. *Angew. Chem. Int. Ed.* **2003**, *42*, 5834.
(59) James, D. K.; Tour, J. M. *Chem. Mater.* **2004**, *16*, 4423.
(60) McCreery, R. L. *Chem. Mater.* **2004**, *16*, 4477.
(61) Luo, L.; Choi, S. H.; Frisbie, C. D. *Chem. Mater.* **2011**, *23*, 631.
(62) Liu, H.; Yu, C.; Gao, N.; Zhao, J. *ChemPhysChem* **2010**, *11*, 1895.
(63) Davis, W. B.; Svec, W. A.; Ratner, M. A.; Wasielewski, M. R. *Nature* **1998**, *396*, 60.
(64) Ho Choi, S.; Kim, B.; Frisbie, C. D. *Science* **2008**, *320*, 1482.
(65) Hines, T.; Diez-Perez, I.; Hihath, J.; Liu, H.; Wang, Z.-S.; Zhao, J.; Zhou, G.; Müllen, K.; Tao, N. *J. Am. Chem. Soc.* **2010**, *132*, 11658.
(66) Bunz, U. H. F. *Chem. Rev.* **2000**, *100*, 1605.
(67) Jenny, N. M.; Mayor, M.; Eaton, T. R. *Eur. J. Org. Chem.* **2011**, *2011*, 4965.

(68) Tour, J. M.; Rawlett, A. M.; Kozaki, M.; Yao, Y.; Jagessar, R. C.; Dirk, S. M.; Price, D. W.; Reed, M. A.; Zhou, C.-W.; Chen, J.; Wang, W.; Campbell, I. *Chem. Eur. J.* **2001**, *7*, 5118.
(69) Kaliginedi, V.; Moreno-García, P.; Valkenier, H.; Hong, W.; García-Suárez, V. M.; Buiter, P.; Otten, J. L. H.; Hummelen, J. C.; Lambert, C. J.; Wandlowski, T. *J. Am. Chem. Soc.* **2012**, *134*, 5262.
(70) Hu, W.; Jiang, J.; Nakashima, H.; Luo, Y.; Kashimura, Y.; Chen, K.-Q.; Shuai, Z.; Furukawa, K.; Lu, W.; Liu, Y.; Zhu, D.; Torimitsu, K. *Phys. Rev. Lett.* **2006**, *96*, 027801.
(71) Lu, Q.; Liu, K.; Zhang, H.; Du, Z.; Wang, X.; Wang, F. *ACS Nano* **2009**, *3*, 3861.
(72) Lu, Q.; Yao, C.; Wang, X.; Wang, F. *J. Phys. Chem. C* **2012**, *116*, 17853.
(73) Tour, J. M.; Jones, L.; Pearson, D. L.; Lamba, J. J. S.; Burgin, T. P.; Whitesides, G. M.; Allara, D. L.; Parikh, A. N.; Atre, S. *J. Am. Chem. Soc.* **1995**, *117*, 9529.
(74) Valkenier, H.; Huisman, E. H.; van Hal, P. A.; de Leeuw, D. M.; Chiechi, R. C.; Hummelen, J. C. *J. Am. Chem. Soc.* **2011**, *133*, 4930.
(75) Wang, C.; Batsanov, A. S.; Bryce, M. R.; Martín, S.; Nichols, R. J.; Higgins, S. J.; García-Suárez, V. c. M.; Lambert, C. J. *J. Am. Chem. Soc.* **2009**, *131*, 15647.
(76) Kamenetska, M.; Quek, S. Y.; Whalley, A. C.; Steigerwald, M. L.; Choi, H. J.; Louie, S. G.; Nuckolls, C.; Hybertsen, M. S.; Neaton, J. B.; Venkataraman, L. *J. Am. Chem. Soc.* **2010**, *132*, 6817.
(77) Grunder, S.; Huber, R.; Horhoiu, V.; González, M. T.; Schönenberger, C.; Calame, M.; Mayor, M. *J. Org. Chem.* **2007**, *72*, 8337.
(78) Sonogashira, K. *J. Organomet. Chem.* **2002**, *653*, 46.
(79) Ramey, M. B.; Hille; Rubner, M. F.; Tan, C.; Schanze, K. S.; Reynolds, J. R. *Macromolecules* **2004**, *38*, 234.
(80) Khatyr, A.; Ziessel, R. *J. Org. Chem.* **2000**, *65*, 3126.
(81) van der Sluis, P.; Spek, A. L. *Acta Crystallographica Section A* **1990**, *46*, 194.
(82) Lee, S. H.; Nakamura, T.; Tsutsui, T. *Org. Lett.* **2001**, *3*, 2005.
(83) Wang, C.; Batsanov, A. S.; Bryce, M. R. *J. Org. Chem.* **2005**, *71*, 108.
(84) Xue, C.; Luo, F.-T. *Tetrahedron* **2004**, *60*, 6285.
(85) Osowska, K.; Miljanic, O. S. *Chem. Commun.* **2010**, *46*, 4276.
(86) Li, Q.; Sue, C.-H.; Basu, S.; Shveyd, A. K.; Zhang, W.; Barin, G.; Fang, L.; Sarjeant, A. A.; Stoddart, J. F.; Yaghi, O. M. *Angew. Chem. Int. Ed.* **2010**, *49*, 6751.
(87) Quek, S. Y.; Kamenetska, M.; Steigerwald, M. L.; Choi, H. J.; Louie, S. G.; Hybertsen, M. S.; Neaton, J. B.; Venkataraman, L. *Nat Nanotechnol* **2009**, *4*, 230.
(88) Newton, M. D.; Smalley, J. F. *PCCP* **2007**, *9*, 555.
(89) Hong, W.; Valkenier, H.; Mészáros, G.; Manrique, D. Z.; Mishchenko, A.; Putz, A.; García, P. M.; Lambert, C. J.; Hummelen, J. C.; Wandlowski, T. *Beilstein Journal of Nanotechnology* **2011**, *2*, 699.
(90) Mishchenko, A.; Zotti, L. A.; Vonlanthen, D.; Bürkle, M.; Pauly, F.; Cuevas, J. C.; Mayor, M.; Wandlowski, T. *J. Am. Chem. Soc.* **2011**, *133*, 184.
(91) Martin, C. A.; Ding, D.; Sørensen, J. K.; Bjørnholm, T.; van Ruitenbeek, J. M.; van der Zant, H. S. J. *J. Am. Chem. Soc.* **2008**, *130*, 13198.
(92) Wold, D. J.; Haag, R.; Rampi, M. A.; Frisbie, C. D. *J. Phys. Chem. B* **2002**, *106*, 2813.
(93) Ishida, T.; Mizutani, W.; Aya, Y.; Ogiso, H.; Sasaki, S.; Tokumoto, H. *J. Phys. Chem. B* **2002**, *106*, 5886.
(94) Moreno-García, P.; Gulcur, M.; Manrique, D. Z.; Pope, T.; Hong, W.; Kaliginedi, V.; Huang, C.; Batsanov, A. S.; Bryce, M. R.; Lambert, C.; Wandlowski, T. *J. Am. Chem. Soc.* **2013**, *135*, 12228.
(95) Liu, H.; Wang, N.; Zhao, J.; Guo, Y.; Yin, X.; Boey, F. Y. C.; Zhang, H. *ChemPhysChem* **2008**, *9*, 1416.
(96) Yamada, R.; Kumazawa, H.; Noutoshi, T.; Tanaka, S.; Tada, H. *Nano Lett.* **2008**, *8*, 1237.

(97) Sedghi, G.; Garcia-Suarez, V. M.; Esdaile, L. J.; Anderson, H. L.; Lambert, C. J.; Martin, S.; Bethell, D.; Higgins, S. J.; Elliott, M.; Bennett, N.; Macdonald, J. E.; Nichols, R. J. *Nat Nanotechnol* **2011**, *6*, 517.
(98) Yamada, R.; Kumazawa, H.; Tanaka, S.; Tada, H. *Appl Phys Express* **2009**, *2*, 025002.
(99) Adams, D. M.; Brus, L.; Chidsey, C. E. D.; Creager, S.; Creutz, C.; Kagan, C. R.; Kamat, P. V.; Lieberman, M.; Lindsay, S.; Marcus, R. A.; Metzger, R. M.; Michel-Beyerle, M. E.; Miller, J. R.; Newton, M. D.; Rolison, D. R.; Sankey, O.; Schanze, K. S.; Yardley, J.; Zhu, X. *J. Phys. Chem. B* **2003**, *107*, 6668.
(100) Edwards, P. P.; Gray, H. B.; Lodge, M. T. J.; Williams, R. J. P. *Angew. Chem. Int. Ed.* **2008**, *47*, 6758.
(101) Zhao, X.; Huang, C.; Gulcur, M.; Batsanov, A. S.; Baghernejad, M.; Hong, W.; Bryce, M. R.; Wandlowski, T. *Chem. Mater.* **2013**, *25*, 4340.
(102) Sautet, P.; Joachim, C. *Chem. Phys. Lett.* **1988**, *153*, 511.
(103) Kocherzhenko, A. A.; Grozema, F. C.; Siebbeles, L. D. A. *J. Phys. Chem. C* **2010**, *114*, 7973.
(104) Kocherzhenko, A. A.; Siebbeles, L. D. A.; Grozema, F. C. *J. Phys. Chem. Lett.* **2011**, *2*, 1753.
(105) Markussen, T.; Stadler, R.; Thygesen, K. S. *Nano Lett.* **2010**, *10*, 4260.
(106) Solomon, G. C.; Andrews, D. Q.; Hansen, T.; Goldsmith, R. H.; Wasielewski, M. R.; Van Duyne, R. P.; Ratner, M. A. *J. Chem. Phys.* **2008**, *129*, 054701.
(107) Solomon, G. C.; Andrews, D. Q.; Goldsmith, R. H.; Hansen, T.; Wasielewski, M. R.; Van Duyne, R. P.; Ratner, M. A. *J. Am. Chem. Soc.* **2008**, *130*, 17301.
(108) Solomon, G. C.; Andrews, D. Q.; Van Duyne, R. P.; Ratner, M. A. *J. Am. Chem. Soc.* **2008**, *130*, 7788.
(109) Arroyo, C. R.; Tarkuc, S.; Frisenda, R.; Seldenthuis, J. S.; Woerde, C. H. M.; Eelkema, R.; Grozema, F. C.; van der Zant, H. S. J. *Angew. Chem. Int. Ed.* **2013**, *52*, 3152.
(110) Aradhya, S. V.; Meisner, J. S.; Krikorian, M.; Ahn, S.; Parameswaran, R.; Steigerwald, M. L.; Nuckolls, C.; Venkataraman, L. *Nano Lett.* **2012**, *12*, 1643.
(111) Hanss, D.; Walther, M. E.; Wenger, O. S. *Chem. Commun.* **2010**, *46*, 7034.
(112) Ke, S.-H.; Yang, W.; Baranger, H. U. *Nano Lett.* **2008**, *8*, 3257.
(113) Venkataraman, L.; Park, Y. S.; Whalley, A. C.; Nuckolls, C.; Hybertsen, M. S.; Steigerwald, M. L. *Nano Lett.* **2007**, *7*, 502.
(114) Chen, W.; Widawsky, J. R.; Vazquez, H.; Schneebeli, S. T.; Hybertsen, M. S.; Breslow, R.; Venkataraman, L. *J. Am. Chem. Soc.* **2011**, *133*, 17160.
(115) Leary, E.; Higgins, S. J.; van Zalinge, H.; Haiss, W.; Nichols, R. J. *Chem. Commun.* **2007**, 3939.
(116) Li, H.; Powell, D. R.; Hayashi, R. K.; West, R. *Macromolecules* **1998**, *31*, 52.
(117) González, M. T.; Díaz, A.; Leary, E.; García, R.; Herranz, M. Á.; Rubio-Bollinger, G.; Martín, N.; Agraït, N. *J. Am. Chem. Soc.* **2013**, *135*, 5420.
(118) Haley, M. M.; Tykwinski, R. R. *Carbon-Rich Compounds : From Molecules to Materials,* Wiley-VCH, Weinheim, 2006.
(119) Diederich, F.; Stang, P. J.; Tykwinski, R. R. *Acetylene Chemistry: Chemistry, Biology and Material Science*; Wiley-VCH, Weinheim, 2005.
(120) Guldi, D. M.; Illescas, B. M.; Atienza, C. M.; Wielopolski, M.; Martin, N. *Chem. Soc. Rev.* **2009**, *38*, 1587.
(121) Rodriguez-Perez, L.; Herranz, M. a. A.; Martin, N. *Chem. Commun.* **2013**, *49*, 3721.
(122) Chen, D.; Zhang, H.; Liu, Y.; Li, J. *Energ. Environ. Sci.* **2013**, *6*, 1362.
(123) Diederich, F. *Nature* **1994**, *369*, 199
(124) Chalifoux, W. A.; Tykwinski, R. R. *C. R. Chim.* **2009**, *12*, 341.
(125) Cataldo, F. *Polyynes: Synthesis Properties and Applications.* CRC Press. Taylor & Francis Group, Boca Raton, FL, 2006.
(126) Jahnke, E.; Tykwinski, R. R. *Chem. Commun.* **2010**, *46*, 3235.

(127) Vail, S. A.; Krawczuk, P. J.; Guldi, D. M.; Palkar, A.; Echegoyen, L.; Tomé, J. P. C.; Fazio, M. A.; Schuster, D. I. *Chem. Eur. J.* **2005**, *11*, 3375.
(128) Wang, C.; Pålsson, L.-O.; Batsanov, A. S.; Bryce, M. R. *J. Am. Chem. Soc.* **2006**, *128*, 3789.
(129) Pålsson, L.-O.; Wang, C.; Batsanov, A. S.; King, S. M.; Beeby, A.; Monkman, A. P.; Bryce, M. R. *Chem. Eur. J.* **2010**, *16*, 1470.
(130) Cataldo, F.; Ravagnan, L.; Cinquanta, E.; Castelli, I. E.; Manini, N.; Onida, G.; Milani, P. *J. Phys. Chem. B* **2010**, *114*, 14834.
(131) Dral, P. O.; Clark, T. *J. Phys. Chem. A* **2011**, *115*, 11303.
(132) Cornil, J.; Beljonne, D.; Calbert, J. P.; Brédas, J. L. *Adv. Mater.* **2001**, *13*, 1053.
(133) Slepkov, A. D.; Hegmann, F. A.; Eisler, S.; Elliott, E.; Tykwinski, R. R. *J. Chem. Phys.* **2004**, *120*, 6807.
(134) Crljen, Ž.; Baranović, G. *Phys. Rev. Lett.* **2007**, *98*, 116801.
(135) Garcia-Suarez, V. M.; Lambert, C. J. *Nanotechnology* **2008**, *19*, 455203.
(136) Eastmond, R.; Johnson, T. R.; Walton, D. R. M. *Tetrahedron* **1972**, *28*, 4601.
(137) Kendall, J.; McDonald, R.; Ferguson, M. J.; Tykwinski, R. R. *Org. Lett.* **2008**, *10*, 2163.
(138) Rubin, Y.; Lin, S. S.; Knobler, C. B.; Anthony, J.; Boldi, A. M.; Diederich, F. *J. Am. Chem. Soc.* **1991**, *113*, 6943.
(139) Gibtner, T.; Hampel, F.; Gisselbrecht, J.-P.; Hirsch, A. *Chem. Eur. J.* **2002**, *8*, 408.
(140) Mohr, W.; Stahl, J.; Hampel, F.; Gladysz, J. A. *Chem. Eur. J.* **2003**, *9*, 3324.
(141) Klinger, C.; Vostrowsky, O.; Hirsch, A. *Eur. J. Org. Chem.* **2006**, 1508.
(142) Movsisyan, L. D.; Kondratuk, D. V.; Franz, M.; Thompson, A. L.; Tykwinski, R. R.; Anderson, H. L. *Org. Lett.* **2012**, *14*, 3424.
(143) Zhao, C.; Kitaura, R.; Hara, H.; Irle, S.; Shinohara, H. *J. Phys. Chem. C* **2011**, *115*, 13166.
(144) Chalifoux, W. A.; Tykwinski, R. R. *Nat. Chem.* **2010**, *2*, 967.
(145) Ziessel, R.; Suffert, J.; Youinou, M.-T. *J. Org. Chem.* **1996**, *61*, 6535.
(146) Eglinton, G.; Galbraith, A. R. *J. Chem. Soc.* **1959**, 889.
(147) Bruce, M. I.; Low, P. J.; Werth, A.; Skelton, B. W.; White, A. H. *J. Chem. Soc., Dalton Trans.* **1996**, 1551.
(148) Gulia, N.; Osowska, K.; Pigulski, B.; Lis, T.; Galewski, Z.; Szafert, S. *Eur. J. Org. Chem.* **2012**, 4819.
(149) Štefko, M.; Tzirakis, M. D.; Breiten, B.; Ebert, M.-O.; Dumele, O.; Schweizer, W. B.; Gisselbrecht, J.-P.; Boudon, C.; Beels, M. T.; Biaggio, I.; Diederich, F. *Chem. Eur. J.* **2013**, *19*, 12693.
(150) Zotti, L. A.; Kirchner, T.; Cuevas, J.-C.; Pauly, F.; Huhn, T.; Scheer, E.; Erbe, A. *Small* **2010**, *6*, 1529.
(151) Xing, Y.; Park, T.-H.; Venkatramani, R.; Keinan, S.; Beratan, D. N.; Therien, M. J.; Borguet, E. *J. Am. Chem. Soc.* **2010**, *132*, 7946.
(152) Qu, W.; Kung, M. P.; Hou, C.; Oya, S.; Kung, H. F. *J. Med. Chem.* **2007**, *50*, 3380.
(153) Song, H.; Reed, M. A.; Lee, T. *Adv. Mater.* **2011**, *23*, 1583.
(154) van der Molen, S. J.; Liao, J.; Kudernac, T.; Agustsson, J. S.; Bernard, L.; Calame, M.; van Wees, B. J.; Feringa, B. L.; Schönenberger, C. *Nano Lett.* **2009**, *9*, 76.
(155) Yasuda, S.; Nakamura, T.; Matsumoto, M.; Shigekawa, H. *J. Am. Chem. Soc.* **2003**, *125*, 16430.
(156) Lykkebo, J.; Gagliardi, A.; Pecchia, A.; Solomon, G. C. *ACS Nano* **2013**, *7*, 9183.
(157) Markussen, T.; Schiötz, J.; Thygesen, K. S. *J. Chem. Phys.* **2010**, *132*, 224104.
(158) Fracasso, D.; Valkenier, H.; Hummelen, J. C.; Solomon, G. C.; Chiechi, R. C. *J. Am. Chem. Soc.* **2011**, *133*, 9556.
(159) Guedon, C. M.; Valkenier, H.; Markussen, T.; Thygesen, K. S.; Hummelen, J. C.; van der Molen, S. J. *Nat Nanotechnol* **2012**, *7*, 305.

(160) Valkenier, H.; Guedon, C. M.; Markussen, T.; Thygesen, K. S.; van der Molen, S. J.; Hummelen, J. C. *PCCP* **2014**, *16*, 653.
(161) Lim, J.; Albright, T. A.; Martin, B. R.; Miljanić, O. Š. *J. Org. Chem.* **2011**, *76*, 10207.
(162) Zhou, C.-Z.; Liu, T.; Xu, J.-M.; Chen, Z.-K. *Macromolecules* **2003**, *36*, 1457.
(163) Wang, C.; Batsanov, A. S.; Bryce, M. R. *J. Org. Chem.* **2006**, *71*, 108.
(164) Jester, S.-S.; Shabelina, N.; Le Blanc, S. M.; Höger, S. *Angew. Chem. Int. Ed.* **2010**, *49*, 6101.
(165) Atienza, C.; Insuasty, B.; Seoane, C.; Martin, N.; Ramey, J.; Rahman, G. M. A.; Guldi, D. M. *J. Mater. Chem.* **2005**, *15*, 124.
(166) Goeb, S.; Ziessel, R. *Org. Lett.* **2007**, *9*, 737.
(167) Kaae, B. H.; Harpsøe, K.; Kvist, T.; Mathiesen, J. M.; Mølck, C.; Gloriam, D.; Jimenez, H. N.; Uberti, M. A.; Nielsen, S. M.; Nielsen, B.; Bräuner-Osborne, H.; Sauerberg, P.; Clausen, R. P.; Madsen, U. *ChemMedChem* **2012**, *7*, 440.
(168) Wender, P. A.; Lesser, A. B.; Sirois, L. E. *Angew. Chem. Int. Ed.* **2012**, *51*, 2736.
(169) Yamada, S.; Kinoshita, K.; Iwama, S.; Yamazaki, T.; Kubota, T.; Yajima, T. *RSC Advances* **2013**, *3*, 6803.